



Published in final edited form as:

Prog Oceanogr. 2018 January ; 160: 186–212. doi:10.1016/j.pocean.2018.01.001.

An overview of approaches and challenges for retrieving marine inherent optical properties from ocean color remote sensing

P. Jeremy Werdell^{a,*}, Lachlan I.W. McKinna^{a,b}, Emmanuel Boss^c, Steven G. Ackleson^d, Susanne E. Craig^{a,e}, Watson W. Gregg^f, Zhongping Lee^g, Stéphane Maritorena^h, Collin S. Roeslerⁱ, Cécile S. Rousseaux^{e,f}, Dariusz Stramski^j, James M. Sullivan^k, Michael S. Twardowski^k, Maria Tzortziou^{l,m}, and Xiaodong Zhangⁿ

^aNASA Goddard Space Flight Center, Code 616, Greenbelt, MD, USA

^bGo2Q Pty Ltd, Sunshine Coast, QLD, Australia

^cSchool of Marine Sciences, University of Maine, Orono, Maine, USA

^dNaval Research Laboratory, Washington, DC, USA

^eUniversities Space Research Association, Columbia, MD, USA

^fNASA Global Modeling and Assimilation Office, Greenbelt, MD, USA

^gSchool for the Environment, University of Massachusetts Boston, Boston, MA, USA

^hEarth Research Institute, University of California, Santa Barbara, CA, USA

ⁱDepartment of Earth and Oceanographic Science, Bowdoin College, Brunswick, ME, USA

^jScripps Institution of Oceanography, University of California San Diego, La Jolla, CA, USA

^kHarbor Branch Oceanographic Institute, Florida Atlantic University, Fort Pierce, FL, USA

^lDepartment of Earth and Atmospheric Science, The City College of New York, New York, NY, USA

^mNASA Goddard Space Flight Center, Code 614, Greenbelt, MD, USA

ⁿDepartment of Earth System Science and Policy, University of North Dakota, Grand Forks, ND, USA

Abstract

Ocean color measured from satellites provides daily global, synoptic views of spectral waterleaving reflectances that can be used to generate estimates of marine inherent optical properties (IOPs). These reflectances, namely the ratio of spectral upwelled radiances to spectral downwelled irradiances, describe the light exiting a water mass that defines its color. IOPs are the spectral absorption and scattering characteristics of ocean water and its dissolved and particulate constituents. Because of their dependence on the concentration and composition of marine constituents, IOPs can be used to describe the contents of the upper ocean mixed layer. This information is critical to further our scientific understanding of biogeochemical oceanic processes,

*Corresponding author: jeremy.werdell@nasa.gov.

such as organic carbon production and export, phytoplankton dynamics, and responses to climatic disturbances. Given their importance, the international ocean color community has invested significant effort in improving the quality of satellite-derived IOP products, both regionally and globally. Recognizing the current influx of data products into the community and the need to improve current algorithms in anticipation of new satellite instruments (e.g., the global, hyperspectral spectroradiometer of the NASA Plankton, Aerosol, Cloud, ocean Ecosystem (PACE) mission), we present a synopsis of the current state of the art in the retrieval of these core optical properties. Contemporary approaches for obtaining IOPs from satellite ocean color are reviewed and, for clarity, separated based their inversion methodology or the type of IOPs sought. Summaries of known uncertainties associated with each approach are provided, as well as common performance metrics used to evaluate them. We discuss current knowledge gaps and make recommendations for future investment for upcoming missions whose instrument characteristics diverge sufficiently from heritage and existing sensors to warrant reassessing current approaches.

Keywords

Ocean color; satellite remote sensing; bio-optics; inherent optical properties

1 Introduction

Understanding oceanic response to the Earth's changing climate, the ocean's role in land-ocean-atmosphere carbon cycles, regional marine ecosystems' responses to hazards, variations across systems, and the health of aquatic fisheries and other critical habitats – to name only a few – requires access to substantial volumes of marine biogeochemical information (IOCCG, 2008; IOCCG, 2009). Ocean color satellite instruments not only collect data on temporal and spatial scales that cannot currently be achieved by conventional *in situ* or aircraft sampling platforms, but also provide data records that allow retrospective analyses of spatiotemporal trends. These instruments provide estimates of spectral water-leaving radiances – the light exiting a water mass that defines its color, leading to the colloquial discipline name *ocean color*. The scientific community has invested significant effort in the development of algorithms to derive marine biogeochemical and optical quantities from satellite measurements of ocean color (IOCCG, 2006; IOCCG, 2014). With these algorithms, ocean color data records provide invaluable resources to study global and large-scale regional (e.g., Southern Ocean and North Atlantic) carbon stocks (Allison et al., 2010; Duforet-Gaurier et al., 2010; Gardner et al., 2006; Loisel et al., 2002; Siegel et al., 2014; Siegel et al., 2005; Stramska, 2009; Stramska & Stramski, 2005), phytoplankton population diversity and succession (IOCCG, 2014), phytoplankton physiology (Westberry et al., 2016; Westberry & Siegel, 2006), and oceanic productivity (Antoine et al., 1996; Behrenfeld et al., 2005; Saba et al., 2011; Uitz et al., 2010).

The continuous global data record from polar orbiting ocean color satellites in low Earth orbit (LEO) now spans twenty years and includes, but is not limited to, data collected by the following instruments: the NASA Sea-viewing Wide Field of View Sensor (SeaWiFS; 1997–2010), the NASA Moderate Resolution Imaging Spectroradiometers onboard Terra

(MODIST; 1999-present) and Aqua (MODISA; 2002-present), the ESA Medium Resolution Imaging Spectrometer (MERIS; 2002–2012), the NASA-NOAA Suomi National Polar-orbiting Partnership Visible Infrared Imaging Radiometer Suite (VIIRS; 2012-present), and the ESA Ocean and Land Colour Instrument (OLCI; 2016-present). Over this time span, the number of derived data products increased substantially given improvements in computing power, better and more diverse *in situ* measurements, improved knowledge of ocean optics, unlimited access to the data records, and the varied instrument characteristics of the satellite missions (e.g., their spectral, spatial, and temporal resolutions). The interest in using satellite data records to support coupled hydrodynamic-biological modeling efforts (Dutkiewicz et al., 2015; Gnanadesikan et al., 2010; Mannino et al., 2016; Rousseaux & Gregg, 2015) and management and decision making activities (Schaeffer et al., 2015) has also grown. Looking forward, upcoming instruments, such as the spectrometer to be flown as part of the NASA Plankton, Aerosol, Cloud, ocean Ecosystem mission (PACE; launch planned for 2022), will extend current ocean color records and will provide improved sensing systems, including increased spectral resolution (and, possibly, polarization information from a second instrument) that will undoubtedly expand interest in ocean color data records and stimulate derived product development activities.

Recognizing the current influx of data products into the community and the forthcoming need to develop enhanced approaches that exploit the characteristics of new instruments, we present a synopsis of the current state of the art in the retrieval of a core suite of properties used in studying ocean biogeochemistry, namely spectral marine inherent optical properties (IOPs). IOPs are insensitive to changes in the light field and encompass the absorption and scattering properties of seawater and its particulate and dissolved constituents. Ocean color satellite instruments measure the spectral radiance emanating from the top of the atmosphere, $L_t(\lambda)$ ($\mu\text{W cm}^{-2} \text{ nm}^{-1} \text{ sr}^{-1}$) at, at least, discrete visible (VIS; 400–700 nm) and near-infrared (NIR; 700–1000 nm) wavelengths. Generally speaking, two approaches exist to retrieve IOPs from satellite measurements of ocean color. The first approach, used in standard agency processing (e.g., NASA, NOAA, and ESA), applies atmospheric correction (AC) algorithms to remove the contribution of the atmosphere from the total signal at the top of the atmosphere and produce estimates of remote-sensing reflectances, $R_{rs}(\lambda)$ (sr^{-1}), the light exiting the water normalized to a hypothetical condition of an overhead Sun and no atmosphere (Gordon & Clark, 1980; Gordon & Wang, 1994) (paths 1 \rightarrow 2 \rightarrow 4 or 1 \rightarrow 2 \rightarrow 3 \rightarrow 4 in Fig. 1). In the field, $R_{rs}(\lambda)$ is calculated as the ratio of water-leaving radiance, $L_w(\lambda)$ ($\mu\text{W cm}^{-2} \text{ nm}^{-1} \text{ sr}^{-1}$), to downwelling irradiance just above the air-sea interface, $E_s(\lambda)$ ($\mu\text{W cm}^{-2} \text{ nm}^{-1}$). Since $R_{rs}(\lambda)$ is an apparent optical property, that is, it is dependent upon the details of the light field, field measurements are generally made as close to the time of the local satellite overpass(es) as possible. Algorithms are then applied to the $R_{rs}(\lambda)$ to produce estimates of geophysical properties, such as IOPs (IOCCG, 2006; Werdell et al., 2013a). The second approach relates $L_t(\lambda)$ directly to IOPs or an optical proxy for a biogeochemical stock (Hu, 2009; Matthews et al., 2012; Wynne et al., 2013), circumventing the need for AC that can sometimes be confounded by absorbing aerosols and optically complex water masses (path 1 \rightarrow 4 in Fig. 1).

Algorithms for quantifying IOPs from ocean color adopt numerous forms and are used to generate varied optical data products to serve diverse purposes. The total IOPs, those that

result from additive contributions of all water constituents with optical signatures, determine the propagation of light within an aquatic medium and, hence, the changes in the magnitude and spectral composition of the light field throughout the water column. They are the major determinants of $R_{rs}(\lambda)$ and thereby play a critical role in the interpretation of ultraviolet-to-near infrared remote-sensing data. The component IOPs associated with specific types of water constituents, such as phytoplankton, non-algal particles (NAP), and colored dissolved organic matter (CDOM), carry information about ocean properties and processes that have specific biological and biogeochemical significance, including standing stocks and rate processes of aquatic carbon pools. For example, spectral absorption coefficients of phytoplankton provide essential parameters for quantifying primary production (Bannister, 1974; Kiefer & Mitchell, 1983; Lee et al., 1996b; Marra et al., 2007). Phytoplankton absorption coefficients arguably also provide the single best parameters for optically-based assessments of phytoplankton community composition that is typically described in terms of community size structure and pigment composition (Bracher et al., 2017; Brewin et al., 2011; Bricaud et al., 2007; Ciotti et al., 2002; Devred et al., 2011; Hirata et al., 2008; Hoepffner & Sathyendranath, 1993; Lohrenz et al., 2003; Moisan et al., 2011; Organelli et al., 2013; Sathyendranath et al., 2001; Sathyendranath et al., 2005; Uitz et al., 2015). Likewise, spectral absorption coefficients of CDOM provide biogeochemically useful proxies of aquatic dissolved organic carbon (DOC) (Fichot & Benner, 2011; Mannino et al., 2008; Matsuoka et al., 2012; Vantrepotte et al., 2015; Vodacek et al., 1997), allowing the estimation of this carbon pool from optical measurements in some aquatic environments.

The flow of this paper is as follows. First, we review the state of the art in approaches for obtaining IOPs from satellite ocean color. We separate the approaches based on common methods in either inversion methodology or the type of IOPs sought. We next provide summaries of known uncertainties associated with the approaches and common performance metrics. Both of the latter merit (and could fill) full reviews, but doing so exceeds the scope of this review, so only synopses are provided. We then discuss knowledge gaps and recommendations for future investment and conclude with a discussion of recommendations for the upcoming missions, including PACE, whose instrument characteristics diverge sufficiently from heritage and existing sensors such that novel and/or refined approaches will be required to best exploit and take advantage of these characteristics.

2 Heritage algorithmic approaches

2.1 Equations and assumptions

2.1.1 Relating $R_{rs}(\lambda)$ to IOPs—Considerable effort has focused on the development of analytical frameworks for deriving unknown marine IOPs from sensor-observed $R_{rs}(\lambda)$, recognizing that these frameworks cannot be exactly reduced to an analytical equation or expression (IOCCG, 2006). Mathematically, deriving IOPs requires solution of an inverse problem that can be solved by developing an appropriate forward model, F , that explicitly relates the observed quantity (in this case, $R_{rs}(\lambda)$) to a set of unknown variables-of-interest (IOPs):

$$R_{rs}(\lambda) = F[IOP_S(\lambda)] \quad (1)$$

Given that $R_{rs}(\lambda)$ is an apparent optical property (AOP) that depends on the geometry of the light field, F must explicitly or implicitly account for angular variations associated with illumination conditions. Once a suitable forward model has been developed, it is often possible to derive IOPs from sensor-observed $R_{rs}(\lambda)$ using an inverse solution method:

$$IOP_S(\lambda) = F^{-1}[R_{rs}(\lambda)] \quad (2)$$

The inverse solution method is often mathematically ill-posed, however, as different combinations of IOPs can result in the same $R_{rs}(\lambda)$ spectrum in the visible (VIS) domain (DefoinPlatel & Chami, 2007; Sydor et al., 2004; Twomey, 1977). This is particularly the case when the number of independent observations (i.e. number of sensor VIS wavelengths) is small compared to the number of unknown IOP variables, or when uncertainty in the observed $R_{rs}(\lambda)$ is high. Historically, two distinct forward modeling approaches have been routinely used to develop the relationship between R_{rs} and IOPs: (1) scalar radiative transfer (RT) simulations; and (2) approximation to the RT such as the quasi-single scattering approximation (QSSA). RT simulations comprehensively quantify the fate of the incident downwelling photon flux as it interacts with optically significant constituent matter. The QSSA is a simplified analytical model that approximates $R_{rs}(\lambda)$ as a function of spectral IOPs. Note that statistical and neural network approaches also exist that directly relate measured $R_{rs}(\lambda)$ and IOPs, thus simplifying Eq. (1) further. We review these methods in Section 2.2.3.

Many RT codes have been developed that compute $R_{rs}(\lambda)$ from user-input IOPs and other key environmental parameters (e.g. sea surface state, atmospheric transmittance, solar geometry, viewing geometry, and water column depth). Historically, hydrological RT codes have been either Monte Carlo ray tracing-based methods (Boynton & Gordon, 2002; Gordon & Boynton, 1998; Kattawar & Adams, 1989; Zhai et al., 2008) or direct solutions to the RT equation (Mobley et al., 1993), with the latter being most common in recent ocean optics studies. A substantial benefit of hydrologic RT codes is they can capture the effects of multiple scattering, inelastic radiative processes, and vertical water-column structure. In addition, hydrologic and atmospheric RT codes can be coupled to simulate sensor-observed $L_r(\lambda)$. Note, however, that RT simulations can be computationally intensive, are conceptually complex, rely on accurate user inputs (e.g., IOP measurements or models), and can be limited by any assumptions associated with measurement gaps, including bio-optical models that may be used to parameterize input IOPs (Gordon et al. 1988). In addition, most RT codes in use are scalar and do not account for polarization. Including polarization may result in significantly different (~ 50%) values relative to heritage scalar results (Harmel et al., 2012; Mobley, 2015), opening the door for retrieval of more information about atmospheric and oceanic particles.

The QSSA was first derived for ocean color applications by Gordon (1973). Essentially, the QSSA assumes most scattering occurs in the forward direction and, accordingly, that the color and shape of the upward propagating light field is primarily determined by absorption and singlescattering at large angles (rather than multiple scattering at small angles), respectively (Gordon, 1993). Using this assumption, several analytical expressions have been developed that approximate the sub-surface remote-sensing reflectance, $r_{rs}(\lambda)$ (sr^{-1}) as a function of total absorption, $a(\lambda)$ (m^{-1}), and backscattering, $b_b(\lambda)$ (m^{-1}) coefficients (Gordon et al., 1988; Morel, 1988; Morel & Prieur, 1977). Alternatively, the QSSA can be used to model subsurface irradiance reflectance, $R(\lambda)$ (unitless), defined as the ratio of subsurface upwelling irradiance, $E_u(\lambda)$, to subsurface downwelling irradiance, $E_d(\lambda)$, (both with units of $\mu\text{W cm}^{-2} \text{nm}^{-1}$). Other models have additionally included explicit dependencies on the volume scattering function (VSF) (Jerlov, 1976; Zaneveld, 1982; Zaneveld, 1995). The major benefit of QSSA models is the provision of an explicit analytical relation between IOPs and $r_{rs}(\lambda)$. Establishing this relationship, however, requires various assumptions of boundary conditions, such as an infinitely deep and a homogeneous water column. Furthermore, QSSAs cannot capture extreme multiple scattering effects, require an additional module to consider inelastic processes, do not account for the polarization, and are not as accurate as RT codes. Some formulations exist that address bottom reflectance (Lee et al., 1994; Lee et al., 1998a; Philpot, 1987; Sathyendranath & Platt, 1988), but we do not discuss them in detail in this review.

2.1.2 Common QSSA equations—Most contemporary ocean color applications employ QSSA models that express $r_{rs}(\lambda)$ as a function of IOPs. In these cases, it is necessary to convert the $R_{rs}(\lambda)$ observed by the satellite instrument to $r_{rs}(\lambda)$ using a relationship such as Lee et al. (2002):

$$r_{rs}(\lambda) = \frac{R_{rs}(\lambda)}{0.52 + 1.7R_{rs}(\lambda)} \quad (3)$$

Note that in conventional NASA processing, the input $R_{rs}(\lambda)$ includes “exact” normalization to account for bidirectional reflectance distribution function (BRDF) effects (Morel et al., 2002). We assume $R_{rs}(\lambda)$ to be normalized as such in this review, which effectively removes most of the effects of the Sun being off-zenith. The most commonly employed relationships to express $r_{rs}(\lambda)$ as a function of IOPs can be represented in the expression developed by (Gordon et al., 1988):

$$r_{rs}(\lambda) = \sum_{i=1}^2 G_i(\lambda)[u(\lambda)]^i \quad (4)$$

where the $G(\lambda)$ coefficients represent the combined influence of illumination conditions and geometry, sea surface properties, and the shape of the marine VSF and , $u(\lambda)$ is described as:

$$u(\lambda) = \frac{b_b(\lambda)}{a(\lambda) + b_b(\lambda)} \quad (5)$$

as obtained from the QSSA approximation. Eq. (4) has a unique positive solution for $u(\lambda)$ when $r_{rs}(\lambda)$ and $G(\lambda)$ are all positive. Common methods for estimating the $G(\lambda)$ functions include Gordon et al. (1988), where $G_1(\lambda)$ and $G_2(\lambda)$ are spectrally fixed as 0.0949 and 0.0794 (see Lee et al. (2002) and Lee et al. (2011) for alternative coefficients) and the tabulated results of Morel et al. (2002), where $G_1(\lambda)$ is estimated for given solar and sensor geometries and chlorophyll-a concentrations (C_a ; mg m^{-3}) and $G_2(\lambda)$ is set to 0. Appendix A provides an alternate list of expressions for Eq. (4). In current practice, these methods for estimating $G(\lambda)$ cannot represent all illumination conditions and geometries, sea surface properties, and shapes of the particle VSF. Alternative representations of $G(\lambda)$ within a QSSA have emerged to address the uncertainties associated with these specific effects being poorly defined (see Section 5.3).

2.1.3 Common IOP component definitions and equations—The total spectral absorption coefficient is a conservative property and thus, by definition, can be expressed as the sum of all individual absorbing constituents:

$$a(\lambda) = \sum_{i=1}^N a_i(\lambda) \quad (6)$$

where index i indicates the i^{th} of N total individual absorbing constituents. Practically, similar constituents are grouped into components (Roesler et al., 1989; Stramski et al., 2001):

$$a(\lambda) = a_w(\lambda) + \sum_{i=1}^{N_{ph}} a_{ph,i}(\lambda) + \sum_{i=1}^{N_{nap}} a_{nap,i}(\lambda) + \sum_{i=1}^{N_{cdom}} a_{cdom,i}(\lambda) \quad (7)$$

where the subscripts w , ph , nap , and $cdom$ indicate contributions by water, phytoplankton, NAP, and CDOM and the index i may indicate a number of individual constituents (i.e., phytoplankton cells) or sub-components (i.e., multiple phytoplankton communities) enumerated as N_{ph} . Similarly, N_{nap} and N_{cdom} are the number of different types of NAP and CDOM present. Further, each absorbing component can be expressed as the product of its normalized spectral absorption coefficient (shape; a^*) and its magnitude (A):

$$a(\lambda) = a_w(\lambda) + \sum_{i=1}^{N_{ph}} A_{ph,i} a_{ph,i}^*(\lambda) + \sum_{i=1}^{N_{nap}} A_{nap,i} a_{nap,i}^*(\lambda) + \sum_{i=1}^{N_{cdom}} A_{cdom,i} a_{cdom,i}^*(\lambda) \quad (8)$$

where the term “normalized” is used here to describe the process of obtaining a representation of absorption spectral shape. Multiple approaches have been adopted (Bricaud et al., 1995; Bricaud et al., 1998; Roesler et al., 1989), as expanded upon in Section 2.1.4, and the units of A and a^* depend upon the choice of normalization. For example, when the phytoplankton component absorption spectrum is scaled to the chlorophyll-a concentration, the term $A_{ph,i}$ is equivalent to the chlorophyll-a concentration (mg m^{-3}) and $a^*_{ph,i}(\lambda)$ is the chlorophyll-a specific absorption coefficient ($\text{m}^2 \text{mg}^{-1}$) associated with the i^{th} phytoplankton type present. The shapes of $a_{nap}(\lambda)$ and $a_{cdom}(\lambda)$ are spectrally similar, and for simplicity, or when the degrees of freedom are low, they are often treated in combination:

$$a_{dg}(\lambda) = a_{nap}(\lambda) + a_{cdom}(\lambda) \quad (9)$$

where a_{dg} is a heritage term, namely absorption by detrital particulate matter and gelbstoff, although NAP encompasses more than detrital particulate matter (i.e., living and detrital particulate organic matter, exclusive of in vivo phytoplankton pigments, as well as inorganic particulates) and CDOM operationally includes sub-micron particles. The term $A_{dg,i}$ (m^{-1}) is accordingly introduced for scaling the magnitude of the i^{th} normalized CDOM + NAP coefficient, $a_{dg}^*(\lambda)$ (unitless). The total absorption coefficient from Eq. (8) now becomes:

$$a(\lambda) = a_w(\lambda) + \sum_{i=1}^{N_{ph}} A_{ph,i} a^*_{ph,i}(\lambda) + \sum_{i=1}^{N_{dg}} A_{dg,i} a^*_{dg,i}(\lambda) \quad (10)$$

Note, however, that this simplification is not ubiquitous and several algorithms derive the $a_{cdom}(\lambda)$ and $a_{nap}(\lambda)$ components separately from one another, as described in Section 2.1.4.

The total spectral backscattering coefficient can be similarly expanded as (Stavn & Richter, 2008; Stramski et al., 2001):

$$b_b(\lambda) = b_{bw}(\lambda) + \sum_{i=1}^{N_{ph}} b_{bph,i}(\lambda) + \sum_{i=1}^{N_{nap}} b_{bnap,i}(\lambda). \quad (11)$$

As for absorption, we can express each constituent within the components of $b_b(\lambda)$ as the product of a normalized backscattering spectrum (shape; b^*) and its magnitude (B). The total backscattering coefficient can thus be expressed as:

$$b_b(\lambda) = b_{bw}(\lambda) + \sum_{i=1}^{N_{ph}} B_{bph,i} b^*_{bph,i}(\lambda) + \sum_{i=1}^{N_{nap}} B_{bnap,i} b^*_{bnap,i}(\lambda). \quad (12)$$

As the two non-water backscattering components are considered spectrally similar, Eq. (12) is often reduced to:

$$b_b(\lambda) = b_{bw}(\lambda) + \sum_{i=1}^{N_p} B_{bp,i} b_{bp,i}^*(\lambda). \quad (13)$$

For the inversion problem to be well-posed, the number of unknown IOP variables must not exceed the number of observed independent variables (spectral bands). Contemporary oceancolor sensors are multi-spectral, having between 5 and 8 VIS bands suitable for use in inversion algorithms. We note, however, that the number of unknown parameters one can actually solve for may be significantly less than the number of bands available depending on the uncertainties in the measured input reflectances and the amount of un-correlated information within them (e.g. Twomey 1977). We expect that for future missions with hyperspectral spectrometers from the ultraviolet (UV; ~350 nm) to the NIR (~900 nm), such as PACE, the number of retrievable parameters will be much fewer than the number of wavebands, but the uncertainty in the retrieved parameters will be much lower. In the simplest formulation described by Eqs. (4), (5), (10) and (13) and with $N_p=N_{pl}=1$, only three normalized spectral shapes are required ($a_{ph}^*(\lambda)$, $a_{dg}^*(\lambda)$, and $b_{bp}^*(\lambda)$) and three unknown IOP magnitudes, (A_{ph} , A_{dg} and B_p), are retrieved. Methods used to partition $a(\lambda)$ and $b_b(\lambda)$ into additional subcomponents and mathematical solution methods to invert IOPs from $r_{rs}(\lambda)$ are described in Sections 2.1.4 and 2.2, respectively.

2.1.4 Approaches to Retrieving Component IOPs from Reflectance—Broadly speaking, many variants of several approaches exist to invert $R_{rs}(\lambda)$ or $r_{rs}(\lambda)$ to IOPs, all of which require varied degrees of knowledge of IOP component spectral shapes. Methods for assigning spectral shapes or partitioning total IOPs into their components, however, are not often mutually exclusive from the inverse solution method. Next, we present IOP spectral shape parameterization and partitioning approaches. A detailed discussion of solution methods is presented separately in Section 2.2. For the purposes of this section, it is convenient and necessary to introduce two solution concepts for deriving component IOPs: (A) a simultaneous solution of $b_{bp}(\lambda)$, $a_{ph}(\lambda)$, and $a_{dg}(\lambda)$ (or, $a_{cdom}(\lambda)$ and $a_{nap}(\lambda)$) (path 2→4 in Fig. 1); and (B) a two-part solution where first $b_{bp}(\lambda)$ and $a(\lambda)$ are determined, then $a(\lambda)$ is subsequently decomposed into its components (path 2→3→4 in Fig. 1). For reference, these two concepts map most directly to the solution methods presented in Sections 2.2.1 and 2.2.2.

2.1.4.1 Seawater absorption and backscattering: A number of values for $a_w(\lambda)$ have been estimated from laboratory measurements of pure water samples (Pope & Fry, 1997) or modeled using *in situ* samples collected from hyper-oligotrophic regions of the ocean (Lee et al., 2015; Morel et al., 2007; Smith & Baker, 1981). Several sets of spectral $b_{bw}(\lambda)$ have been derived previously from theory (Buiteveld et al., 1994; Morel, 1974; Shifrin, 1988). Theoretical values from Zhang and Hu (2009) and Zhang et al. (2009) are considered the current state of the art, agreeing to within 2% on average with the only pure water scattering measurements made by Morel (1968). The vibrational states and thermodynamic properties of seawater, and hence its optical properties, vary with changes in temperature (T) and/or salinity (S) in specific spectral regions. Accordingly, recent efforts have focused on modeling the spectral shapes of $a_w(\lambda)$ (Pegau et al., 1997; Röttgers et al., 2014; Sullivan et

al., 2006; Twardowski et al., 1999) and $b_{bw}(\lambda)$ (Pegau et al., 1997; Röttgers et al., 2014; Zhang et al., 2009) as functions of T and S . Satellite observations of sea surface temperature (SST; Kilpatrick et al. (2001) and sea surface salinity (SSS; Lagerloef et al. (2008), as well as climatological values (Antonov et al., 2010; Reynolds et al., 2002), have made it possible to implement T - S dependent $b_{bw}(\lambda)$ within inverse algorithms (Werdell et al., 2013b).

2.1.4.2 Phytoplankton, NAP, and CDOM absorption: Partitioning total absorption, $a(\lambda)$, into several broadly-defined components associated with CDOM, phytoplankton, and NAP is possible because of the availability of routine experimental methodologies for determinations of $a_{cdom}(\lambda)$, $a_{ph}(\lambda)$, $a_{nap}(\lambda)$, and $a_p(\lambda) (= a_{nap}(\lambda) + a_{ph}(\lambda))$ (Bricaud et al., 1981; Bricaud & Stramski, 1990; Ferrari & Tassan, 1999; Kishino et al., 1985; Miller et al., 2002; Mitchell et al., 2003; Mitchell & Holm-Hansen, 1991; Pegau et al., 2003; Röttgers & Doerffer, 2007; Röttgers et al., 2007; Stramski et al., 2015; Twardowski et al., 1999), with the understanding that interpretation of these components remains constrained by their operational definitions and measurement protocols. For example, whereas $a_{cdom}(\lambda)$ is defined by the 0.2 μm pore size of the filter used to establish the dissolved fraction of the sample, $a_p(\lambda)$ is typically measured with a filter-pad method by collecting particles on GF/F glass-fiber filters (Mitchell et al., 2003). Thus, the filter-pad method does not account for a certain fraction of particulate absorption associated with submicron particles (Stramski, 1990) and closure in the nominal size range 0.2 μm to 0.7 μm is lacking unless the missing fraction is measured (Simeon et al., 2003). Note that partitioning $a(\lambda)$ in the actual methodological sense is practically equivalent to partitioning of the non-water absorption coefficient, $a_{nw}(\lambda) = a(\lambda) - a_w(\lambda)$, because $a_w(\lambda)$ is assumed to be known (see above).

2.1.4.2.1 Simultaneous partitioning methodology: Most heritage IOP models pursue a simultaneous solution (path 2→4 in Fig. 1), which requires assumptions about the spectral shapes of $a_{ph}(\lambda)$ and $a_{dg}(\lambda)$. These approaches often parameterize a single spectral shape for $a_{ph}^*(\lambda)$ based on *in situ* measurements (Garver & Siegel, 1997; Maritorena et al., 2002; Roesler & Perry, 1995; Sathyendranath et al., 1989), multiple $a_{ph}^*(\lambda)$ spectra associated with different pigment-based taxonomic groups (Roesler & Boss, 2003; Roesler et al., 2004; Werdell et al., 2014), or as empirically-derived Gaussian-based approximations to measurements (Hoge & Lyon, 1996; Lee et al., 1996a). Spectral variations in $a_{ph}^*(\lambda)$ do exist, however, due to the types and relative concentrations of phytoplankton present and their physiological responses to growth conditions including light, nutrient availability, and temperature. This leads to temporal, spatial and depth variations in the spectral shapes of $a_{ph}^*(\lambda)$ that are encountered in the ocean. During pixel-by-pixel processing $a_{ph}^*(\lambda)$ is either treated as a spectral constant or a bio-optical model is used in an attempt to capture its variability. Commonly used approaches for parameterizing $a_{ph}^*(\lambda)$ are summarized in Table 1.

A fixed shape for $a_{dg}^*(\lambda)$ is typically modeled with the exponential function:

$$a_{dg}^*(\lambda) = \exp(-S_{dg}\lambda), \quad (14)$$

where the exponential decay coefficient, S_{dg} , which typically varies between 0.01 and 0.02 nm^{-1} (Roesler et al., 1989), is assigned as a constant value (Hoge & Lyon, 1996; Maritorena et al., 2002; Roesler & Perry, 1995). The choice of S_{dg} is sometimes based on region-specific *in situ* measurements (Brando et al., 2012), global *in situ* datasets (Lee et al., 2009), or by optimally tuning the inverse algorithm's bio-optical parameters with a training dataset (Maritorena et al., 2002). Alternatively, the approach of Lee et al. (2009) estimates S_{dg} dynamically from an empirical dependence on the blue to green reflectance ratio:

$$S_{dg} = 0.015 + \frac{0.002}{0.6 + r_{rs}(443)/r_{rs}(55x)}, \quad (15)$$

where the reference wavelength, $55x$, is centered on the greenest wavelength of the satellite instrument (e.g. 555 nm for SeaWiFS and 547 nm for MODIS). This method does not permit S_{dg} to fall below 0.015 nm^{-1} and predicts a decrease in S_{dg} as water becomes clearer (through an increasing 443–55x ratio), which has not been ubiquitously observed, particularly in the presence of photobleaching. Generally speaking, the magnitudes of S_{dg} (or S_g) and $a_{dg}(440)$ (or $a_g(440)$) share an inverse relationship (Bricaud et al. 2012), a model parameterization explored in Brewin et al. (2015a). Twardowski et al. (2004) suggested that exponential relationships do not accurately represent the spectral shape of CDOM, offering power-laws as the alternative and demonstrating that S_{dg} values will vary dependent on specified spectral range used to compute it (see also Nelson and Siegel (2002). Most recently, Cael and Boss (2017) demonstrated that a stretched exponential provides a better model than Eq. (14) or a power-law for $a_{dg}(\lambda)$.

2.1.4.2.2. Two-step partitioning methodology: Many emerging IOP models pursue a two-step solution (path 2→3→4 in Fig. 1) for partitioning $a(\lambda)$ into its subcomponents. One pathway begins with decomposing of $a_{nw}(\lambda)$ into $a_p(\lambda)$ and $a_{cdom}(\lambda)$ and then subsequently subdividing $a_p(\lambda)$ into $a_{ph}(\lambda)$ and $a_{nap}(\lambda)$. (Bricaud & Stramski, 1990; Cleveland & Perry, 1994; Hoepffner & Sathyendranath, 1993; Lin et al., 2013; Morrow et al., 1989; Roesler et al., 1989; Wang et al., 2008; Zheng & Stramski, 2013a). This multiple-step approach has had limited applicability within the remote sensing context, primarily because of difficulties in directly estimating $a_p(\lambda)$ and $a_{cdom}(\lambda)$ from ocean color measurements. Currently, the most common pathway involves partitioning of $a_{nw}(\lambda)$ into $a_{ph}(\lambda)$ and $a_{dg}(\lambda)$ (Eq. (10); for examples of partitioning methods in this category see Table 2.

Despite its convenience within the remote-sensing paradigm, combining $a_{nap}(\lambda)$ and $a_{cdom}(\lambda)$ into one term, $a_{dg}(\lambda)$, has disadvantages when linking IOPs to ocean biogeochemical processes. NAP and CDOM can originate from different sources, are affected by different physical and biogeochemical processes and are associated with different pools and residence times in the ocean. In addition, NAP is assumed to contribute to scattering significantly while CDOM's contribution is assumed negligible. As such, they cannot always be expected to demonstrate strong covariation in coastal or open ocean waters. Furthermore, while NAP and CDOM both show an exponential decrease in absorption with increasing wavelength, their spectral slopes are typically considerably different, with S_{nap} and S_{cdom} encompassing 0.005–0.015 nm^{-1} and 0.01–0.03 nm^{-1} ,

respectively (Babin et al., 2003; Roesler et al., 1989; Tzortziou et al., 2007). Ultimately, retrieving S_{cdom} from satellite observations is desirable as it provides a reliable indicator of the source, molecular size, aromatic content and extent of photochemical versus microbial degradation of organic matter in aquatic environments (e.g. Blough & Green, 1995; Chin et al., 1994; Helms et al., 2008; Tzortziou et al., 2011). Similarly, retrieving S_{nap} may enable the relative proportions of mineral and organic matter to be determined (Babin et al., 2003). As such, effort has focused on the development of partitioning approaches to derive $a_{ph}(\lambda)$ and separate $a_{dg}(\lambda)$ into $a_{nap}(\lambda)$ and $a_{cdom}(\lambda)$ (Chang & Dickey, 1999; Claustre et al., 2000; Dong et al., 2013; Gallegos & Neale, 2002; Lin et al., 2013; Schofield et al., 2004; Zheng et al., 2015).

Similar to other categories of absorption partitioning models, methods developed to partition $a(\lambda)$ into $a_{ph}(\lambda)$, $a_{nap}(\lambda)$, and $a_{cdom}(\lambda)$ typically carry significant limitations associated with restrictive assumptions about model outputs, the use of ancillary input data, and region-specific parameterizations. Several models employ a single spectral shape or a linear combination of a small number of predefined spectral shapes for $a_{ph}^*(\lambda)$ (Devred et al., 2011; Gallegos & Neale, 2002; Schofield et al., 2004). Nearly all assume an exponential function for the spectral shapes of both $a_{nap}^*(\lambda)$ and $a_{cdom}^*(\lambda)$, in some cases with a fixed value for one of the two (Dong et al., 2013). Many use empirical parameterizations requiring input ancillary data, such as C_a (Claustre et al., 2000), $R_{rs}(\lambda)$ and/or $b_b(\lambda)$ (Dong et al., 2013), or even direct measurements of $a_{cdom}(\lambda)$ (Chang & Dickey, 1999). Furthermore, most models in this category have features or parameterizations that reflect intended applicability only to specific regions or *in situ* measurements taken with specific instruments (Chang & Dickey, 1999; Claustre et al., 2000; Gallegos & Neale, 2002; Schofield et al., 2004; Zheng et al., 2015).

2.1.4.3 Particulate backscattering: The total backscattering coefficient of seawater, $b_b(\lambda)$, is most commonly represented as a sum of only two components, the pure seawater backscattering coefficient free from particulate matter, $b_{bw}(\lambda)$, and the particulate backscattering coefficient, $b_{bp}(\lambda)$ (Eq. (13)). The pure seawater component is assumed to be known *a priori* or predictable as described previously. Particulate backscattering is typically assumed to include the contributions from all kinds of suspended particles pooled together into a single particulate component, $b_{bp}(\lambda)$. In some models, the particulate component has been further partitioned into two components such as organic and inorganic particle components (Bukata et al., 1995), large-sized and small-sized particle components (Roesler & Perry, 1995), and phytoplankton and NAP components (Brando et al., 2012) (Eq. (11)).

Many IOP models adopt a power-law to describe the spectral shape of $b_{bp}^*(\lambda)$ (Gordon & Morel, 1983; Morel & Prieur, 1977):

$$b_{bp}^*(\lambda) = \lambda^{-S_{bp}} b_p, \quad (16)$$

where S_{bp} typically varies between 0 and 3, largely driven by varying proportions of large and small particles (Reynolds et al., 2016; Sathyendranath et al., 1989; Stramska et al.,

2003). Note, this relationship is not exhaustively based on *in situ* or laboratory measurements and deserves systematic evaluation in the future. Stramska et al. (2003) and Reynolds et al. (2016) show *in situ* determinations of backscattering versus wavelength and the power function for these data. Based on $b_{bp}(\lambda)$ values from 394 to 852 nm collected in the Arctic, Reynolds et al. (2016) reported the range of S_{bp} from 0.13 to 3.01 with the majority of data (80%) between 0.5 and 1.5, a median value of 1, and a mean value of 1.5. In some inverse models, the value of S_{bp} is treated as constant based on *in situ* measurements with values of 0.5 used in coastal waters and values of 1.0 for oceanic waters (Mobley, 1994). When $r_{rs}(\lambda)$ are known, methods to estimate S_{bp} from $r_{rs}(\lambda)$ or C_a also exist (Table 3). Roesler and Boss (2003) proposed an alternative approach that does not assume a power-law spectra for particulate backscattering, but rather assumes a spectrally constant particulate back-scattering ratio, $\tilde{b}(\lambda) = b_{bp}(\lambda)/b_p(\lambda)$ and a power-law spectral dependence for particulate beam attenuation, S_c (which is consistent with measurements):

$$b_{bp}(\lambda) = \tilde{b}(\lambda) \left[c_p(\lambda_0) \left(\frac{\lambda}{\lambda_0} \right)^{-S_c} - a_p(\lambda) \right] \quad (17)$$

where, λ_0 is a reference wavelength and $c_p(\lambda_0)$ is the particulate beam attenuation coefficient at λ_0 . For $a_p(\lambda)$, *a priori* assumptions about the spectral shape of the model output of particulate backscattering components can be highly restrictive, especially for application at arbitrary time and location within the global ocean. Loisel and Stramski (2000) developed an approach that does not require *a priori* assumptions about the spectral shape of output IOPs by providing solutions for $b_b(\lambda)$ and $a(\lambda)$ at different light wavelengths independently. The particulate component $b_{bp}(\lambda)$ is calculated from $b_b(\lambda)$ by subtracting the known or assumed values of $b_{bw}(\lambda)$. Similarly, $a_{nw}(\lambda)$ is calculated by subtracting the known or assumed values of $a_w(\lambda)$ from $a(\lambda)$. Loisel and Stramski (2000) provides one example where absorption components must be retrieved in a second step from the derived $a_{nw}(\lambda)$, as described above.

2.2 Solution methods

2.2.1 Semi-analytical inversion approaches—Semi-analytical inversion algorithms (SAAs) estimate marine IOPs from sensor-observed $R_{rs}(\lambda)$ using a combination of empiricism and radiative transfer theory. SAAs attempt to simultaneously estimate the magnitudes of $a_{ph}(\lambda)$, $a_{dg}(\lambda)$, and $b_{bp}(\lambda)$ (Brando et al., 2012; Brewin et al., 2015a; Bukata et al., 1995; Devred et al., 2006; Garver & Siegel, 1997; Hoge & Lyon, 1996; IOCCG, 2006; Maritorena et al., 2002; Roesler & Perry, 1995; Wang et al., 2005; Werdell et al., 2013a). These SAAs generally assign constant spectral values for $a_w(\lambda)$ and $b_{bw}(\lambda)$, parameterize the spectral dependency of the IOPs of non-water constituents ($a_{ph}^*(\lambda)$, $a_{dg}^*(\lambda)$, and $b_{bp}^*(\lambda)$) for all sensor bands in the VIS part of the spectrum, or at a few specific bands, and retrieve the magnitudes of these constituents (A_{ph} , A_{dg} , and B_{bp}). They primarily differ only in the assumptions employed to define component IOP spectral shapes (see Sections 2.1.4), the inverse relation between $r_{rs}(\lambda)$ and IOPs (see Section 2.1.2), and the mathematical method applied to calculate the magnitude of the component IOPs.

Generally speaking, SAAs fall into four broad classes based on their solution method: (i) nonlinear spectral optimization, (ii) direct linear inversion, (iii) spectral deconvolution, and (iv) bulk inversion (Table 4). SAA methods (i) and (ii) use $R_{rs}(\lambda)$ and normalized spectral shapes as inputs and estimate the amplitudes for absorption and backscattering components via linear or nonlinear least squares inversion of Eqs. (4) and (5). Roesler and Perry (1995), for example, used the nonlinear least-squares Levenberg-Marquardt optimization scheme. Hoge and Lyon (1996) later showed the problem could be linearized and, thus, directly solved by simple linear matrix inversion (single solution). The system is over-determined when the number of input $R_{rs}(\lambda)$ wavelengths exceeds the number of unknowns, in which case the single solution obtained is the best in the least-square sense (Wang et al., 2005). These two classes best represent the simultaneous solution described as concept (A) in Section 2.1.4.

SAA method (iii), spectral deconvolution, assigns spectral shapes for some components and proceeds in a step-wise fashion to sequentially determine the component IOPs, unlike methods (i) and (ii) that iteratively run the forward model to find the optimal solution of the amplitudes. Examples of class (iii) are described in Lee et al. (2002) and Smyth et al. (2006). Note that SAAs in this class first determine total absorption and backscattering (unlike spectral optimization approaches) and, therefore, can be employed to explore multiple approaches to decompose $a(\lambda)$ and $b_{bp}(\lambda)$ into their component parts (for reference, path 2→3→4 in Fig. 1). A key difference between the spectral deconvolution and the other methods is that there is no residual difference between input and output $R_{rs}(\lambda)$ spectra in the bulk inversion scheme, whereas residual differences between input and output $R_{rs}(\lambda)$ spectra are inherent to the other inversion schemes (with the residuals used as performance metrics, see Section 4, or to assign spectral variations to retrieved absorption constituents not captured by input spectral shapes (Roesler & Perry, 1995). Accordingly, spectral deconvolution approaches are inherently sensitive to biases in sensor-observed $R_{rs}(\lambda)$ data due to sensor miscalibration and/or sub-optimal AC.

Finally, SAAs in method class (iv), bulk inversions, do not assign shape-components – that is, they do not predefine spectral shapes for the absorption or backscattering coefficients when deriving the total absorption coefficients. The approach introduced in Loisel and Stramski (2000) is a widely used example. In practice, SAAs in this class determine IOPs at each wavelength independently and, therefore, can be used to calculate spectral shape functions (e.g., S_{bp}) dynamically. These SAAs, however, require additional assumptions and/or intermediate products, such as spectral diffuse attenuation coefficients of downwelling irradiance ($K_d(\lambda)$; m^{-1}). Appendix A of Werdell et al. (2013a) provides a detailed discussion of these broad SAA classes.

An emerging generation of SAAs adopts ensemble approaches, employing either ranges of shape-components (Brando et al., 2012; Wang et al., 2005) or on-the-fly identification of optical water types, which can conceptually be used to assign corresponding shape-components (Moore et al., 2009; Vantrepotte et al., 2012). In the former, ranges of shape-components for unknown parameters are applied iteratively. The final unknown parameters are either calculated as the median of all valid values retrieved during the iteration, or selected from a range of retrievals based on threshold and/or best-fit metrics. In the latter,

shape-components are dynamically assigned for each satellite pixel based on an environmental classification metric, thus minimizing assumptions that singular shape-components represent all water types and conditions at all times.

2.2.2 Look-up-table approaches—Look-up table (LUT) solution methods first use a forward model to generate a database of $R_{rs}(\lambda)$ and/or $L_r(\lambda)$. Each $R_{rs}(\lambda)$ or $L_r(\lambda)$ spectrum in the LUT corresponds to a unique combination of water column properties (IOPs and, if relevant, depth and seafloor reflectance) and atmospheric properties (if relevant, cloud cover, surface conditions, and sun geometry). The LUT is constructed by running a forward model (QSSA or RT) for each combination of parameters to be considered (Hedley et al., 2009; Liu & Miller, 2008; Mobley et al., 2005). The IOPs used in the forward modeling arise from either *in situ* datasets or are generated with bio-optical models using constituent-specific parameterizations, such as mass-specific properties at reference wavelengths and associated spectral shape functions (see Sections 2.1.3 and 2.1.4).

To derive IOPs, the sensor-observed $R_{rs}(\lambda)$ or $L_r(\lambda)$ for a given image pixel is compared with the spectra stored in the LUT. The LUT is searched until an entry or suite of entries is found that best match the sensor-observed spectrum. A best match is determined once the cost function (distance measure) achieves a pre-defined threshold, in a manner similar to spectral optimization. The returned IOP solution is defined as that which corresponds to the closest-matching forwardmodeled $R_{rs}(\lambda)$ or $L_r(\lambda)$ in the LUT. If the search returns a solution set – all spectra within a prescribed uncertainty tolerance, ϵ , of the measured spectrum – the solution might be computed as the average of all associated parameters consistent with the retrieved spectra. An advantage to this approach is that ϵ can be defined as a function of known sources of uncertainty, such as those associated with the remote sensor and data/parameterizations used to generate the database, and the divergence of the various consistent solutions can provide a measure of the uncertainty in retrieved IOPs. The cost function can be spectrally weighted to account for band-specific instrument noise and sensitivity to constituent variability.

Mobley et al. (2005) and Liu and Miller (2008) constructed RT-based LUTs using the commercial software HydroLight (Mobley & Sundman, 2008). Mobley et al. (2005) generated a LUT containing 41,591 spectra for various combinations of water constituent IOPs, bottom type reflectance, water depth, sun angle, wind speed, and sky conditions from their study region. The approach was developed for inverting airborne-based hyperspectral $R_{rs}(\lambda)$ imagery to derive IOPs, seafloor type, and water-column depth without the need for *in situ* ancillary data. Liu and Miller (2008) used a C_a -based bio-optical model to parameterize IOPs and included inelastic scattering effects, resulting in a LUT with 22,575 individual spectra. Their LUT-derived IOPs compared well with both *in situ* and model-simulated hyperspectral data.

The LUT methodology offers several useful features. It does not require uniqueness of solution and can return a suite of solutions with which an estimate of uncertainty can be derived for each retrieved parameter. Inelastic processes can be easily incorporated in forward models, such as C_a and CDOM fluorescence if robust quantum efficiencies are well described. LUTs can be easily tuned to a region of interest based on known environmental

conditions, thus reducing the required search space. While it is typical to assume vertical homogeneity within the water column, vertical structure can, in principle, be included. The LUT methodology also includes a number of limitations. The utility of the LUT requires accurate characterization of the IOPs and because limited analytic or empirical models (e.g., C_a -based IOP models) are used, the internal dependences may not reflect natural sources of variability and non-covariability. Generating the LUT with RT code can be computationally expensive, although this is generally an infrequent investment. Searching for solutions can also be computationally expensive. Even with limited sets of IOPs (e.g., ten $a^*(\lambda)$ or $b^*(\lambda)$), the number of spectra in the LUT database will be 100^m , where m is the number of different constituents. This burden can be eased somewhat using suitable LUT search algorithms and with improved computational power. Hedley et al. (2009), for example, dynamically constructed a LUT by adaptively constraining model runs to reduce the LUT size. Each sensor-observed $R_{rs}(\lambda)$ is projected onto principle component space and passed through a binary decision tree until it is optimally matched with similar spectra. Hedley et al. (2009) found this approach to be computationally comparable to spectrum matching approaches (c.f. SAA class (i) methods), such as Levenberg-Marquardt nonlinear optimization.

2.2.3 Empirical approaches—Empirical algorithms derive IOPs from some predictor variable(s), typically sensor-observed $R_{rs}(\lambda)$ or derived parameters (e.g. C_a), using a large data set derived from *in situ* observations or AOP/IOP datasets synthesized using RT modeling. Most approaches follow statistical methods including, but not limited to, univariate polynomial regression (Lee et al., 1998b), multiple linear regression (MLR) (Mannino et al., 2014), principal component regression (PCR) (Craig et al., 2012), and machine learning algorithms (Chang, 2015; Doerffer & Schiller, 2007; Ioannou et al., 2011; Jamet et al., 2012). While these approaches diverge from the RT and QSSA methods and spectral shape parameterizations presented to this point, their inclusion in this review remains relevant as they provide viable methods for deriving IOPs from satellite ocean color radiometry.

Several univariate empirical models relate an IOP to C_a using both linear and non-linear regression methods (Bricaud et al., 1995; Gordon & Morel, 1983; Huot et al., 2008; Loisel & Morel, 1998; Morel, 1988). While these methods are useful for oceanic waters where phytoplankton dominate the in-water optical field, they can be confounded in optically complex waters with elevated CDOM and high inorganic particle loads. Univariate methods also exist that predict IOPs as a function of $R_{rs}(\lambda)$ (Lee et al., 1998b; Stramska et al., 2003; Stramski et al., 1999). The empirical model developed by Lee et al. (1998b), for example, relates the total absorption coefficient at a green or red reference wavelength to a $r_{rs}(\lambda)$ band ratio via polynomial regression. This model initiates the quasi-analytical algorithm (QAA, the SAA class (iii) inversion scheme of Lee et al. (2002)). It is important to recognize that such empirical relationships often form the base of the spectral shape parameterizations presented in Section 2.1.4, such as Eq. (15) and the contents of Tables 1 and 3, and thereby inherently reside within the some of the SAA and LUT inversion methods reviewed above.

MLR models allow IOPs to be derived from sets of multiple predictors, for example, absolute $R_{rs}(\lambda)$ values, $R_{rs}(\lambda)$ differences, and/or $R_{rs}(\lambda)$ ratios. Mannino et al. (2014) and Cao et al. (2018), for example, demonstrated an MLR that effectively derived $a_{cdom}(\lambda)$ and

S_{cdom} from $R_{rs}(\lambda)$. MLRs, however, become unstable when the set of predictor variables exhibits co-linearity (that is, one or more of the predictor variables are highly correlated). To address this, a data reduction method is often employed to decrease the number of variables used in the model. Mannino et al. (2014) used a stepwise backward approach and reduced the number of input $R_{rs}(\lambda)$ from five to two. Other approaches, such as principal component analysis (PCA; an orthogonal linear transform, also known as empirical orthogonal function (EOF) analysis (Preisendorfer & Mobley, 1988), can also be used to reduce dimensionality of the predictor variable set without an appreciable loss of information (Barnes et al., 2014; Craig et al., 2012; Soja-Wo niak et al., 2017).

Using principal component regression (PCR; a combination of PCA and MLR), Craig et al. (2012) developed an algorithm for deriving C_a and $a_{ph}(\lambda)$ from $R_{rs}(\lambda)$ in optically complex waters. The first four PCs were used in an MLR model as they cumulatively explained over 99% of variance in the $R_{rs}(\lambda)$ predictor dataset. Similarly, Fichot et al. (2008) and Cao et al. (2014) used a PCR model to retrieve $K_d(\lambda)$ in the range 320–490 nm from multi-spectral $R_{rs}(\lambda)$ for a variety of water bodies ranging from oligotrophic to turbid estuarine systems. Barnes et al. (2014) used PCR to derive $K_d(\lambda)$ in the UV from satellite-observed $R_{rs}(\lambda)$ in optically shallow reef waters. Thus far, the limitation of PCA-based approaches appears to be reliance on training with region-specific data in order to perform optimally. One might also argue that PCR approaches are not mechanistic. Careful interpretation of the spectral behavior of the principal component (PC) loadings, however, can reveal coherent features that are clearly related to absorption, fluorescence, and scattering processes (Craig et al., 2012; Fichot et al., 2008; Soja-Wo niak et al., 2017). Barnes et al. (2014) noted that PCs that cumulatively explain the bulk of the variance in the predictor dataset do not always serve as the best predictor variables but they can be used to identify important physical or biological driving forces *a posteriori*. They proposed that consideration of all PCs during MLR development and their reduction through suitable variable selection procedures (for example, stepwise forward addition) may be more robust.

Advanced machine learning methods exist to derive IOPs, including artificial neural networks (D'Alimonte et al., 2012; Doerffer & Schiller, 2007; Ioannou et al., 2011; Ioannou et al., 2013; Tanaka et al., 2004) and gene expression programming (Chang, 2015). Artificial neural networks (ANNs) have shown promise for retrieving $K_d(\lambda)$, constituent matter concentrations (C_a and NAP), and $a_{cdom}(\lambda)$ (Chen et al., 2014a; D'Alimonte et al., 2012; Doerffer & Schiller, 2007; Dzwonkowski & Yan, 2005; Schiller & Doerffer, 1999; Tanaka et al., 2004). ANN approaches also exist solely for deriving IOPs (Chen et al., 2014b; Chen et al., 2015; Ioannou et al., 2011; Ioannou et al., 2013). Krasnopolsky and Schiller (2003) recommended training two ANNs that act as forward and inverse models, respectively. By employing the forward and inverse ANNs in concert, an ANN-based algorithm can then dynamically assess its retrieval skill and flag poor quality values (Doerffer & Schiller, 2007). Ioannou et al. (2011) demonstrated an ANN-based approach using independent validation data and benchmarking with the SAAs of Lee et al. (2002) and Maritorea et al. (2002). They also demonstrated ANN handling of noise (10–20%) in the input $R_{rs}(\lambda)$ dataset without compromised performance. Like all empirical approaches, however, machine learning methods require a large $R_{rs}(\lambda)$ /IOP training dataset (order of 1,000 records per Ioannou et al. (2011) and order of 100,000 records per Doerffer and Schiller (2007) that

spans a wide range of optical conditions. Accordingly, ANN approaches are often tuned and applied regionally (D'Alimonte et al., 2012; Doerffer & Schiller, 2007); however, through the appropriate use of RT modeling and/or *in situ* datasets, the development of globally-applicable ANN-based algorithms has been demonstrated (Chen et al., 2014b; Ioannou et al., 2011).

3 Sources and derivation of uncertainties

3.1 IOP measurement uncertainties

In situ and laboratory measurements of IOPs are used to develop and refine algorithms and to assess their performance. For algorithm development, IOP measurement uncertainties, and any associated assumptions required where IOP measurements are lacking, propagate directly into the algorithms. For performance assessment, IOP measurement uncertainties must be considered to isolate satellite instrument performance, along with uncertainties in the radiometric measurements serving as algorithm input. This section briefly summarizes known uncertainties in and limitations of relevant IOP measurements and their potential impacts on remote-sensing algorithms and products. The NASA Ocean Optics Protocol series (<https://oceancolor.gsfc.nasa.gov/docs/technical>) has far greater detail on this subject. In general, availability of more than one technology to measure a parameter (e.g. instrumental closure) may improve estimates of the true uncertainty associated with a parameter of interest.

3.1.1 *In situ* absorption, attenuation, and total scattering measurements—

The community standard approach for measuring *in situ* $a(\lambda)$ and $c(\lambda)$ for the last twenty years has been WET Labs *ac* meters (Twardowski et al., 1999; Zaneveld et al., 1992). These instruments have two flow tubes, typically 0.25 m in length, with the $a(\lambda)$ tube having a reflective quartz sleeve and the $c(\lambda)$ tube having a non-reflective matt black finish. Total scattering is then calculated as $b(\lambda) = c(\lambda) - a(\lambda)$. Measurements made with *ac* meters have associated uncertainties due to their inability to measure exactly these parameters (e.g., finite acceptance angle, inability to collect all the scattered light), the effect of flow in and around each flow tube that possibly disrupts/disaggregates and reorients particles, random electronic noise, and bias errors due to factors such as calibration uncertainty.

All *ac* meters require periodic calibration to some reference medium, typically purified water, to track drift. With careful attention to instrument protocols and repetition in calibrations, uncertainties of 0.005 to 0.01 m^{-1} and 0.01 to 0.015 m^{-1} are achievable for absorption and attenuation, respectively. Note that these values vary spectrally, with the largest uncertainties near 400 nm. Instrument drift remains of particular concern when working in clear waters, where calibrations are carried out daily to ensure data quality. Absorption and attenuation measurements also require correction for the dependence of pure water absorption on T and S in the NIR (Pegau et al., 1997; Sullivan et al., 2006). Because these corrections can be significant, associated uncertainties in $a(\lambda)$ and $c(\lambda)$ are expected to be greater in the NIR relative to the VIS.

An ongoing area of research focuses on quantifying the correction for the reflective flow tube for $a(\lambda)$ that does not direct all scattered light towards a diffuse director, and can be of

order 30–50% of the derived absorption coefficient (Stockley et al. 2017). Zaneveld et al. (1994) suggested several approaches for this scattering correction, all with assumptions and associated uncertainties. Their *baseline* correction, traditionally applied to bench-top spectrophotometers, subtracts the NIR offset, which assumes that scattering does not vary spectrally. Their *proportional* correction incorporates the observed spectral scattering variability and assumes a spectrally constant ratio of the scattering correction to an approximation of total scattering. Both corrections also assume null absorption in the NIR, which does not follow many recent observations in areas where NAP concentrations are significant (Babin & Stramski, 2004; Bowers & Binding, 2006; McKee et al., 2013; Röttgers et al., 2014; Röttgers & Gehnke, 2012; Stramski et al. 2004b; Stramski et al., 2007; Tassan & Ferrari, 1995; Tassan & Ferrari, 2003) leading to approaches that assume some fraction of the NIR signal is due to absorption.

3.1.2 Laboratory absorption measurements—Absorption measurement of discrete samples is performed using bench-top spectrophotometers. These instruments typically lack the sophisticated optics of the *ac* meters (i.e., collimated beams, reflective tubes, detector-side diffusers) and have 10-cm maximal cuvette pathlengths. In dilute ocean waters, this necessitates concentration of particulate matter, while in more complex waters, scattering by suspended particulates leads to substantially overestimated absorption estimates. Since the 1980s, the traditional approach has been to concentrate the particulate matter onto filters and measure directly in the spectrophotometer in transmission mode (Kiefer & SooHoo, 1982). The advantage of filtering samples, aside from concentrating particulate matter, is the separation of the absorbing components. The filtration separates CDOM from the particulate matter. CDOM absorption can be accurately measured in a cuvette due to the negligible scattering. Particulate matter absorption can be measured directly on the filter.

Glass fiber filters are the standard as they have a small nominal pore size (0.7 μm for Whatman GF/F, the recommended brand and model) and a relatively spectrally flat spectrophotometric signature, with relatively low uncertainty (Roesler, 1998; Stramski et al., 2015). The highly scattering glass fibers significantly increase the optical pathlength, increasing substantially the signal to noise. This effect can be corrected using a pathlength amplification factor, β , determined using a variety of empirical approaches based upon paired measurements in suspensions and on filters (Allali et al., 1997; Arbones et al., 1996; Bricaud & Stramski, 1990; Cleveland & Weidemann, 1993; Finkel & Irwin, 2001; Lohrenz, 2000; Mitchell, 1990; Moore et al., 1995; Nelson et al., 1998; Stramska et al., 2003; Tassan & Ferrari, 1995). The lack of consensus in β results from the suspension measurements used to construct the correction being prone themselves to scattering errors similar to those in the *ac* meters, but with less information for correction. Recent progress has been made to better constrain β (Lefering et al., 2016; Röttgers & Gehnke, 2012; Stramski et al., 2015). Stramski et al. (2015), for example, provide a protocol for measuring absorption by placing the filter inside a large diameter commercially available integrating sphere (Labsphere, Inc), which optimizes the collection of scattered light by the glass fiber filter over the traditional transmission mode measurements. The dual beam configuration allows the absorption by the directly transmitted beam to be separated from the absorption by beams scattered by the sphere. At present, β remains quantified for the VIS range only, and preliminary analysis of

the UV region suggests large uncertainties due to the combination of one or more of the following: weak lamp strength, weak detection capabilities, and strong absorption by the integrating sphere itself and the glass fiber filters, as well as possible instability of the particulate absorption signal in the UV over short temporal scales. The analysis in the UV remains an active area of investigation.

The filter pad approach also offers a capability for separating the particulate absorption into contributions by phytoplankton and NAP. Kishino et al. (1985) proposed the method of measuring the particulate sample, then returning the filter pad to the filtration cup and gently adding methanol to extract the pigments from the cell, filtering the methanol through and rinsing gently with filtered seawater to remove the methanol. The remaining material is the nonpigmented particulate matter, NAP, which is then scanned again. After correction for pathlength amplification (which will be different for the particulate and NAP scans), the phytoplankton absorption is calculated by difference. The more accurate description of this component is the absorption by phytoplankton pigments *in vivo* as the NAP does include the non-pigmented phytoplankton cellular material. Samples with phycobilipigments such as phycoerythrin require an additional treatment with hot water or phosphate buffer (Roesler & Perry, 1995) or buffered Milli-Q water (Sobiechowska-Sasim et al., 2014) to extract the water-soluble pigments. Oxidation with bleach is another approach (Doucha & Kubin, 1976; Ferrari & Tassan, 1999; Röttgers & Gehnke, 2012), although rather than removing the pigments from the sample, the oxidized pigment molecules remain on the filter and their absorption shifts to the far blue and UV portion of the spectrum, and thus should be used with caution. Some investigators have also explored the separation of the NAP into organic and inorganic components using combustion or chemical oxidation (Estapa & Mayer, 2010; Werdell & Roesler, 2003). The efficacy remains elusive because the treatment impacts the absorbing material and because the inorganic particles often have an organic coating. When that coating is removed, the underlying mineral absorption properties are revealed but, in this case, the sum of the components is not conserved.

Uncertainties associated with the spectrophotometric approach vary between instruments, but for a quality dual beam benchtop model, absorbance resolution is of order 10^{-4} , which translates into a signal to noise ratio of about 10^3 . To avoid self-shading and multiple scattering, target absorbances should fall between ~ 0.1 and ~ 0.4 (van de Hulst, 1957), which may require the use of multiple cuvette pathlengths or filter volumes over the UV-VIS range. Generally speaking, filters should not be overloaded such that absorbance exceeds 0.4 to avoid artifacts associated with self-shading (and additional enhancement of multiple scattering). In contrast, with regard to spectrophotometric measurements on suspension, absorbances measured in the beam attenuation configuration should remain generally below ~ 0.13 to keep the optical thickness (the product of beam attenuation and pathlength) below 0.3 (i.e., the single scattering regime) (Mitchell et al., 2003). The variability associated with the filter pad measurement includes filter-to-filter variations, pathlength amplification uncertainties, and sample handling uncertainties. Furthermore, the associated uncertainties for replicate samples far exceed the instrument resolution and are typically of order a few percent. It should also be noted that the sample condition can yield higher uncertainties due to uneven distribution of material on the filter. This is often due to gelatinous or

polysaccharides in the sample. In such cases, multiple readings per filter and replicate filters are required to reduce uncertainties.

3.1.3 VSF and backscattering measurements—The coefficients $b(\lambda)$ and $b_b(\lambda)$ can be computed from VSF measurements via straightforward integration, however, only several prototype sensors capable of VSF measurements over broad angular ranges exist (e.g. Chami et al., 2014; Harmel et al., 2016; Lee & Lewis, 2003; Twardowski et al., 2012). The Multi Angle Scattering Optical Tool (MASCOT), calibrated with NIST-traceable micro spherical beads and measuring the VSF in 10° increments from 10° to 170° relative to the incident beam, has demonstrated uncertainties of 2% at each angle and ~1% for integrated $b_b(\lambda)$ (Sullivan et al., 2013; Twardowski et al., 2012). The Multispectral Volume Scattering Meter (MVSM) (Berthon et al., 2007; Lee & Lewis, 2003; Zhang et al., 2012) measures the VSF with an angular resolution of 0.25° from 0.5 to 179° at eight wavelengths. The MVSM and the MASCOT can be used with the Sequoia Scientific LISST-100X that measures the VSF at 532 nm from 0.07° to 13.9° (e.g. Slade & Boss, 2006). The combination of the measurements by these two instrument forms a more complete angular resolution of the VSF at 532 nm and inter-instrument comparisons shows agreement to within 10% in both forward and backward angles (Zhang & Gray, 2015). At the time of this writing, the new Sequoia Scientific LISST-VSF had not been fully characterized.

The WET Labs ECO-BB and HOBI Labs Hydrosat instruments provide commercially available spectral backscattering sensors that make a VSF measurement with broad angular weighting at a single fixed geometry (the ECO-BB has a centroid angle of 124° and the Hydrosat has a centroid angle of 140°). In addition, WET Labs ECO-VSF sensors make a VSF measurement at several fixed geometries (centroid angles at 104°, 131°, and 150°). Estimation of $b_b(\lambda)$ from these instruments requires a conversion coefficient, χ , that is specific to each angular measurement geometry (Sullivan et al., 2013). Historical χ factors have been based on both modeled and/or measured VSF shape analyses that effectively assume a single constant, representative shape for natural waters (Berthon et al., 2007; Boss & Pegau, 2001; Chami et al., 2006; Maffione & Dana, 1997; Oishi, 1990; Sullivan & Twardowski, 2009; Zhang et al., 2014). Typically, derivations of χ adopt a spectrally independent VSF shape in the backward direction. This assumption has been examined both theoretically and experimentally, where in many cases, the shape has been found to be spectrally independent within measurement uncertainties (e.g. Berthon et al., 2007; Boss & Pegau, 2001; Maffione & Dana, 1997; Mobley et al., 2002; Twardowski et al., 2001; Ulloa et al., 1994; Vaillancourt et al., 2004; Whitmire et al., 2007; Whitmire et al., 2010). That said, the conditions for applicability of this assumption remain under active investigation (Chami et al., 2006; Harmel et al., 2016; Jonasz & Fournier, 2007; Sullivan & Twardowski, 2009; Zhang et al., 2014; Zhang et al., 2017). Current estimation of uncertainties associated with applying χ to derive $b_b(\lambda)$ range from 1–2% when the geometry of the VSF measurement is well known and the centroid of the measurement is near 120° (Sullivan et al., 2013). After calibration with NIST-traceable micro-spherical beads and analytical derivation of angular weighting functions, WET Labs ECO sensors show total estimated uncertainties of 5% (Sullivan et al., 2013), whereas HOBI Labs (Bellevue, WA) Hydrosat sensors are calibrated using a Spectralon plaque and with similar estimated uncertainties. Instrumental closure

between a Hydrosat and a Wet Labs ECO-VSF showed differences $< 2\%$ (Boss et al., 2004). A recent comparison of three WET Labs single angle backscattering sensors (ECO-FLBB, ECO-BB and MCOMS) deployed on hundreds of profiling floats, however, found consistent differences of up to 30%, which is inconsistent with the above discussion (Poteau et al., 2017). At the time of this writing, this discrepancy results from the manufacturer applying the wrong calibration constant, with steps underway to provide a remedy (A. Barnard, WET Labs, personal communication).

All scattering sensors suffer from attenuation along the path. A correction is typically warranted when the pathlength between source, sample volume, and receiver exceeds several cm (Sullivan et al., 2013; Twardowski et al., 2012). For WET Labs ECO sensors, this correction is $< 1\%$ when absorption (including water) is $< 0.5 \text{ m}^{-1}$. For the Hydrosat, which has a pathlength of 0.15 m, the correction is $\sim 50\%$ when c is 1 m^{-1} . Doxaran et al. (2016) provides additional analysis of this problem and improved correction methods.

3.1.4 Pure seawater measurements—Backscattering by pure seawater is often considered to be constant and well-known in remote sensing algorithms (IOCCG, 2006) and common practice for several decades has been to use a constant pure seawater backscattering spectra originating from Morel (1974). As described in Section 2.1.4.1, Zhang et al. (2009) provides the most recent theoretical description of pure seawater scattering as a function of the physical properties of water with variables of T , S , and pressure. The physical constants in the calculations are all known with excellent precision ($< 0.1\%$), with the exception of the depolarization ratio. The currently recommended value for this parameter is 0.039 from measurements by Farinato and Rowell (1976). Pure water scattering in the blue decreases by more than 10% when using a value of 0.039 relative to the value of 0.09 used by Morel (1974). The Zhang and Hu (2009) computations of pure water scattering with a value of 0.039 produce volume scattering functions that match experimental measurements by Morel (1968) within 2% (Jonasz & Fournier, 2007). Nonetheless, this important parameter deserves additional experimental evaluation to further reduce uncertainties in pure water scattering values.

To date, Mason et al. (2016) provides the most recent laboratory measurements of pure water absorption in the UV and VIS domain. These values are much lower than previously measured in the UV (Pope & Fry, 1997; Smith & Baker, 1981). Lee et al. (2015) derived higher values for seawater in the UV, which possibly result from contributing UV absorption by dissolved inorganic constituents in seawater. Lee et al. (2015) derived their values via analytical inversion of a remote sensing reflectance inversion model, in lieu of direct experimental measurement. Given the lack of closure amongst the varied methods, additional research is necessary to understand the effects of dissolved inorganic substances in the UV and associated uncertainties.

3.1.5 *In situ* sampling—Assessment of how well *in situ* observations compare with remotely sensed observations must include uncertainties associated with sampling a dynamic environment with multiple scales of variability. Temporally, it is rare for *in situ* observations to be made simultaneously with remote measurements. Following, any temporal offset must at least consider the time scales of environmental change to address how conditions imaged

at time t_a compare with the water mass that was observed at time t_b when $t_a \neq t_b$. In dynamic coastal environments, uncertainties can grow rapidly as $t = t_b - t_a$ increases and will scale with both advective velocities and spatial variability. Likewise, uncertainties are also associated with observations made at dissimilar spatial scales, both horizontally and vertically. Horizontally, discrete water samples and *in situ* optical measurements may represent conditions at a point location representing $O(1 \text{ m}^2)$ (depending how long the water was sampled and advective velocities), whereas sensor-observed $R_{rs}(\lambda)$, even if measured simultaneously, is a vertically integrated value averaged laterally across the ground sampling distance (GSD) of the system (1 km^2 , for example, in the cases of SeaWiFS and PACE). Vertically, discrete samples of IOPs, C_p , or parameters related to phytoplankton community composition collected at only one or few depths in the upper optical depth prohibit reconstruction and true representation of the full optically-weighted signal observed by the satellite (Gordon & Clark, 1980; Smith, 1981; Zaneveld, 1995). Optical depths vary spectrally such that satellite retrieved spectral absorption comes from different optical depths – and, thus, phytoplankton and particle populations – suggesting that satellite algorithm development and data product validation activities benefit from (and are better informed by) continuous depth resolved measurements (Werdell & Bailey, 2005; Werdell et al., 2014).

Temporal scales of variability in the open ocean are dominated by biological dynamics (e.g., phytoplankton production and loss processes), as well as physical dynamics (e.g. mixed-layer dynamics, horizontal stretching, folding, and mixing). During the day, when passive remote sensing is possible, near-surface C_p , $a(\lambda)$, and $b_p(\lambda)$ can change by as much as a factor of two (Siegel et al., 1989; Dickey et al., 1991). Within shallow coastal waters where $R_{rs}(\lambda)$ is often dominated by non-living, organic and inorganic particles, temporal scales of variability in these biological and optical properties are typically minutes to hours as the result of advection by changing tidal currents, suspension of bottom sediments by waves and currents, and land-ocean exchanges of optically-important materials. In the vertical direction, stratification in the concentration and composition of near-surface optical constituents with depth is common within shallow coastal waters in association with current and wave suspension of bottom sediments, thin, sub-surface biological layers, and buoyant plumes. If the gradients are large enough and close enough to the surface, they affect $R_{rs}(\lambda)$ as observed by ocean color sensors (Andre, 2002; Petrenko et al., 1998; Yang et al., 2013).

While it is impossible to remove all sampling uncertainty, uncertainties can be minimized with sampling approaches devised with understanding of the sources and magnitudes of environmental variability. Understanding the statistics of the underlying parameter (e.g. its probability distribution) in space and time can provide guidance as to how uncertainties are reduced when aggregating independent matchups (e.g. can the simple $1/N^{1/2}$ decrease in the standard error of the mean apply, with N being the number of independent match-ups). Knowledge of such variability suggests that minimizing sampling uncertainty requires collection of *in situ* observations as close to the time of the remote observations as possible and at spatial scales that resolve sub-pixel variability and depth scales to resolve the exponentially-weighted IOPs over spectrally varying optical depths. Acknowledging that temporal and spatial variability are correlated through advection, spatial uncertainty associated with sub-pixel variability can be reduced by increasing the number of sub-pixel observations in space or time (Moses et al., 2016; Werdell et al., 2013b).

3.1.6 Closure between measured IOPs and $R_{rs}(\lambda)$ —Understanding the quality of measured IOPs and AOPs is often accomplished through RT-*in situ* closure experiments. These closure experiments are conducted by using *in situ* IOPs as input into a RT model that simulates AOPs. RT-modeled AOPs are then compared to *in situ* AOPs to see how well they agree. The degree of agreement in closure exercises is typically quantified using metrics such as the coefficient of determination, root mean square difference, absolute difference and root mean square relative difference at a few wavelengths (Tonizzo et al., 2017). All components of the closure exercise have uncertainties – the IOPs and AOPs suffer from measurement error (as described above), while the RT model has assumptions, typically regarding IOPs not directly measured (e.g., VSF), horizontal homogeneity, inelastic scattering contributions, sky/sun models, the air-sea interface, and polarization effects (as described in Section 2.1). Despite these caveats, when performing careful measurements and understanding the impacts of various assumptions, it remains possible to obtain closure (often within 20–30%) and use such an exercise to evaluate biases introduced by different measurement methods (Lefering et al., 2016; Mobley et al., 2002; Tonizzo et al., 2017; Tzortziou et al., 2006; Werdell et al., 2014).

3.2 Uncertainties in derived IOPs

Characterization of errors and uncertainties associated with ocean color products allows endusers to determine if the derived product is fit-for-purpose. Uncertainty estimates are key to interpretation of higher level modeling efforts that incorporate ocean color products (e.g., primary production and data assimilation in ecosystem or biogeochemical models) (Gould et al., 2014; Sheng et al., 2014). This requires complete documentation of uncertainties associated with an IOP product and their method of determination on a pixel-by-pixel basis. Satellite-to-*in situ* analyses provide one suitable way to characterize the uncertainty of derived IOP products (Bailey & Werdell, 2006). These matchup analyses, however, provide only a general estimate of IOP algorithm uncertainty, remain limited to coverage by the existing at-sea optics sampling platforms (ships of opportunity, buoys, floats, and gliders), and do not adequately resolve variability in either time or space (Valente et al., 2016; Werdell & Bailey, 2005).

Errors and uncertainties in derived IOP products mainly result from three sources: (i) uncertainties in input $R_{rs}(\lambda)$ data due to sensor noise and atmospheric correction error; (ii) the forward model used, its general formulation and parameterization, and the assumptions and approximations it carries; and, (iii) the inverse solution method used (IOCCG, 2006; Werdell et al., 2013a). In theory, these factors should be collectively considered when deriving error estimates, but it is generally difficult to do so in practice. Several approaches exist for generating uncertainty estimates for various ocean color products, including IOPs (Mélin & Franz, 2014; Salama et al., 2012). Algebraic error propagation analysis provides one way to assess model sensitivity and quantify uncertainties in IOPs (Lee et al., 2010; Neukermans et al., 2014; Neukermans et al., 2009). Lee et al. (2010), for example, estimated how uncertainty in an early stage of the QAA algebraic algorithm propagates to IOP components derived in subsequent steps of the algorithm, thereby assessing how uncertainties in specific model parameters (e.g., S_{bp} and S_{dg}) influence the accuracy of derived absorption components. Conceptually, the propagation of radiometric uncertainty

could be accomplished analytically for ocean color AC as well, however, this requires the difficult characterization of uncertainties in ancillary input data and for all of the major steps of data processing (Mobley et al., 2016).

Spectral matching inversion models often provide uncertainties estimated from gradient-based methods. Non-linear least squares inversions use matrix algebra to combine information about how small changes in the best-fit retrieved IOP parameters affect the forward modeled $R_{rs}(\lambda)$ and ultimately derive the standard error of the retrieved products from the covariance matrix (Bates & Watts, 1988; Press et al., 1992). This gradient-based approach is used in several ocean color SAAs that derive IOPs (Maritorena et al., 2010; Maritorena & Siegel, 2005; Salama et al., 2009; Van Der Woerd & Pasterkamp, 2008; Werdell et al., 2013a). In addition, Salama et al. (2011) developed a gradient-based approach for estimating uncertainties associated with varying the inverse model parameterization without the need for performing an inversion. Some non-linear curve fitting techniques can also account for the uncertainties in the observed reflectance (if known; see Maritorena et al. (2010). It is important to recognize that uncertainty estimates from non-linear least square generally rely on the difference between observed and modeled reflectance and are thus influenced by the forward reflectance model approximations and parameterization. Gradient-based methods do not handle uncertainties due to sensor noise and/or AC error (Salama et al., 2011). It has also been shown that gradient-based uncertainty estimates tend to be proportional to the magnitude of the retrieved variables (Maritorena & Siegel, 2005; Salama et al., 2009).

Ensemble-type methods (e.g., Monte Carlo) provide another technique for estimating IOP uncertainties. In this approach, each AOP input and/or the inverse model parameterization is perturbed m times, with a set of m candidate IOP solutions returned. The IOP solution and its uncertainty are derived from the distribution of candidates. Using this approach, Wang et al. (2005) computed the absolute uncertainty of IOPs apportioned to noise in the input $R_{rs}(\lambda)$ data. Median IOPs and their associated uncertainties were then computed from a subset of the ensemble capable of reproducing the input $R_{rs}(\lambda)$ throughout the spectrum within a defined range. Similarly, Schiller and Doerffer (1999) and Salama (2012) used ensemble-based approaches to quantify IOP uncertainties in ANNs and stochastic inverse IOP models, respectively. While a powerful tool for estimating uncertainties in derived IOPs, ensemble methods are computationally expensive, often requiring thousands of perturbations per pixel, and often do not account for correlative errors between variables. Ensemble-based approaches also make assumptions about noise characteristics of sensor-observed $R_{rs}(\lambda)$ (e.g., ranges, statistical distributions, and spectral correlations) that may not always be appropriate for all conditions at all times.

Other approaches have been developed for estimating uncertainties in $R_{rs}(\lambda)$ and/or C_a that could be extended to IOP retrieval models (Frouin & Pelletier, 2015; Mélin et al., 2010; Mélin et al., 2016; Moore et al., 2009; Moore et al., 2015). The approach of Moore et al. (2009) can be used to assign an uncertainty value to each pixel of a product (e.g., C_a) derived from $R_{rs}(\lambda)$. For each $R_{rs}(\lambda)$ spectra, a fuzzy classification scheme assigns a fractional membership corresponding to each of the predefined optical classes that allows for non-discrete uncertainty estimates when the matchup statistics are applied. This method is

model-independent and can be applied to virtually any ocean color product; however, it is limited by the quantity and representativeness of matchup data available. Frouin and Pelletier (2015) used a Bayesian approach to predict $R_{rs}(\lambda)$ from $L_r(\lambda)$, which can conceptually be extended to IOPs. A Bayesian inverse modeling approach allows the definition of a confidence domain of the predicted quantity and as such, in the particular case of ocean color remote sensing, can provide a measure of its uncertainty at each pixel. Uncertainties associated with C_a or $R_{rs}(\lambda)$ have also been assessed by comparing the coincident daily data records from pairs of sensors (Mélin et al., 2010; Mélin et al., 2016). This co-location approach characterizes uncertainties associated with random effects and can be used either with a particular sensor serving as the reference or by treating each sensor equally. The approach enables IOP uncertainties to be spatially resolved for pairs of sensors, but has not yet been applied to evaluate its ability to assess temporal variations of uncertainties, particularly over short time scales for which only few satellite-to-*in situ* pairs are available.

4 Performance Metrics

Recognizing the current influx of algorithms into the community, the forthcoming need to develop enhanced approaches that exploit new instruments' characteristics, and the varied portabilities of globally parameterized algorithms to specific regions, development and implementation of rigorous metrics to assess algorithm performance is essential. Broadly speaking, the choice of algorithm often depends on: (i) precision and dynamic range requirements that dictate the repeatability and distributions of desired retrievals; (ii) biases, imposed most often by the applicability of algorithm parameterizations and training data sets (and their sizes and broad representativeness) to specific regions of interest; (iii) robustness, defined by spatial and temporal stability, frequency of invalid retrievals and uncertainty requirements; and, (iv) the computational efficiency of an algorithm and computational resources available. Deep discussions related to algorithm selection for particular applications or specific statistical metrics for use in algorithm comparisons exceed the scope of this review (we refer the reader to Brewin et al. (2015b)); however, several features of contemporary inverse IOP models that are typically overlooked or minimized in algorithm evaluation activities merit presentation in the context of this review. They include algorithm internal consistency metrics, internally applied geophysical restraints, and data transformations.

Internal consistency verifications exist to assess the quality of derived IOPs once an algorithm returns a solution. Comparisons of model-derived remote-sensing reflectances, $R_{rs}^{mod}(\lambda)$ – those remote-sensing reflectances calculated using the forward model with the derived IOPs as inputs – with the sensor-observed remote-sensing reflectances, $R_{rs}^{obs}(\lambda)$, provide a similarity metric that is commonly embedded within an algorithm. When the computed distance measure falls below some predefined tolerance, the $R_{rs}^{mod}(\lambda)$ and $R_{rs}^{obs}(\lambda)$ are deemed suitably similar and the algorithm reports the computed IOPs. This process is akin to *in situ* closure experiments, discussed in Section 3.1.6. Boss and Roesler (2006) and Werdell et al. (2013a) assessed algorithm closure in this manner by computing their absolute percent relative difference:

$$\Delta R_{rs}(\lambda) = 100\% \frac{|R_{rs}^{mod}(\lambda) - R_{rs}^{obs}(\lambda)|}{R_{rs}^{obs}(\lambda)} \quad (18)$$

These authors considered internal consistency achieved when the R_{rs} fell below a predefined value over a predefined wavelength range. Boss and Roesler (2006) used 10% for any band within the wavelength range 400–555 nm and Werdell et al. (2013a) used 33% for the average R_{rs} for all wavelengths within 400–670 nm (the current NASA implementation of Werdell et al. (2013a) uses 400–600 nm). These algorithms return a non-solution when the value of R_{rs} exceeds their threshold values. Note that several alternatively suitable distance measures exist, including the Euclidean distance, Chi square distance, root mean square error, and relative root mean squared error (Brando et al., 2012; Brewin et al., 2015b; Hedley et al., 2009). In general, errors result from residual biases, not normally distributed random error, so non-parametric metrics should also be explored. They are also, in general, less sensitive to outliers compared to parametric distance measures and do not assume a probability distribution of R_{rs} . Note also that internal consistency verification does not directly apply to, nor is possible for, all algorithms, such as Lee et al. (2002) and others in the spectral deconvolution class defined in Section 2.2.1.

Standard satellite data processing provides another series of internal verifications through quality flags, such as the *I2_flags* product reported by the NASA SeaWiFS Data Analysis System (SeaDAS; <https://seadas.gsfc.nasa.gov>). During routine processing, a pixel is considered of poor quality if one or more key flags are activated by algorithm failure or the presence of, for example, clouds, ice, land, saturated radiances, or straylight (Robinson et al., 2003).

Even with suitable internal algorithm closure, IOPs with unrealistic or non-physical values may be returned as a solution given that the inversion is mathematically ill-posed. Inspection of derived IOP ranges counters this to ensure they fall within a suitably realistic range that is consistent with known natural variability. Werdell et al. (2013a), for example, applied a series of inequality constraints after the non-water IOP solutions have been derived, specifically:

$$\begin{aligned} -0.05b_{bw}(\lambda) < b_{bp}(\lambda) < 0.05[m^{-1}] \\ -0.05a_w(\lambda) < a_{ph}(\lambda) < 5.0[m^{-1}] \\ -0.05a_w(\lambda) < a_{dg}(\lambda) < 5.0[m^{-1}] \end{aligned} \quad (19)$$

In this case, when one or more of the derived IOPs fall outside the defined range, the algorithm returns a non-solution. We note that the inequality constraints in Eq. (19) allow for slightly negative solutions. This should be allowed given uncertainties in the *in situ* measurements (if it is not allowed, the match-up statistics will be biased high). As an alternative to using inequality constraints to check the validity of derived IOPs, it is possible

to constrain the solution method such that the solution space search is limited to a predefined range (Garcia et al., 2014; McKinna et al., 2015). Constrained solution methods, however, can potentially interfere with the mathematical mechanism for searching multi-parameter solution space and can result in IOP solutions that sit on the edge of the solution space (Garcia et al., 2014; Huang et al., 2013).

Characterization of bias and uncertainties for ocean constituents occasionally benefit from data transformations. Satellite C_p for example, are nearly log-normally distributed in space (Campbell, 1995), as confirmed when viewing frequency distributions of untransformed and logtransformed SeaWiFS chlorophyll data for May 1998 (Fig. 2). As normally distributed data are required for parametric statistical tests to retain their meaning, interpretations of statistical results can be misleading if non-normally distributed data are used for characterization. In application of log-transformed SeaWiFS chlorophyll comparisons, Gregg and Casey (2004) derived an RMS log error of 31.0%. In this case, 76% of the comparisons fell below this error level, which is reasonably close to the definition of the RMS. When using untransformed data, the RMS contained 95% of the data, which deviates significantly from the expected 67%, strongly suggesting erroneous application of the RMS due to a non-normal data set (Fig. 2). The extent to which other optical constituents or IOPs possess spatial or temporal deviations that differ significantly from normal (Gaussian) distributions remains understudied and non-parametric descriptors of uncertainty and bias should be explored. Frequency diagrams demonstrate the nature of the distributions and may guide the choice of statistical applications and transforms. Means and medians should also be computed – medians are less sensitive to data distribution, such that it is likely that the data are not normally distributed when the median differs substantially from the mean. Comparison between frequency distributions of derived products and those measured *in situ* (e.g., in databases) are critical to assess the applicability of the specific dataset to derive inversion algorithms on global scales, as a non-representative dataset is likely to bias the global algorithm (Werdell et al., 2009; Werdell et al., 2013a). Care should be applied to subsample the dataset to be spatially (and if possible temporally) representative of the variability of the full domain of interest.

5 Looking forward

In the following sections, we briefly overview new and upcoming missions, knowledge gaps in IOP bio-optical models and measurements, and the future of inverse methods, uncertainty considerations, and methods for algorithm assessment. A number of recent and soon-to-launch ocean color missions will carry novel sensor payloads with unprecedented observing capabilities (Table 5). It is useful to briefly contextualize these missions to consider existing knowledge gaps in IOP retrieval methodologies and recommend paths forward. Furthermore, building upon Section 2.2 where heritage algorithmic approaches were reviewed, it is important to identify knowledge and measurement gaps that require attention to further improve upon inverse IOP modeling efforts in the PACE era. In particular, we discuss gaps in absorption and backscattering coefficients, additional data needed to improve algorithms, non-conventional approaches, and future machine learning approaches.

5.1 Future sensing technologies

Future technologies suitable for IOP remote sensing can roughly be split into three categories: (i) high spatial O(10 m) pixel sensor instruments in low Earth orbits (LEO), (ii) sensors in geostationary Earth orbits (GEO) with moderate resolution O(1 km) pixels, and (iii) moderate spatial O(1 km) pixel resolution LEO sensors. These three categories clearly demonstrate the tradeoffs required for remote sensing – there is only so much radiant energy emanating from the ocean and each sensor optimizes on spatial resolution at the expense of spectral and/or temporal resolution and vice versa. A summary of recently launched and soon-to-be launched sensors applicable to retrieving IOPs is given in Table 5.

High spatial resolution sensors have recently provided remarkable insights into sub-mesoscale processes in coastal regions (Franz et al., 2015; Vanhellemont & Ruddick, 2014). However, as current instruments with high spatial resolution (OLI and MSI) were primarily designed for terrestrial observations, they have limited and relatively wide bands sets (typically four VIS bands) and signal-to-noise characteristic not ideal for remote sensing dark ocean targets. Nonetheless, much work is underway to improve the radiometric quality of high spatial resolution data and AC correction, to support heritage IOP methodologies (Franz et al., 2015; Pahlevan et al., 2014; Pahlevan et al., 2017; Vanhellemont & Ruddick, 2015; Vanhellemont & Ruddick, 2016). A present limitation of high spatial resolution sensors is their swath width, which is typically O(100 km), their repeat time O(10 days), and the fact they are typically not tasked to image the open ocean away from coastlines. Collectively, this means that existing high resolution sensors in LEO are not conducive to providing near-daily basin-scale measurements of oceanic IOPs.

The capabilities of GEO satellites have recently been demonstrated using meteorological satellites (Murakami, 2016; Neukermans et al., 2009; Neukermans et al., 2012) and with the Geostationary Ocean Color Imager (GOCI) (Choi et al., 2012). GEO sensors offer the ability to observe diurnal marine processes by capturing multiple images of a region throughout the day. With better temporal resolution compared to LEO, GEO sensors can resolve dynamic marine processes such as suspended sediment plumes (Choi et al., 2013) and diurnal variability in phytoplankton blooms (Lou & Hu, 2014). In addition, multiple GEO images can provide more spatially complete daily snapshots of a region when averaged together. However, like high resolution LEO sensors, GEO sensors do not provide near-daily global coverage and are multispectral with band sets similar to heritage ocean color missions such as SeaWiFS. We note, however, potential synergies between high radiometric quality LEO sensor data and high temporal frequency GEO sensor data have recently been considered, specifically approaches for combining the two data types for the purpose of producing improved temporally-rich ocean color data suitable for observing coastal waters (Peschoud et al., 2017; Vanhellemont et al., 2014).

Moderate spatial resolution sensors have been, and continue to be, used for deriving near-daily global IOP data products. They are well-calibrated sensors with dynamic ranges and signal-to-noise characteristics necessary for observing ocean properties (Hu et al., 2012). These polar orbiting LEO sensors completely image the Earth's surface in O(1 day) and are the critical for climate-quality synoptic-scale observations of marine biogeochemical processes. Most inverse IOP methods detailed in Section 2.2 were developed for application

to moderate spatial resolution LEO sensors with measured success. We note that the number of spectral bands observed by existing (MODIS, OLCI, VIIRS) and most future (SGLI, OCM-3) moderate spatial resolution LEO sensors are only slightly better than historical instruments (e.g. SeaWiFS, MERIS, OCM-1, OCM-2) with the exception of the primary PACE instrument, which will be a hyperspectral sensor. We discuss the capabilities of the PACE mission in the following section.

5.1.1 The PACE Mission—The PACE mission spacecraft will carry its primary instrument, the Ocean Color Imager (OCI), in a polar LEO providing global coverage every two days. The OCI spectroradiometer will have higher spectral resolution (~5 nm contiguous bands) than historical and contemporary satellite sensors (see Table 5), ranging from the UV (~350 nm) to NIR (~900 nm), and will potentially be flown with a multi-angle polarimeter as a second instrument in its payload. Accordingly, it is prudent to pursue inverse IOP methods that take maximal advantage of these new features.

The PACE spectroradiometer has the potential to discriminate optical constituent matter in ways previously impracticable with multispectral data. High-resolution spectral capabilities can better inform SAA approaches such as those presented above (Vandermeulen et al., 2017; Wolanin et al., 2016) and also allow common spectroscopy approaches, such as derivative analysis, to be utilized (Bracher et al., 2009). It is also expected that $R_{rs}(UV)$ measurements will enable improved separation of $a_{cdom}(\lambda)$ and $a_{nap}(\lambda)$, as S_{cdom} exceeds S_{nap} and hence typically $a_{cdom}(\lambda) > a_{nap}(\lambda)$ in the UV. The PACE spectrometer also has the potential to improve estimates of phytoplankton community composition through its continuous measurements of spectral features aligned with accessory pigment absorption (Bracher et al., 2017; Torrecilla et al., 2011; Vandermeulen et al., 2017). For example, existing ocean color sensors lack appropriately placed yellow/orange spectral bands (560–650 nm) needed to detect phycobilipigments, such as phycocyanin, indicative of cyanobacteria (McKinna, 2015).

Finally, measurements of polarized $R_{rs}(\lambda)$ (or reflectance) show sensitivity to microphysical properties of hydrosols (marine particles), such as their composition (e.g., refractive index), size, and shape (Chowdhary et al., 2012; Kattawar, 2013; Lotsberg & Stamnes, 2010). Loisel et al. (2008), for example, demonstrated the use of polarized radiometry to distinguish organic and inorganic particles near the mouth of the Amazon River. Accordingly, it is anticipated that polarimetric remote sensing will provide additional information for inverse IOP methods (Harmel, 2016; Ibrahim et al., 2016) that can, in principle, lead to improved methods for determining pigment concentrations, particles sizes, and phytoplankton taxonomy.

5.2 IOP theoretical models and measurements

5.2.1 Knowledge gaps in absorption—Particulate absorption measurements from UV to NIR may still have significant biases that need to be addressed. *In situ* measurements, currently made largely using WET Labs *ac* meters, still suffer from large uncertainties due to the necessity to scatter correct the measurements as discussed in section 3.1.1. This issue appears most acute in coastal environments where particulate absorption cannot be assumed

to be vanishingly small at NIR wavelengths, an assumption that may be reasonable in clear open ocean conditions. Improved scattering corrections have been proposed, but they require companion measurements collected using a VSF sensor to independently calculate the scattering error to derive uncertainties (McKee et al., 2013; Tonizzo et al., 2017; Stockley et al. 2017). We note, however, that these corrections have not been widely adopted as they do not seem to merge with offshore solutions. Integrating cavity absorption sensors have recently been commercialized (e.g., the Turner Design Integrating Cavity Absorption Meter (ICAM) and the Trios Online hyperSpectral integrating Cavity Absorption meter (OSCAR), which theoretically collect all, or nearly all, scattered light, and can potentially derive absorption with reduced uncertainties. These sensors, however, are only now being fully characterized, including considerations for inelastic scattering.

For pure seawater absorption, there is a clear need for research to better understand the role of absorption by dissolved inorganics in the UV such as oxygen, NO_3 , Br^- , and other salt ions comprising sea salts that have significant absorption in the UV (Armstrong & Boalch, 1961; Copin-Montegut et al., 1971; Johnson & Coletti, 2002; Lenoble, 1956; Ogura & Hanya, 1966; Shifrin, 1988). These effects have received scarce attention in recent literature. At 230 nm, these constituents all maintain more than an order of magnitude higher absorption than the values of pure water absorption, with steeply increasing absorption at shorter UV wavelengths. How substantially these constituents absorb at wavelengths longer than 300 nm remains unresolved, as the tail absorption effects have typically not been studied with high accuracy. Even relatively small contributions could be significant since pure water absorption is very low, particularly in the 320 to 420 nm range ($< 0.01 \text{ m}^{-1}$). Armstrong and Boalch (1961) found significant effects of sea salt absorption out to 400 nm, but rigorous purification steps were not taken, so it is unclear if their additions of artificial sea salts introduced organic contaminants.

For inverse IOP methods, such as SAAs, there is no generalized bio-optical model that can parameterize the spectral shape $a^*_{ph}(\lambda)$ in the UV. Additional characterization of UV phytoplankton absorption, including contributions of absorbing compounds such as mycosporine-like amino acids (MAAs) is essential to resolve this gap. Given that phytoplankton community structure varies with environmental conditions, however, additional review of how measurements of T , S , nutrients, and light can better inform or constrain $a^*_{ph}(\lambda)$ within the context of remote sensing will also improve the skill of IOP inversions. We note, however, that while laboratory absorption techniques in the VIS have become significantly more robust (Stramski et al., 2015), accurate quantification of UV absorption with a filter-pad method remains a challenge, particularly because the absorption signal in this spectral region may exhibit significant drift on relatively short time scales comparable with the duration of spectral scan. Additionally, commercially-available *in situ* UV absorption meters do not currently exist.

5.2.2 Knowledge gaps in backscattering—Successfully partitioning of $b_{bp}(\lambda)$ into multiple components is currently limited by insufficient knowledge about natural variability in particle backscattering properties in the ocean. Whereas technological and methodological capabilities to derive total $b_{bp}(\lambda)$ *in situ* exist, and there are inversion approaches to derive particulate scattering components from VSF measurements (Twardowski et al., 2012; Zhang

et al., 2012; Zhang et al., 2014; Zhang et al., 2011), there is a lack of routine experimental methodologies for directly determining particle type-specific backscattering data for multiple particulate backscattering components (e.g., $b_{ph}(\lambda)$ and $b_{nap}(\lambda)$). A continued need for further advancements in understanding of particulate backscattering, such as the roles of different particle types, remains an important challenge (Stramski et al., 2004a). Furthermore, in support of upcoming missions with expanded spectral ranges, investing in the development of hyperspectral backscattering instruments that span UV-NIR should be pursued. Current commercially-available sensors (WET Labs ECO-BB and HOBI Labs HydroScat) measure $b_{bp}(\lambda)$ at a finite number of wavelengths (3–9 channels). Additional gaps are associated with how the spectral shape of the particulate backscattering coefficient is parameterized. For example, the appropriateness of its assignment as a power-law (Eq. 16) and under what circumstances the particulate backscattering ratio can be assumed to be spectrally constant (Eq. 17) (Gordon et al., 2009).

As reviewed in Sections 2.1.4.1 and 3.1.4, Zhang and Hu (2009) and Zhang et al. (2009) describe the physical relationships to derive the currently recommended values for $b_{bw}(\lambda)$. The largest remaining uncertainty is the depolarization ratio. As mentioned, we recommend a δ value 0.039 at this time, however uncertainty in this parameter is at least 50% based on the range in values measured by Farinato and Rowell (1976), the only set of experimental measurements we are aware of in the last 50 years. Additional research is required to improve the accuracy of δ , and to ascertain any associated dependencies (e.g., spectral, T , S).

5.3 Inverse models

5.3.1 Inverting AOPs to IOPs with additional optical information—In addition to the widely applied QSSA of Gordon et al. (1988), other approximations with potential value for IOP inverse models exist that have not widely been adopted in standard ocean color data processing schemes (Appendix A). Zaneveld (1982; 1989; 1995), for example, derived an analytical expression for $r_{rs}(\lambda)$ that explicitly includes treatment of the VSF (in lieu of relying on average parameterizations such as the $G_f(\lambda)$ in Eq. 4) (Appendix B). From a remote-sensing perspective, such an expression enables application of algorithms that explicitly contain the shape of the VSF. By doing so, it also merges two separate, disconnected steps in current QSSA algorithm work: (i) the BRDF correction of input $R_{rs}(\lambda)$ based on tables from Morel et al. (2002) (see Section 2.1.2), and (ii) the subsequent inverse model. Combining these steps in a single, rigorous relationship allows explicit assessment of errors in component variables. In the current two-step approach, errors associated with, for example, the VSF are dispersed in several poorly defined parameters that are empirically tuned. Furthermore, approximations that retain as much of the functional form of the RT equation as possible presumably remain inherently more stable. Zaneveld (1989) provided an inversion approach for his analytical expression that would benefit from renewed assessment by the community.

Only a subset of contemporary inversion methods explicitly includes inelastic processes, such as Raman scattering or fluorescence (e.g. Lee et al., 1994; Loisel & Stramski, 2000; Sathyendranath et al., 2001), although generalized methods for their inclusion now exist

(Lee et al., 2013; McKinna et al., 2016; Westberry et al., 2013). To date, no treatment of Raman scattering accounts for T and S effects, although implementing T and S corrections within an inversion algorithm has been demonstrated (Werdell et al., 2013b). Walrafen (1967), Walrafen et al. (1986) and Becucci et al. (1999) all provide information on the temperature dependence of Raman scattering. Becucci et al. (1999) provides information on the salinity dependence of Raman scattering (through the use of synthetic seawater). On average, the observed effects were on the order of 20% from 10 to 30°C and 10% from 0 to 26 ppt. In contrast, Bartlett et al. (1998) found no evidence for a salinity effect on Raman in seawater samples, which suggests that further review is necessary. Broadly speaking, neither C_a or CDOM fluorescence are considered in IOP inversions (for an exception, see Lee et al. 1994). Given observed variability in C_a and CDOM fluorescence (Del Castillo et al., 2001; Falkowski & Kolber, 1995; Green & Blough, 1994; Hoge et al., 1993), further study is needed to assess how to best parameterize these inelastic scattering processes within inverse IOP methods.

5.3.2 Optically shallow waters—Interest has steadily increased in utilizing ocean color data to monitor ecosystem health in optically shallow shelf waters (Devlin et al., 2015; Hedley et al., 2016). However, most inverse IOP methods used to process global datasets were designed for optically deep oceanic waters with some exceptions (Lee et al., 2001; Lee et al., 1999). These algorithms are easily confounded by light reflected off the seafloor in clear, shallow waters resulting in biased IOP retrievals (Barnes et al., 2013; McKinna et al., 2015). A number of SAAs have been developed for remote sensing shallow waters using either multi- or hyperspectral airborne spectroradiometric data (Dekker et al., 2011), however, historical approaches have focused more on bathymetry and seafloor mapping rather than deriving water-column properties (Brando et al., 2009; Werdell & Roesler, 2003). Dedicated optically shallow ocean color algorithms have started to become available for deriving IOPs (Barnes et al., 2017; Barnes et al., 2013; McKinna et al., 2015). It is challenging, however, to incorporate these approaches into global data processing, as optically shallow waters make up only a small fraction of overall pixels and no robust mechanism currently exists to adequately flag their location during routine processing. In the approach of McKinna et al. (2015), for example, ancillary bathymetry and benthic albedo datasets are needed to help to constrain the dimensionality of the solution space to three unknowns (A_{pb} , A_{dg} , B_p). The need for large region-specific ancillary benthic albedo and bathymetry datasets can be alleviated, however, through the recently-developed algorithm of (Barnes et al., 2017); an approach that would be well-suited to spectrally-rich ocean color data collected by missions such as PACE.

As described in Section 3.1.4, coastal waters are often optically heterogeneous, making validation of algorithms difficult. This is compounded in optically shallow regions where withinpixel seafloor and bathymetric variability and stray light from adjacent features (e.g. sand cays and breaking waves) further complicate algorithm validation efforts. Not only are appropriate sampling protocols and methodologies required, but also a publicly accessible archive of *in situ* AOP/IOP data for algorithm development and validation. To that end, it is likely that the recently initiated NASA-funded COral Reef Airborne Laboratory (CORAL;

<https://coral.jpl.nasa.gov/>) project will contribute greatly to the afore-mentioned knowledge gaps.

5.3.3 Non-conventional approaches for estimating IOPs from ocean color—

Methods that relate $L_A(\lambda)$ to IOPs have recently emerged and will benefit from further review and development (path 1→4 in Fig. 1). These approaches circumvent the need for AC (path 1→2 in Fig. 1) that can sometimes be confounded by absorbing aerosols and optically complex water masses. Two broad classes of approaches exist, specifically empirical models and coupled atmosphere-ocean algorithms models. Common empirical methods for deriving IOPs from $R_{rs}(\lambda)$ were described in Section 2.2.3. Coupled atmosphere-ocean approaches operate similarly to the methods described in Sections 2.2.1 and 2.2.2, but solve for both atmospheric and marine variables simultaneously (e.g. Chomko & Gordon, 1998; Chomko et al., 2003; Gordon et al., 1997; Kuchinke et al., 2009a; Kuchinke et al., 2009b; Li et al., 2008; Spurr et al., 2007; Stamnes et al., 2003; Steinmetz et al., 2011). In general, this approach involves the combination of a model that accounts for aerosol properties and a model to express hydrosol (i.e. water components) via IOPs and/or other constituents, such as C_a . The number of unknown variables in coupled models exceeds typical SAAs due to the combination of aerosol and marine expressions and, as such, coupled models generally require more spectral observations (bands) than traditional SAAs. When applied to data from current ocean color instruments, coupled models use $L_A(\lambda)$ from both the VIS and NIR bands. The retrieval of the aerosol and hydrosol variables then reduces to a classic inverse problem where modeled $L_A(\lambda)$ is fitted to match sensor-observed $L_A(\lambda)$. Both non-linear and linearization techniques have been developed to solve for the aerosol and marine parameters.

The main benefits of a coupled atmosphere-ocean approach lie in its potential to better identify and account for absorbing aerosols and non-negligible NIR radiances, both of which require special consideration in the classic decoupled AC scheme. Nonetheless, the ability of a coupled model to perform well under a wide variety of atmospheric and oceanic conditions remains dependent upon the general formulation of the aerosol and marine components, which unavoidably include inherent limitations and uncertainties. Furthermore, coupled oceanatmosphere approaches are historically computationally demanding and often require retrievals to be constrained to avoid unrealistic or unambiguous solutions.

5.3.4 Improved computational capabilities and statistical methods—

Computational processing capabilities have historically driven the design and implementation of remote sensing algorithms. Most LUT, ANN, and coupled ocean-atmosphere approaches require additional computation capabilities relative to SAAs and, as such, have received less attention in operational ocean color processing environments with near-real-time data delivery requirements. We expect these limitations to be progressively alleviated as computing power continues to grow and new hardware accelerator technologies such as graphic processing units (GPUs) are utilized. Furthermore, with the spectrally rich data expected from PACE, we anticipate the ocean color community will benefit from pursuing integration into the realm of computer (data) science, following the path of the terrestrial remote sensing (Verrelst et al., 2015) and medical imaging (Jiang et al., 2010) communities.

Statistical methods with large(r) computational requirements, such as random forests and support vector machines, have only recently been explored for IOP inverse modeling, several of which have been shown to be effective for deriving constituent matter concentrations (Camps-Valls et al., 2006; Chang, 2015; Kim et al., 2014). Clustering methods are used to partition marine waters into distinct optical types (Mélin & Vantrepotte, 2015; Moore et al., 2009; Neukermans et al., 2016). Those that provide weighted water types per satellite pixel allow blending of multiple algorithms that have been tuned to specific water types (Moore et al., 2001; Moore et al., 2014; Wo niak et al., 2010). Statistical methods have also been shown to be highly effective in reducing solution spaces or finding a solution neighborhood, thereby speeding up the search for an optimal solution (De Noia et al., 2015; Hedley et al., 2009). In addition, as the capabilities of modern computers continue to expand alongside improvements in RT code and innovative machine learning tools, such as TensorFlow (Abadi et al., 2016), the burden of simulating large synthesized datasets to enable development of advanced empirical algorithms will also diminish.

5.4 Uncertainties

While the term *uncertainty* is used in virtually all of the studies mentioned in Section 3.2, the actual values presented often represent different mathematical constructs that are not always comparable. This may be due to the lack of consensus on the type and characteristics of the uncertainties required by space agencies or by the user-community. For space agencies, uncertainty metrics are useful for quality assurance and product assessment, while for ocean modelers, uncertainties are useful during data assimilation and when performing modelobservation comparisons. Additional work is necessary to define uncertainties and recommend their computation. The IOCCG Working Group on Uncertainties in Ocean Color Remote Sensing (<http://ioccg.org/group/uncertainties/>) provides additional guidance on the subject.

Furthermore, it remains critical for measurement technology to continue to improve (thereby reducing measurement uncertainties) to ensure our ability to perform closure and validate remotely sensed products. Looking towards PACE, for example, hyperspectral measurements that extend into the UV will be critical. Specific technology gaps exist in: (i) *in situ* spectral $b_{\beta}(\lambda)$ and VSF measurements – commercial or prototypical hyperspectral backscattering sensors do not yet exist; (ii) *in situ* absorption measurements with significantly reduced uncertainties associated with scattering correction and extension to the UV – emerging commercial instrumentation do not require such a correction but, these instruments are only recently being validated; and, (iii) polarized IOPs that report the 12 and 22 elements of the Mueller Matrix (at least) to better model the polarized underwater light field –instrumentation that provides more accurate estimates of polarized IOPs will reduce uncertainties in AOP-IOP closure. In addition, methods for closing the scale gap between *in situ* and satellite measurements when matched up (see Section 3.1.5) must be explored. This might be accomplished through increased spatial resolution of satellites, particularly in coastal areas (Moses et al., 2016), as well as through the use of moving *in situ* platforms (e.g., gliders and flow-through systems) that travel significant distances in a relatively short time periods to provide information on and quantify satellite subpixel variability (e.g., Werdell et al., 2013c).

5.5 Performance metrics

Varied validation methods exist to evaluate derived IOPs using independent measurements designated to be truth. Generally speaking, the most common encompass comparisons of IOPs derived from synthesized $R_{rs}(\lambda)$ with synthesized IOPs (IOCCG, 2006; Werdell et al., 2014) and IOPs derived from *in situ* or satellite-observed $R_{rs}(\lambda)$ with coincident *in situ* IOPs (Brewin et al., 2015b; IOCCG, 2006; Werdell et al., 2013a). Other emerging approaches include, but are not limited to, simulating $R_{rs}(\lambda)$ from the derived IOPs using the forward model or an alternative RT model for comparison with independent *in situ* measurements of $R_{rs}(\lambda)$ (Tonizzo et al., 2017) and time-series and population statistical analyses when sufficient volumes of *in situ* data exist (Kostadinov et al., 2007; Werdell et al., 2009). With the exception of the latter, most validation methods ultimately rely on interpretation of regression results and one-to-one scatter plots to quantitatively assess algorithm performance.

Broadly speaking, the community has not achieved absolute consensus on the best statistical metrics for assessing algorithm performance and, as previously stated, we do not make recommendations here, other than to request further study. While r^2 values, regression slopes and intercepts, biases, absolute and relative percent differences, RMS, and biased and unbiased root mean square errors have evolved as the most popular to determine how closely derived IOPs represent the truth measurements, many of these metrics overlap in their meaning and interpretation and other metrics exist (Brewin et al., 2015b; Willmott et al., 2017). Multi-dimensional tools have also shown promise and merit increased consideration, including Taylor and Target plots (Jolliff et al., 2009; Taylor, 2001), as do population statistics such as temporal and spatial frequency distributions, cumulative distribution functions, and long-term time series when sufficient truth data can be accumulated. Since different IOPs are related in nature in ways that may not be parametrized in a specific inversion schemes, these relationships can also be used to test the skill of an inversion (e.g., verifying that distributions of retrieved $a_{nap}(\lambda) / a_{ph}(\lambda)$ achieve consistency with *in situ* observations).

For satellite applications, we also encourage the consideration of temporal and spatial variability and stability (e.g., rates of failures and appearances of outliers and anomalies). Other topics for future consideration include evaluation of regional versus global performance, additional comparisons of multiple satellite instruments with varied spectral bands that may impart inherent differences in IOP retrievals, and, in the coming hyperspectral era of NASA's PACE mission, development of decision support metrics to drive execution of validation activities on all available wavelengths versus a subset of identified key wavelengths.

6 Summary and recommendations

We have presented the current state of the art in approaches to obtain IOPs from ocean color remote sensing, as well as outlined the areas where uncertainties and knowledge gaps remain. As an increasing number of space-based instruments measure ocean color simultaneously, uncertainties in $L(\lambda)$ and $R_{rs}(\lambda)$ are expected to become better constrained through sensor intercomparisons and growth of the invested community. As computing

power continues to increase, computationally expensive methods such as ANN and LUTs are likely to be used routinely and comparisons between IOPs generated from all the methods outlined above will increase, resulting in more robust ensemble results, such as those derived from ensembles of weather prediction models. Significantly more *in situ* data needs to be collected using community adopted measurement protocols to assess the performance and utility of the different methods across space and time, and sub-pixel variability and uncertainties in the *in situ* measurements need to be better characterized. These measurements will become the basis for international databases for novel algorithm refinement and developments. Below we provide a set of recommendations that could help improve IOP inversion algorithm further.

Data and measurements

We recommend:

- Development of new, commercially available instrumentation for measuring $a(\lambda)$, $c(\lambda)$, $b(\lambda)$, $b_b(\lambda)$ and the VSF(λ) from UV to NIR at high spectral resolution (~ 5 nm);
- Development of instrumentation and methods to measure the polarized scattering elements of the Mueller matrix and radiance fields *in situ*;
- Additional research into UV absorption of dissolved inorganic constituents of seawater;
- Additional research into the depolarization ratio for pure water scattering;
- Assembly of additional publicly-available *in situ* and simulated hyperspectral datasets for algorithm development and testing, with attention to the temporal, spatial, and biogeochemical representativeness of these datasets; and,
- Continued collection, assembly, and public dissemination of key biogeochemical variables that can be directly inferred from IOPs including, but not limited to: particle size distributions, phytoplankton pigment concentrations, phytoplankton classes and metrics of community composition, and particulate and dissolved organic carbon.

Algorithm and radiative transfer codes

We recommend:

- Sharing of algorithm code (e.g., open-source distribution) to encourage maximization of knowledge transfer and testing/vetting of novel approaches;
- Development and distribution of vector RT codes for application in aquatic environments to study the effects of polarization on $R_{rs}(\lambda)$;
- Evaluation of the use of additional environmental information (e.g., T , S , and distance from shore) to help inform and constrain IOP inversion algorithms; and,
- Assessment of the increase in information that multi-angle polarimetry introduces to inform and better constrain IOP inversions and prepare for future

missions (e.g., PACE) where polarimeter and radiometer may observe the Earth simultaneously.

System uncertainty

We recommend:

- Increased assessment and quantification of uncertainty budgets, including those associated with the satellite instrument, sub-pixel variability, atmospheric correction algorithms, bidirectional reflectance characterizations and simplified AOP-IOP relationships, in-water algorithms, and *in situ* and laboratory measurements, so that efforts can target reduction of the largest sources of uncertainty.

Acknowledgements

The NASA Ocean Biology and Biogeochemistry Program supported all authors through membership on the NASA PACE Science Team. We thank Paula Bontempi, Jacek Chowdhary, Betsy Edwards, Georges Fournier, Bryan Franz, Mati Kahru, Timothy Moore, Michael Ondrusek, and Lorraine Remer for their comments, advice, and participation in science team meetings and workshops related to this review paper. We also thank Brian Barnes and one anonymous reviewer for their valuable comments and feedback regarding this work.

Appendix A

In addition to the widely applied radiative transfer approximation of Gordon et al. (1988), other numerical approximations exist to relate $R_{rs}(\lambda)$ or $r_{rs}(\lambda)$ to IOPs. This appendix serves to provide a brief summary of several common alternatives, all of which can be used in place of Eq. (4).

Jerome et al. (1996) suggests that nadir-viewing $r_{rs}(\lambda)$ can be expressed as:

$$r_{rs}(\lambda) = -0.00042 + 0.112 \frac{b_b(\lambda)}{a(\lambda)} - 0.0455 \left(\frac{b_b(\lambda)}{a(\lambda)} \right)^2$$

Morel and Gentili (1993) expresses $r_{rs}(\lambda)$ as:

$$r_{rs}(\lambda) = \frac{f(\lambda) b_b(\lambda)}{Q(\lambda) a(\lambda)}$$

where $f(\lambda)$ represents the combined influence of illumination conditions and geometry and sea surface properties and $Q(\lambda)$ defines the ratio of upwelling irradiance to upwelling radiance. Morel et al. (2002) provides a LUT for $f(\lambda) / Q(\lambda)$ for various sensor-viewing and solar zenith angles, tabulated at seven wavelengths [412.5, 442.5, 490, 510, 560, 620, and 660 nm] and for six C_a [0.03, 0.1, 0.3, 1, 3, and 10 mg m⁻³].

Albert and Mobley (2003) generated the following expression for $r_{rs}(\lambda)$ using Hydrolight:

$$r_{rs}(\lambda) = p_1 u(\lambda) \left(1 + p_2 u(\lambda) + p_3 u(\lambda)^2 + p_4 u(\lambda)^3 \right) \left(1 + p_5 \frac{1}{\cos(\theta_s)} \right) \left(1 + p_6 W \right) \left(1 + p_7 \frac{1}{\cos(\theta_v)} \right)$$

where $p_{1...7} = [0.0512, 4.6659, -7.8387, 5.4571, 0.1098, -0.0044, 0.4021]$, W is wind speed, θ_s is solar zenith angle, and θ_v is the sensor-viewing angle.

Lee et al. (2004) explicitly account for the phase function effect of molecular and particulate scattering (Morel & Loisel, 1998) and express $r_{rs}(\lambda)$ as:

$$r_{rs}(\lambda) = g_w \frac{b_{bw}(\lambda)}{a(\lambda) + b_b(\lambda)} + g_p(\lambda) \frac{b_{bp}(\lambda)}{a(\lambda) + b_b(\lambda)}$$

Using Hydrolight, they defined g_w as 0.113 and $g_p(\lambda)$ as:

$$g_p(\lambda) = 0.197 \left[1 - 0.636 \exp \left(-2.552 \frac{b_{bp}(\lambda)}{a(\lambda) + b_b(\lambda)} \right) \right]$$

Park and Ruddick (2005) parameterized $R_{rs}(\lambda)$ as follows using Hydrolight:

$$R_{rs}(\lambda) = \sum_{i=1}^4 G_i u(\lambda)^i$$

with G_i tabulated in a LUT for various θ_s , θ_v , relative azimuth angles, and ratios of $b_{bp}(\lambda) / b_b(\lambda)$.

Appendix B

In addition to the widely applied radiative transfer approximation of Gordon et al. (1988) (Eq. 4), there are other approximations that may additionally have value in AOP-IOP inversions. In particular, Zaneveld (1982; 1989; 1995) derived analytically from the radiative transfer equation an expression of remote sensing reflectance $r_{rs}(\theta, \phi)$:

$$r_{rs}(\theta, \phi) = \frac{1}{\mu_d K_{Lu}(\theta, \phi) \left| \cos\theta \right| + a + b_b - (f_L(\theta, \phi) - 1) b_f} \frac{f_b(\theta, \phi) \frac{b_b}{2\pi}}{\quad} \quad (\text{B1})$$

For brevity in this Appendix, spectral dependence is implied, but not denoted. In Eq. (B1), μ_d is the average cosine of downwelling irradiance, K_{Lu} is the diffuse attenuation coefficient of the upwelling nadir radiance $L_u(\theta, \phi)$, b_f is the forward scattering coefficient,

$$f_b(\theta, \phi) = \frac{\int_0^{2\pi} \int_0^{\pi/2} \beta(\theta, \phi, \theta', \phi') L(\theta', \phi') \sin\theta' d\theta' d\phi'}{E_{od} b_b / 2\pi} \quad (\text{B2})$$

$$f_L(\theta, \phi) = \frac{\int_0^{2\pi} \int_{\pi/2}^{\pi} \beta(\theta, \phi \cdot \theta' \cdot \phi') L(\theta', \phi') \sin\theta' d\theta' d\phi'}{b_f L_u(\theta, \phi)} \quad (\text{B3})$$

In Eq. (B2), the shape factor f_b represents the ratio of the light actually scattered into the direction (θ, ϕ) by scattering of downwelling radiance to the light that would be received if the VSF was constant and equal to $b_b/2\pi$. In Eq. (B3), f_L represents the ratio of the light actually scattered into the direction (θ, ϕ) by scattering of upwelling radiance to the light that would be received if the upwelling radiance were isotropic and equal to $L_u(\theta, \phi)$ and if the VSF was constant and equal to $b_f/2\pi$. Assuming the volume scattering function and the radiance distribution are continuous within their respective angular ranges, the shape factor f_b can be rewritten as:

$$f_b(\theta, \phi) = \frac{\beta(\gamma_m) \int_0^{2\pi} \int_0^{\pi/2} L(\theta', \phi') \sin\theta' d\theta' d\phi'}{E_{od} b_b / 2\pi} = \frac{2\pi \beta(\gamma_m)}{b_b} \quad (\text{B4})$$

where $\beta(\gamma_m)$ represents the downwelling radiance distribution less the weighted mean volume scattering function and γ_m the corresponding scattering angle. Inserting Eq. (B4) into Eq. (B1), we have:

$$r_{rs}(\theta, \phi) = \frac{1}{\mu_d K_{Lu}(\theta, \phi) |\cos\theta| + a + b_b - (f_L(\theta, \phi) - 1)b_f} \beta(\gamma_m) \quad (\text{B5})$$

Note that Eq. (B5) explicitly includes the VSF in defining the remote sensing reflectance. Zaneveld (1989) provided an inversion for Eq. (B5) that has not been rigorously assessed by the community to date. It is important to note that inelastic processes such as Raman scattering are not included in the above relationships.

Eq. (B5) has several attractive aspects from a remote sensing algorithm perspective. First, it would seem desirable to develop algorithms that explicitly contain the shape of the VSF. As Morel and Gentili (1993) point out, the BRDF which describes the shape of the upwelling radiance distribution, "... is essentially controlled by the shape of the VSF..." Exclusively using integrated coefficients such as b_b must introduce some approximate error. Second, using a relationship such as Eq. (B5) merges two separate, disconnected steps in current QSSA algorithm work – recall that in current NASA processing, for example, $R_{rs}(\lambda)$ are first "exactly" normalized following Morel et al. (2002) to account for varied solar geometry, then the IOP inversion is executed. Combining these steps in a single, rigorous relationship allows explicit assessment of errors in component variables. In the current two-step approach, errors associated with, for example, the VSF are dispersed in several poorly defined parameters that are empirically tuned. Finally, approximations that retain as much of the functional form of the RT equation as possible would seem to be inherently more stable.

Abbreviations

AC	atmospheric correction
ANN	artificial neural network
AOP	apparent optical property
BRDF	bidirection reflectance distribution function
Ca	chlorophyll-a
CDOM	colored dissolved organic matter
CORAL	CORal Reef Airborne Laboratory
DLR	German Aerospace Center
DOC	dissolved organic matter
EnMAP	Environmental Mapping and Analysis Program
EOF	empirical orthogonal function
ESA	European Space Agency
GEO	geostationary Earth orbit
GSD	ground sampling distance
GOCI	Geostationary Ocean Color Imager
IOCCG	International Ocean Colour Coordinating Group
IOPs	Inherent Optical Properties
ISRO	Indian Space Research Organisation
JAXA	Japanese Aerospace Exploration Agency
KIOST	Korean Institute of Ocean Science and Technology
LEO	low Earth orbit
LUT	look-up-table
MAAs	mycosporine-like amino acids
MASCOT	Multi Angle Scattering Optical Tool
MERIS	Medium Resolution Imaging Spectroradiometer
MLR	multiple linear regression
MODISA	Moderate Resolution Imaging Spectroradiometer aboard the Aqua spacecraft

MODIST	Moderate Resolution Imaging Spectroradiometer aboard the Terra spacecraft
MSI	MultiSpectral Instrument
MVSM	Multispectral Volume Scattering Meter
NAP	non-algal particles
NASA	National Aeronautics and Space Administration
NIR	near-infrared
NOAA	National Oceanic and Atmospheric Administration
OCI	Ocean Color Instrument
OCM	Ocean Color Monitor
OCTS	Ocean Color Temperature Scanner
OLCI	Ocean and Land Colour Instrument
OLI	Operational Land Imager
PACE	Plankton, Aerosol, Cloud, ocean, Ecosystem mission
PC	principal component
PCA	principal component analysis
PCR	principal component regression
RT	radiative transfer
QSSA	quasi single scattering approximation
S	salinity
SAs	semi-analytical inversion algorithms
SeaWiFS	Sea-viewing Wide-Field-of-view Sensor
SGLI	Second-generation Global Imager
SSS	sea surface salinity
SST	sea surface temperature
T	temperature
USGS	United States Geological Survey
UV	ultraviolet
VIIRS	Visible Infrared Imaging Radiometer Suite

VIS	visible
VSF	volume scattering function
VSWIR	Visible ShortWave InfraRed sensor

References

- Abadi M, Agarwal A, Barham P, Brevdo E, Chen Z, Citro C, Corrado GS, Davis A, Dean J, Devin M, 2016 Tensorflow: Large-scale machine learning on heterogeneous distributed systems. arXiv, 1603.04467.
- Albert A, Mobley C, 2003 An analytical model for subsurface irradiance and remote sensing reflectance in deep and shallow case-2 waters. *Optics Express*, 11, 2873–2890. [PubMed: 19471407]
- Allali K, Bricaud A, Claustre H, 1997 Spatial variations in the chlorophyll-specific absorption coefficients of phytoplankton and photosynthetically active pigments in the equatorial Pacific. *Journal of Geophysical Research*, 102 (C6), 12413–12423.
- Allison DB, Stramski D, Mitchell BG, 2010 Seasonal and interannual variability of particulate organic carbon within the Southern Ocean from satellite ocean color observations. *Journal of Geophysical Research*, 115, C06002, 10.1029/2009jc005347.
- Andre JM, 2002 Ocean color remote sensing and the subsurface vertical structure of phytoplankton pigments. *Deep Sea Res. I*, 39, 763–779.
- Antoine D, Andre JM, Morel A, 1996 Oceanic primary production .2. Estimation at global scale from satellite (coastal zone color scanner) chlorophyll. *Global Biogeochemical Cycles*, 10, 57–69.
- Antoine D, Siegel DA, Kostadinov T, Maritorena S, Nelson NB, Gentili B, Vellucci V, Guillocheau N, 2011 Variability in optical particle backscattering in contrasting bio-optical oceanic regimes. *Limnology and Oceanography*, 56, 955–973.
- Antonov JI, Seidov D, Boyer TP, Locarnini RA, Mishonov AV, Garcia HE, Baranova OK, Zweng MM, Johnson DR, 2010 World Ocean Atlas 2009, Volume 2: Salinity, NOAA NESDIS 68. In Levitus S (Ed.) (p. 39). Washington DC.
- Arbones B, Figueiras F, Zapata M, 1996 Determination of phytoplankton absorption coefficient in natural seawater samples: evidence of a unique equation to correct the pathlength amplification on glass-fiber filters. *Marine Ecology Progress Series*, 137, 293–304.
- Armstrong F, Boalch G, 1961 The ultra-violet absorption of sea water. *Journal of the Marine Biological Association of the United Kingdom*, 41, 591–597.
- Babin M, Stramski D, 2004 Variations in the mass-specific absorption coefficient of mineral particles suspended in water. *Limnol. Oceanogr*, 49, 756–767.
- Babin M, Stramski D, Ferrari GM, Claustre H, Bricaud A, Obolensky G, Hoepffner N, 2003 Variations in the light absorption coefficients of phytoplankton, nonalgal particles, and dissolved organic matter in coastal waters around Europe. *Journal of Geophysical Research*, 108(C7), 3211, 10.1029/2001JC000882.
- Bailey SW, Werdell PJ, 2006 A multi-sensor approach for the on-orbit validation of ocean color satellite data products. *Remote Sensing of Environment*, 102, 12–23.
- Bannister TT, 1974 General Theory of Steady-State Phytoplankton Growth in a Nutrient Saturated Mixed Layer. *Limnology and Oceanography*, 19, 13–30.
- Barnes BB, Garcia R, Hu C, Lee Z, 2017 Multi-band spectral matching inversion algorithm to derive water column properties in optically shallow waters: An optimization of parameterization. *Remote Sensing of Environment*, 204, 424–438.
- Barnes BB, Hu C, Cannizzaro JP, Craig SE, Hallock P, Jones DL, Lehrter JC, Melo N, Schaeffer BA, Zepp R, 2014 Estimation of diffuse attenuation of ultraviolet light in optically shallow Florida Keys waters from MODIS measurements. *Remote Sensing of Environment*, 140, 519–532.
- Barnes BB, Hu C, Schaeffer BA, Lee Z, Palandro DA, Lehrter JC, 2013 MODIS-derived spatiotemporal water clarity patterns in optically shallow Florida Keys waters: A new approach to remove bottom contamination. *Remote Sensing of Environment*, 134, 377–391.

- Bartlett JS, Voss KJ, Sathyendranath S, Vodacek A, 1998 Raman scattering by pure water and seawater. *Appl. Opt.*, 37, 3324–3332. [PubMed: 18273291]
- Bates DM, Watts DG, 1988 Nonlinear regression: iterative estimation and linear approximations Nonlinear regression analysis and its applications, John Wiley and Sons, Inc., 32–66.
- Becucci M, Cavalieri S, Eramo R, Fini L, Materazzi M, 1999 Accuracy of remote sensing of water temperature by Raman spectroscopy. *Applied Optics*, 38, 928–931. [PubMed: 18305693]
- Behrenfeld MJ, Boss E, Siegel DA, Shea DM, 2005 Carbon-based ocean productivity and phytoplankton physiology from space. *Global Biogeochemical Cycles*, 19, GB1006, doi: 10.1029/2004GB002299.
- Berthon J-F, Shybanov E, Lee ME-G, Zibordi G, 2007 Measurements and modeling of the volume scattering function in the coastal northern Adriatic Sea. *Applied Optics*, 46, 51895203.
- Blough N, Green S, 1995 Spectroscopic characterization and remote sensing of non-living organic matter The Role of Non-living Organic Matter in the Earth's Carbon Cycle (Zepp RG and Sonntag C, eds), John Wiley & Sons Ltd, 23–45.
- Boss E, Pegau W, Lee M, Twardowski M, Shybanov E, Korotaev G, Baratange F, 2004 Particulate backscattering ratio at LEO 15 and its use to study particle composition and distribution. *Journal of Geophysical Research*, 109, C01014, 10.1029/2002JC001514.
- Boss E, Pegau WS, 2001 Relationship of light scattering at an angle in the backward direction to the backscattering coefficient. *Applied Optics*, 40, 5503–5507. [PubMed: 18364835]
- Boss E, Roesler C, 2006 Over constrained linear matrix inversion with statistical selection Remote Sensing of Inherent Optical Properties: Fundamentals, Tests of Algorithms, and Applications, IOCCG, Dartmouth, NS, Canada, IOCCG Rep, 5.
- Bowers DG, Binding CE, 2006 The optical properties of mineral suspended particles: A review and synthesis. *Estuarine Coastal Shelf Science*, 67, 219–230.
- Boydton GC, Gordon HR, 2002 Irradiance inversion algorithm for absorption and backscattering profiles in natural waters: improvement for clear waters. *Applied Optics*, 41, 2224–2227. [PubMed: 12003214]
- Bracher A, Bouman HA, Brewin RJW, Bricaud A, Brotas V, Ciotti AM, Clementson L, Devred E, Di Cicco A, Dutkiewicz S, Hardman-Mountford NJ, Hickman AE, Hieronymi M, Hirata T, Losa SN, Mouw CB, Organelli E, Raitos DE, Uitz J, Vogt M, Wolanin A, 2017 Obtaining Phytoplankton Diversity from Ocean Color: A Scientific Roadmap for Future Development. *Frontiers in Marine Science*, 4, 10.3389/fmars.2017.00055.
- Bracher A, Vountas M, Dinter T, Burrows JP, Rottgers R, Peeken I, 2009 Quantitative observation of cyanobacteria and diatoms from space using PhytoDOAS on SCIAMACHY data. *Biogeosciences*, 6, 751–764.
- Brando VE, Anstee JM, Wettle M, Dekker AG, Phinn SR, Roelfsema C, 2009 A physics based retrieval and quality assessment of bathymetry from suboptimal hyperspectral data. *Remote Sensing of Environment*, 113, 755–770.
- Brando VE, Dekker AG, Park YJ, Schroeder T, 2012 Adaptive semianalytical inversion of ocean color radiometry in optically complex waters. *Applied Optics*, 51, 2808–2833. [PubMed: 22614582]
- Brewin RJW, Devred E, Sathyendranath S, Lavender SJ, Hardman-Mountford NJ, 2011 Model of phytoplankton absorption based on three size classes. *Applied Optics*, 50, 4535–4549. [PubMed: 21833130]
- Brewin RJW, Raitos DE, Dall'Olmo G, Zarokanellos N, Jackson T, Racault MF, Boss ES, Sathyendranath S, Jones BH, Hoteit I, 2015a Regional ocean-colour chlorophyll algorithms for the Red Sea. *Remote Sensing of Environment*, 165, 64–85.
- Brewin RJW, Sathyendranath S, Müller D, Brockmann C, Deschamps P-Y, Devred E, Doerffer R, Fomferra N, Franz B, Grant M, Groom S, Horseman A, Hu C, Krasemann H, Lee Z, Maritorea S, Mélin F, Peters M, Platt T, Regner P, Smyth T, Steinmetz F, Swinton J, Werdell J, White GN, 2015b The Ocean Colour Climate Change Initiative: III. A round-robin comparison on in-water bio-optical algorithms. *Remote Sensing of Environment*, 162, 271–294.
- Bricaud A, Babin M, Morel A, Claustre H, 1995 Variability in the chlorophyll-specific absorption coefficients of natural phytoplankton: Analysis and parameterization. *Journal of Geophysical Research: Oceans*, 100, 13321–13332.

- Bricaud A, Ciotti AM, Gentili B, 2012 Spatial-temporal variations in phytoplankton size and colored detrital matter absorption at global and regional scales, as derived from twelve years of SeaWiFS data (1998–2009). *Global Biogeochemical Cycles*, 26, doi:10.1029/2010GB003952.
- Bricaud A, Mejjia C, Biondeau-Patissier D, Claustre H, Crepon M, Thiria S, 2007 Retrieval of pigment concentrations and size structure of algal populations from their absorption spectra using multilayered perceptrons. *Applied Optics*, 46, 1251–1260. [PubMed: 17318245]
- Bricaud A, Morel A, Babin M, Allali K, Claustre H, 1998 Variations of light absorption by suspended particles with the chlorophyll a concentration in oceanic (Case 1) waters : analysis and implications for bio-optical models. *J. Geophys. Res. Oceans*, 103, 31033–31044.
- Bricaud A, Morel A, Prieur L, 1981 Absorption by dissolved organic matter of the sea (yellow substance) in the UV and visible domains I. *Limnology and Oceanography*, 26, 43–53.
- Bricaud A, Stramski D, 1990 Spectral absorption coefficients of living phytoplankton and nonalgal biogenous matter: A comparison between the Peru upwelling area and the Sargasso Sea. *Limnology and Oceanography*, 35, 562–582.
- Buiteveld H, Hakvoort JHM, Donze M, 1994 The Optical Properties of Pure Water. *Ocean Optics* Xii, 2258, 174–183.
- Bukata RP, Jerome JH, Kondratyev AS, Pozdnyakov DV, 1995 Optical properties and remote sensing of inland and coastal waters: CRC press.
- Cael BB, Boss E, 2017 Simplified model of spectral absorption by non-algal particles and dissolved organic materials in aquatic environments. *Optics Express*, 25, 25486–25491. [PubMed: 29041215]
- Campbell JW, 1995 The lognormal distribution as a model for bio-optical variability in the sea. *Journal of Geophysical Research*, 100, 13237–13254, doi:10.1029/1995JC00458
- Camps-Valls G, Gomez-Chova L, Muñoz-Marí J, Vila-Francis J, Calpe-Maravilla J, 2006 Composite kernels for hyperspectral image classification. *IEEE Geoscience and Remote Sensing Letters*, 3, 93–97.
- Cao F, Fichot CG, Hooker SB, Miller WL, 2014 Improved algorithms for accurate retrieval of UV/visible diffuse attenuation coefficients in optically complex, inshore waters. *Remote Sensing of Environment*, 144, 11–27.
- Cao F, Tzortziou M, Hu C, Mannino A, Fichot C, Del Vecchio R, Najjar R, Novak M, 2018 Remote sensing retrievals of colored dissolved organic matter and dissolved organic carbon dynamics in North American eutrophic estuaries and their margins. *Remote Sensing of Environment*, 205, 151–165, 10.1016/j.rse.2017.11.1014.
- Chami M, Marken E, Stamnes J, Khomenko G, Korotaev G, 2006 Variability of the relationship between the particulate backscattering coefficient and the volume scattering function measured at fixed angles. *Journal of Geophysical Research: Oceans*, 111, 10.1029/2005JC003230.
- Chami M, Thirouard A, Harmel T, 2014 POLVSM (Polarized Volume Scattering Meter) instrument: an innovative device to measure the directional and polarized scattering properties of hydrosols. *Optics Express*, 22, 26403–26428. [PubMed: 25401673]
- Chang C-H, 2015 Development of ocean color algorithms for estimating chlorophyll-a concentrations and inherent optical properties using gene expression programming (GEP). *Optics Express*, 23, 10.1029/2012JC008076.
- Chang GC, Dickey TD, 1999 Partitioning in situ total spectral absorption by use of moored spectral absorption–attenuation meters. *Applied Optics*, 38, 3876–3887. [PubMed: 18319994]
- Chen J, Cui T, Ishizaka J, Lin C, 2014a A neural network model for remote sensing of diffuse attenuation coefficient in global oceanic and coastal waters: Exemplifying the applicability of the model to the coastal regions in Eastern China Seas. *Remote Sensing of Environment*, 148, 168–177.
- Chen J, Quan W, Cui T, Song Q, Lin C, 2014b Remote sensing of absorption and scattering coefficient using neural network model: development, validation, and application. *Remote Sensing of Environment*, 149, 213–226.
- Chen J, Zhu Y, Wu Y, Cui T, Ishizaka J, Ju Y, 2015 A Neural Network Model for K (λ) Retrieval and Application to Global Kpar Monitoring. *PloS one*, 10, e0127514. [PubMed: 26083341]

- Chin Y-P, Aiken G, O'Loughlin E, 1994 Molecular weight, polydispersity, and spectroscopic properties of aquatic humic substances. *Environmental Science & Technology*, 28, 1853–1858. [PubMed: 22175925]
- Choi J-K, Park YJ, Ahn JH, Lim H-S, Eom J, Ryu J-H, 2012 GOCI, the world's first geostationary ocean color observation satellite, for the monitoring of temporal variability in coastal water turbidity. *Journal of Geophysical Research: Oceans*, 117, 10.1029/2012JC008046.
- Choi J-K, Yang H, Han H-J, Ryu J-H, Park Y-J, 2013 Quantitative estimation of suspended sediment movements in coastal region using GOCI. *Journal of Coastal Research*, 1367–1372.
- Chomko RM, Gordon HR, 1998 Atmospheric correction of ocean color imagery: use of the Junge power-law aerosol size distribution with variable refractive index to handle aerosol absorption. *Applied Optics*, 37, 5560–5572. [PubMed: 18286040]
- Chomko RM, Gordon HR, Maritorena S, Siegel DA, 2003 Simultaneous retrieval of oceanic and atmospheric parameters for ocean color imagery by spectral optimization: a validation. *Remote Sensing of Environment*, 84, 208–220.
- Chowdhary J, Cairns B, Waquet F, Knobelspiesse K, Ottaviani M, Redemann J, Travis L, Mishchenko M, 2012 Sensitivity of multiangle, multispectral polarimetric remote sensing over open oceans to water-leaving radiance: Analyses of RSP data acquired during the MILAGRO campaign. *Remote Sensing of Environment*, 118, 284–308.
- Ciotti AM, Cullen JJ, Lewis MR, 1999 A semi-analytical model of the influence of phytoplankton community structure on the relationship between light attenuation and ocean color. *J Geophys Res Oceans*, 104, 1559–1578.
- Ciotti AM, Lewis MR, Cullen JJ, 2002 Assessment of the relationships between dominant cell size in natural phytoplankton communities and the spectral shape of the absorption coefficient. *Limnology and Oceanography*, 47, 404–417.
- Ciotti AM, Bricaud A, 2006 Retrievals of a size parameter for phytoplankton and spectral light absorption by Colored Detrital Matter from water-leaving radiances at SeaWiFS channels in a continental shelf region off Brazil. *Limnology and Oceanography Methods*, 4, 237–253.
- Claustre H, Fell F, Oubelkheir K, Prieur L, Sciandra A, Gentili B, Babin M, 2000 Continuous monitoring of surface optical properties across a geostrophic front: Biogeochemical inferences. *Limnology and Oceanography*, 45, 309–321.
- Cleveland J, Perry M, 1994 A model for partitioning particulate absorption into phytoplanktonic and detrital components. *Deep Sea Research Part I: Oceanographic Research Papers*, 41, 197–221.
- Cleveland J, Weidemann AD, 1993 Quantifying absorption by aquatic particles: A multiple scattering correction for glass-fiber filters. *Limnology and Oceanography*, 38, 1321–1327.
- Copin-Montegut G, Ivanoff A, Saliot A, 1971 Coefficient d'atténuation des eaux de mer dans l'ultra-violet. *CR Acad. Sci. Paris*, 272, 1453–1456.
- Craig SE, Jones CT, Li WK, Lazin G, Horne E, Caverhill C, Cullen JJ, 2012 Deriving optical metrics of coastal phytoplankton biomass from ocean colour. *Remote Sensing of Environment*, 119, 72–83.
- D'Alimonte D, Zibordi G, Berthon J-F, Canuti E, Kajiyama T, 2012 Performance and applicability of bio-optical algorithms in different European seas. *Remote Sensing of Environment*, 124, 402–412.
- De Noia A, Hasekamp OP, van Harten G, Rietjens JHH, Smit JM, Snik F, Henzing JS, de Boer J, Keller CU, Volten H, 2015 Use of neural networks in ground based aerosol retrievals from multi-angle spectropolarimeter observations. *Atmospheric Measurement Techniques*, 8, 281–299.
- Defoin-Platel M, Chami M, 2007 How ambiguous is the inverse problem of ocean color in coastal waters? *Journal of Geophysical Research: Oceans*, 112, 10.1029/2006JC003847.
- Dekker AG, Phinn SR, Antsee J, Bisset P, Brando VE, Casey B, Fearn P, Hedley J, Klonowski W, Lee Z, Lynch MJ, Lyons M, Mobley C, Roelfsema C, 2011 Intercomparison of shallow water bathymetry, hydro-optics, and benthos mapping techniques in Australian and Caribbean coastal environments. *Limnology and Oceanography*, 9, 396–425.
- Del Castillo CE, Coble PG, Conmy RN, Müller-Karger FE, Vanderbloemen L, Vargo GA, 2001 Multispectral in situ measurements of organic matter and chlorophyll fluorescence in seawater: documenting the intrusion of the Mississippi River plume in the West Florida Shelf. *Limnology and Oceanography*, 46, 1836–1843.

- Devlin JM, Petus C, da Silva E, Tracey D, Wolff HN, Waterhouse J, Brodie J, 2015 Water Quality and River Plume Monitoring in the Great Barrier Reef: An Overview of Methods Based on Ocean Colour Satellite Data. *Remote Sensing*, 7, 10.3390/rs71012909.
- Devred E, Sathyendranath S, Stuart V, Maas H, Ulloa O, Platt T, 2006 A two-component model of phytoplankton absorption in the open ocean: Theory and applications. *Journal of Geophysical Research*, 111, 10.1029/2005JC002880.
- Devred E, Sathyendranath S, Stuart V, Platt T, 2011 A three component classification of phytoplankton absorption spectra: Application to ocean-color data. *Remote Sensing of Environment*, 115, 2255–2266.
- Doerffer R, Schiller H, 2007 The MERIS Case 2 water algorithm. *International Journal of Remote Sensing*, 28, 517–535.
- Dong Q, Shang S, Lee Z, 2013 An algorithm to retrieve absorption coefficient of chromophoric dissolved organic matter from ocean color. *Remote Sensing of Environment*, 128, 259–267.
- Doucha J, Kubin S, 1976 Measurement of in vivo absorption spectra of microscopic algae using bleached cells as reference sample. *Arch. Hydrobiol. Suppl.*, 49, 199–213.
- Duforet-Gaurier L, Loisel H, Dessailly D, Nordkvist K, Alvain S, 2010 Estimates of particulate organic carbon over the euphotic depth from in situ measurements. Application to satellite data over the global ocean. *Deep-Sea Research Part I-Oceanographic Research Papers*, 57, 351–367.
- Dutkiewicz S, Hickman AE, Jahn O, Gregg WW, Mouw CB, Follows MJ, 2015 Capturing optically important constituents and properties in a marine biogeochemical and ecosystem model. *Biogeosciences*, 12, 4447–4481.
- Dzwonkowski B, Yan X-H, 2005 Tracking of a Chesapeake Bay estuarine outflow plume with satellite-based ocean color data. *Continental Shelf Research*, 25, 1942–1958.
- Estapa ML, Mayer LM, 2010 Photooxidation of particulate organic matter, carbon/oxygen stoichiometry, and related photoreactions. *Marine Chemistry*, 122, 138–147.
- Evers-King H, Bernard S, Robertson Lain L, Probyn TA, 2014 Sensitivity in reflectance attributed to phytoplankton cell size: forward and inverse modelling approaches. *Optics Express*, 22, 11536–11551. [PubMed: 24921275]
- Falkowski P, Kolber Z, 1995 Variations in chlorophyll fluorescence yields in phytoplankton in the world oceans. *Functional Plant Biology*, 22, 341–355.
- Farinato RS, Rowell RL, 1976 New values of the light scattering depolarization and anisotropy of water. *The Journal of Chemical Physics*, 65, 593–595.
- Ferrari GM, Tassan S, 1999 A method using chemical oxidation to remove light absorption by phytoplankton pigments. *Journal of Phycology*, 35, 1090–1098.
- Fichot CG, Benner R, 2011 A novel method to estimate DOC concentrations from CDOM absorption coefficients in coastal waters. *Geophysical Research Letters*, 38, 10.1029/2010gl046152.
- Fichot CG, Sathyendranath S, Miller WL, 2008 SeaUV and SeaUV C: Algorithms for the retrieval of UV/Visible diffuse attenuation coefficients from ocean color. *Remote Sensing of Environment*, 112, 1584–1602.
- Finkel Z, Irwin A, 2001 Light absorption by phytoplankton and the filter amplification correction: cell size and species effects. *Journal of experimental marine biology and ecology*, 259, 51–61. [PubMed: 11325376]
- Franz BA, Bailey SW, Kuring N, Werdell PJ, 2015 Ocean color measurements with the Operational Land Imager on Landsat-8: implementation and evaluation in SeaDAS. *Journal of Applied Remote Sensing*, 9, 10.1117/1.1111.JRS.1119.096070.
- Frouin R, Pelletier B, 2015 Bayesian methodology for inverting satellite ocean-color data. *Remote Sensing of Environment*, 159, 332–360.
- Gallegos CL, Neale PJ, 2002 Partitioning spectral absorption in case 2 waters: discrimination of dissolved and particulate components. *Applied Optics*, 41, 4220–4233. [PubMed: 12148749]
- Garcia RA, McKinna LI, Hedley JD, Fearn PR, 2014 Improving the optimization solution for a semi-analytical shallow water inversion model in the presence of spectrally correlated noise. *Limnology and Oceanography: Methods*, 12, 651–669.
- Gardner WD, Mishonov A, Richardson MJ, 2006 Global POC concentrations from in-situ and satellite data. *Deep-Sea Research Part Ii-Topical Studies in Oceanography*, 53, 718–740.

- Garver SA, Siegel DA, 1997 Inherent optical property inversion of ocean color spectra and its biogeochemical interpretation: 1. Time series from the Sargasso Sea. *Journal of Geophysical Research: Oceans*, 102, 18607–18625.
- Gnanadesikan A, Emanuel K, Vecchi GA, Anderson WG, Hallberg R, 2010 How ocean color can steer Pacific tropical cyclones. *Geophys. Res. Lett.*, 37, 10.1029/2010GL044514.
- Gordon H, Morel A, 1983 Remote Assessment of Ocean Color for Interpretation of Satellite Visible Imagery: A review. Springer-Verlag NY.
- Gordon HR, 1973 Simple Calculation of the Diffuse Reflectance of the Ocean. *Applied Optics*, 12, 2803–2804. [PubMed: 20125868]
- Gordon HR, 1993 Sensitivity of radiative transfer to small-angle scattering in the ocean: Quantitative assessment. *Applied Optics*, 32, 7505–7511. [PubMed: 20861970]
- Gordon HR, Boynton GC, 1998 Radiance–irradiance inversion algorithm for estimating the absorption and backscattering coefficients of natural waters: vertically stratified water bodies. *Applied Optics*, 37, 3886–3896. [PubMed: 18273356]
- Gordon HR, Brown OB, Evans RH, Brown JW, Smith RC, Baker KS, Clark DK, 1988 A Semianalytic Radiance Model of Ocean Color. *Journal of Geophysical Research*, 93, 10909–10924.
- Gordon HR, Clark DK, 1980 Remote sensing optical properties of a stratified ocean: an improved interpretation. *Applied Optics*, 19, 3428–3430. [PubMed: 20234635]
- Gordon HR, Du T, Zhang T, 1997 Remote sensing of ocean color and aerosol properties: resolving the issue of aerosol absorption. *Applied Optics*, 36, 8670–8684. [PubMed: 18264417]
- Gordon HR, Smyth TJ, Balch WM, Boynton GC, Tarran GA, 2009 Light scattering by coccoliths detached from *Emiliana huxleyi*. *Applied Optics*, 48, 6059–6073. [PubMed: 19881674]
- Gordon HR, Wang M, 1994 Retrieval of water-leaving radiance and aerosol optical thickness over the oceans with SeaWiFS: A preliminary algorithm. *Applied Optics*, 33, 443–452. [PubMed: 20862036]
- Gould RW, McCarthy SC, Coelho E, Shulman I, Richman JG, 2014 Combining satellite ocean color and hydrodynamic model uncertainties in bio-optical forecasts. *Journal of Applied Remote Sensing*, 8, 083652–083652.
- Green SA, Blough NV, 1994 Optical absorption and fluorescence properties of chromophoric dissolved organic matter in natural waters. *Limnology and Oceanography*, 39, 1903–1916.
- Gregg WW, Casey NW, 2004 Global and regional evaluation of the SeaWiFS chlorophyll data set. *Remote Sensing of Environment*, 93, 463–479.
- Haigang Z, Zhong Ping L, Ping S, Chen C, Carder KL, 2003 Retrieval of water optical properties for optically deep waters using genetic algorithms. *Geoscience and Remote Sensing, IEEE Transactions on*, 41, 1123–1128.
- Harmel T, 2016 Recent developments in the use of light polarization for marine environment monitoring from space *Light Scattering Reviews* 10 (pp. 41–84): Springer.
- Harmel T, Gilerson A, Tonizzo A, Chowdhary J, Weidemann A, Arnone R, Ahmed S, 2012 Polarization impacts on the water-leaving radiance retrieval from above-water radiometric measurements. *Applied Optics*, 51, 8324–8340. [PubMed: 23262527]
- Harmel T, Hieronymi M, Slade W, Röttgers R, Roullier F, Chami M, 2016 Laboratory experiments for inter-comparison of three volume scattering meters to measure angular scattering properties of hydrosols. *Optics Express*, 24, A234–A256. [PubMed: 26832578]
- Hedley DJ, Roelfsema MC, Chollett I, Harborne RA, Heron FS, Weeks S, Skirving JW, Strong EA, Eakin MC, Christensen RT, Ticzon V, Bejarano S, Mumby JP, 2016 Remote sensing of coral reefs for monitoring and management: A review. *Remote Sensing*, 8, doi:10.3390/rs8020118.
- Hedley J, Roelfsema C, Phinn SR, 2009 Efficient radiative transfer model inversion for remote sensing applications. *Remote Sensing of Environment*, 113, 2527–2532.
- Helms JR, Stubbins A, Ritchie JD, Minor EC, Kieber DJ, Mopper K, 2008 Absorption spectral slopes and slope ratios as indicators of molecular weight, source, and photobleaching of chromophoric dissolved organic matter. *Limnology and Oceanography*, 53, 955–969.
- Hirata T, Aiken J, Hardman-Mountford N, Smyth TJ, Barlow RG, 2008 An absorption model to determine phytoplankton size classes from satellite ocean colour. *Remote Sensing of Environment*, 112, 3153–3159.

- Hoepffner N, Sathyendranath S, 1993 Determination of the Major Groups of Phytoplankton Pigments from the Absorption-Spectra of Total Particulate Matter. *Journal of Geophysical Research-Oceans*, 98, 22789–22803.
- Hoge FE, Lyon PE, 1996 Satellite retrieval of inherent optical properties by linear matrix inversion of oceanic radiance models: An analysis of model and radiance measurement errors. *Journal of Geophysical Research: Oceans*, 101, 16631–16648.
- Hoge FE, Vodacek A, Blough NV, 1993 Inherent optical properties of the ocean: retrieval of the absorption coefficient of chromophoric dissolved organic matter from fluorescence measurements. *Limnology and Oceanography*, 38, 1394–1402.
- Hu C, Feng L, Lee Z, Davis CO, Mannino A, McClain CR, Franz BA, 2012 Dynamic range and sensitivity requirements of satellite ocean color sensors: learning from the past. *Applied Optics*, 51, 6045–6062. [PubMed: 22945151]
- Hu CM, 2009 A novel ocean color index to detect floating algae in the global oceans. *Remote Sensing of Environment*, 113, 2118–2129.
- Huang S, Li Y, Shang S, Shang S, 2013 Impact of computational methods and spectral models on the retrieval of optical properties via spectral optimization. *Optics Express*, 21, 62576273.
- Huot Y, Morel A, Twardowski MS, Stramski D, Reynolds RA, 2008 Particle optical backscattering along a chlorophyll gradient in the upper layer of the eastern South Pacific Ocean. *Biogeosciences*, 5, 495–507.
- Ibrahim A, Gilerson A, Chowdhary J, Ahmed S, 2016 Retrieval of macro-and microphysical properties of oceanic hydrosols from polarimetric observations. *Remote Sensing of Environment*, 186, 548–566.
- Ioannou I, Gilerson A, Gross B, Moshary F, Ahmed S, 2011 Neural network approach to retrieve the inherent optical properties of the ocean from observations of MODIS. *Applied Optics*, 50, 3168–3186. [PubMed: 21743516]
- Ioannou I, Gilerson A, Gross B, Moshary F, Ahmed S, 2013 Deriving ocean color products using neural networks. *Remote Sensing of Environment*, 134, 78–91.
- IOCCG, 2006 Remote Sensing of Inherent Optical Properties: Fundamentals, Tests of Algorithms, and Applications. Dartmouth, Canada: IOCCG.
- IOCCG, 2008 Why Ocean Colour? The Societal Benefits of Ocean-Colour Technology. Dartmouth, Canada: IOCCG.
- IOCCG, 2009 Remote Sensing in Fisheries and Aquaculture. Dartmouth, Canada: IOCCG.
- IOCCG, 2014 Phytoplankton Functional Types from Space. Dartmouth, Canada: IOCCG.
- Jamet C, Loisel H, Dessailly D, 2012 Retrieval of the spectral diffuse attenuation coefficient $K_d(\lambda)$ in open and coastal ocean waters using a neural network inversion. *Journal of Geophysical Research: Oceans*, 117, 10.1029/2012JC008076.
- Jerlov N, 1976 *Marine Optics*. Amsterdam: Elsevier.
- Jerome J, Bukata R, Miller J, 1996 Remote sensing reflectance and its relationship to optical properties of natural waters. *Remote Sensing*, 17, 3135–3155.
- Jiang J, Trundle P, Ren J, 2010 Medical image analysis with artificial neural networks. *Computerized Medical Imaging and Graphics*, 34, 617–631. [PubMed: 20713305]
- Johnson KS, Coletti LJ, 2002 In situ ultraviolet spectrophotometry for high resolution and long-term monitoring of nitrate, bromide and bisulfide in the ocean. *Deep Sea Research Part I: Oceanographic Research Papers*, 49, 1291–1305.
- Jolliff JK, Kindle JC, Shulman I, Penta B, Friedrichs MAM, Helber R, Arnone RA, 2009 Summary diagrams for coupled hydrodynamic-ecosystem model skill assessment. *Journal of Marine Systems*, 76, 64–82.
- Jonasz M, Fournier G, 2007 *Light scattering by particles in water: Theoretical and experimental constraints*. Acad. Press, San Diego.
- Kattawar GW, 2013 Genesis and evolution of polarization of light in the ocean. *Applied Optics*, 52, 940–948. [PubMed: 23400055]

- Kattawar GW, Adams CN, 1989 Stokes vector calculations of the submarine light field in an atmosphere-ocean with scattering according to a Rayleigh phase matrix: Effect of interface refractive index on radiance and polarization. *Limnology and Oceanography*, 34, 1453–1472.
- Kiefer DA, Mitchell BG, 1983 A Simple, Steady-State Description of Phytoplankton Growth Based on Absorption Cross-Section and Quantum Efficiency. *Limnology and Oceanography*, 28, 770–776.
- Kiefer DA, SooHoo JB, 1982 Spectral absorption by marine particles of coastal waters of Baja California. *Limnology and Oceanography*, 27, 492–499.
- Kilpatrick KA, Podestá GP, Evans R, 2001 Overview of the NOAA/NASA advanced very high resolution radiometer Pathfinder algorithm for sea surface temperature and associated matchup database. *Journal of Geophysical Research: Oceans*, 106, 9179–9197.
- Kim YH, Im J, Ha HK, Choi JK, Ha S, 2014 Machine learning approaches to coastal water quality monitoring using GOCI satellite data. *GIScience & Remote Sensing*, 51.
- Kishino M, Takahashi M, Okami N, Ichimura S, 1985 Estimation of the spectral absorption coefficients of phytoplankton in the sea. *Bulletin of Marine Science*, 37, 634–642.
- Kostadinov TS, Siegel DA, Maritorena S, Guillocheau N, 2007 Ocean color observations and modeling for an optically complex site: Santa Barbara Channel, California, USA. *Journal of Geophysical Research*, 112, C07011 doi: 07010.01029/02006JC003526.
- Krasnopolsky VM, Schiller H, 2003 Some neural network applications in environmental sciences. Part I: forward and inverse problems in geophysical remote measurements. *Neural Networks*, 16, 321–334. [PubMed: 12672428]
- Kuchinke C, Gordon H, Harding L, Voss K, 2009a Spectral optimization for constituent retrieval in Case 2 waters II: Validation study in the Chesapeake Bay. *Remote Sensing of Environment*, 113, 610–621.
- Kuchinke CP, Gordon HR, Franz BA, 2009b Spectral optimization for constituent retrieval in Case 2 waters I: Implementation and performance. *Remote Sensing of Environment*, 113, 571587.
- Lagerloef G, Colomb FR, Le Vine D, Wentz F, Yueh S, Ruf C, Lilly J, Gunn J, Chao YI, Decharon A, Feldman G, Swift C, 2008 The Aquarius/SAC-D mission - Designed to meet the salinity remote-sensing challenge. *Oceanography*, 21, 68–81.
- Lee ME, Lewis MR, 2003 A new method for the measurement of the optical volume scattering function in the upper ocean. *Journal of Atmospheric and Oceanic Technology*, 20, 563–571.
- Lee ZP, Arnone R, Hu CM, Werdell PJ, Lubac B, 2010 Uncertainties of optical parameters and their propagations in an analytical ocean color inversion algorithm. *Applied Optics*, 49, 369–381. [PubMed: 20090801]
- Lee ZP, Carder KL, Arnone RA, 2002 Deriving inherent optical properties from water color: a multiband quasi-analytical algorithm for optically deep waters. *Appl. Opt*, 41, 57555772.
- Lee ZP, Carder KL, Chen RF, Peacock TG, 2001 Properties of the water column and bottom derived from AVIRIS data. *J Geophys Res Oceans*, 106, 11639–11652.
- Lee ZP, Carder KL, Du K, 2004 Effects of molecular and particle scatterings on the model parameter for remote-sensing reflectance. *Applied Optics*, 43, 4957–4964. [PubMed: 15449482]
- Lee ZP, Carder KL, Hawes SK, Steward RG, Peacock TG, Davis CO, 1994 Model for the interpretation of hyperspectral remote-sensing reflectance. *Appl. Opt*, 33, 5721–5732. [PubMed: 20935974]
- Lee ZP, Carder KL, Mobley CD, Steward RG, Patch JS, 1998a Hyperspectral Remote Sensing for Shallow Waters. I. A Semianalytical Model. *Appl. Opt*, 37, 6329–6338. [PubMed: 18286131]
- Lee ZP, Carder KL, Mobley CD, Steward RG, Patch JS, 1999 Hyperspectral remote sensing for shallow waters: 2. Deriving bottom depths and water properties by optimization. *Applied Optics*, 38, 3831–3843. [PubMed: 18319990]
- Lee ZP, Carder KL, Peacock TG, Davis CO, Mueller JL, 1996a Method to derive ocean absorption coefficients from remote-sensing reflectance. *Applied Optics*, 35, 453–462. [PubMed: 21069030]
- Lee ZP, Carder KL, Steward R, Peacock T, Davis C, Patch J, 1998b An empirical algorithm for light absorption by ocean water based on color. *Journal of Geophysical Research: Oceans*, 103, 27967–27978.
- Lee ZP, Carder KL, Steward RG, Perry MJ, 1996b Estimating primary production at depth from remote sensing. *Applied Optics*, 35, 463–474. [PubMed: 21069031]

- Lee ZP, Du KP, Voss KJ, Zibordi G, Lubac B, Arnone R, Weidemann A, 2011 An inherent-optical-property-centered approach to correct the angular effects in water-leaving radiance. *Applied Optics*, 50, 3155–3167. [PubMed: 21743515]
- Lee ZP, Hu C, Shang S, Du K, Lewis M, Arnone R, Brewin R, 2013 Penetration of UV -visible solar radiation in the global oceans: Insights from ocean color remote sensing. *Journal of Geophysical Research: Oceans*, 118, 4241–4255.
- Lee ZP, Lubac B, Werdell PJ, Arnone R, 2009 An update of the Quasi-Analytical Algorithm (QAA_v5) Technical report: International Ocean Colour Coordinating Group (IOCCG) <http://www.ioccg.org/groups/software.html> IOCCG.
- Lee ZP, Wei JW, Voss K, Lewis M, Bricaud A, Huot Y, 2015 Hyperspectral absorption coefficient of "pure" seawater in the range of 350–550 nm inverted from remote sensing reflectance. *Applied Optics*, 54, 546–558.
- Lefering I, Bengil F, Trees C, Röttgers R, Bowers D, Nimmo-Smith A, Schwarz J, McKee D, 2016 Optical closure in marine waters from in situ inherent optical property measurements. *Optics Express*, 24, 14036–14052. [PubMed: 27410565]
- Lenoble J, 1956 Sur le rôle des principaux sels dans l'absorption ultraviolette de l'eau de mer. *Comptes Rendus Hebdomadaires des Séances de l'Académie des Sciences*, 242, 806–808.
- Li W, Stamnes K, Spurr R, Stamnes J, 2008 Simultaneous retrieval of aerosol and ocean properties by optimal estimation: SeaWiFS case studies for the Santa Barbara Channel. *Int. J. Remote Sens*, 29, 5689–5698.
- Lin J, Cao W, Zhou W, Hu S, Wang G, Sun Z, Xu Z, Song Q, 2013 A bio-optical inversion model to retrieve absorption contributions and phytoplankton size structure from total minus water spectral absorption using genetic algorithm. *Chinese journal of oceanology and limnology*, 31, 970–978.
- Liu C-C, Miller RL, 2008 Spectrum matching method for estimating the chlorophyll-a concentration, CDOM ratio, and backscatter fraction from remote sensing of ocean color. *Canadian Journal of Remote Sensing*, 34, 343–355.
- Lohrenz SE, 2000 A novel theoretical approach to correct for pathlength amplification and variable sampling loading in measurements of particulate spectral absorption by the quantitative filter technique. *Journal of plankton research*, 22, 639–657.
- Lohrenz SE, Carroll CL, Weidemann AD, Tuel M, 2003 Variations in phytoplankton pigments, size structure and community composition related to wind forcing and water mass properties on the North Carolina inner shelf. *Continental Shelf Research*, 23, 1447–1464.
- Loisel H, Duforet L, Dessailly D, Chami M, Dubuisson P, 2008 Investigation of the variations in the water leaving polarized reflectance from the POLDER satellite data over two biogeochemical contrasted oceanic areas. *Optics Express*, 16, 12905–12918. [PubMed: 18711530]
- Loisel H, Morel A, 1998 Light scattering and chlorophyll concentration in case 1 waters: A reexamination. *Limnology and Oceanography*, 43, 847–858.
- Loisel H, Nicolas JM, Deschamps PY, Frouin R, 2002 Seasonal and inter-annual variability of particulate organic matter in the global ocean. *Geophysical Research Letters*, 29, 10.1029/2002gl015948.
- Loisel H, Stramski D, 2000 Estimation of the inherent optical properties of natural waters from the irradiance attenuation coefficient and reflectance in the presence of Raman scattering. *Applied Optics*, 39, 3001–3011. [PubMed: 18345226]
- Lotsberg J, Stamnes J, 2010 Impact of particulate oceanic composition on the radiance and polarization of underwater and backscattered light. *Optics Express*, 18, 10432–10445. [PubMed: 20588898]
- Lou X, Hu C, 2014 Diurnal changes of a harmful algal bloom in the East China Sea: Observations from GOCI. *Remote Sensing of Environment*, 140, 562–572.
- Maffione RA, Dana DR, 1997 Recent measurements of the spectral backward-scattering coefficient in coastal waters. *Proceedings SPIE* (pp. 154–159): SPIE International Society for Optical Engineering.
- Mannino A, Novak MG, Hooker SB, Hyde K, Aurin D, 2014 Algorithm development and validation of CDOM properties for estuarine and continental shelf waters along the northeastern US coast. *Remote Sensing of Environment*, 152, 576–602.

- Mannino A, Russ ME, Hooker SB, 2008 Algorithm development and validation for satellite-derived distributions of DOC and CDOM in the U.S. Middle Atlantic Bight. *J. Geophys. Res.*, 113, doi: 10.1029/2007JC004493.
- Mannino A, Signorini SR, Novak MG, Wilkin J, Friedrichs MAM, Najjar RG, 2016 Dissolved organic carbon fluxes in the Middle Atlantic Bight: An integrated approach based on satellite data and ocean model products. *Journal of Geophysical Research-Biogeosciences*, 121, 312–336. [PubMed: 29201582]
- Maritorena S, d'Andon OHF, Mangin A, Siegel DA, 2010 Merged satellite ocean color data products using a bio-optical model: Characteristics, benefits and issues. *Remote Sensing of Environment*, 114, 1791–1804.
- Maritorena S, Siegel DA, 2005 Consistent merging of satellite ocean color data sets using a bio-optical model. *Remote Sensing of Environment*, 94, 429–440.
- Maritorena S, Siegel DA, Peterson AR, 2002 Optimization of a semianalytical ocean color model for global-scale applications. *Applied Optics*, 41, 2705–2714. [PubMed: 12027157]
- Marra J, Trees CC, O'Reilly JE, 2007 Phytoplankton pigment absorption: A strong predictor of primary productivity in the surface ocean. *Deep-Sea Research Part I-Oceanographic Research Papers*, 54, 155–163.
- Mason JD, Cone MT, Fry ES, 2016 Ultraviolet (250–550 nm) absorption spectrum of pure water. *Applied Optics*, 55, 7163–7172. [PubMed: 27607297]
- Matsuoka A, Bricaud A, Benner R, Para J, Sempere R, Prieur L, Belanger S, Babin M, 2012 Tracing the transport of colored dissolved organic matter in water masses of the Southern Beaufort Sea: relationship with hydrographic characteristics. *Biogeosciences*, 9, 925–940.
- Matthews MW, Bernard S, Robertson L, 2012 An algorithm for detecting trophic status (chlorophyll-a), cyanobacterial-dominance, surface scums and floating vegetation in inland and coastal waters. *Remote Sensing of Environment*, 124, 637–652.
- McKee D, Piskozub J, Röttgers R, Reynolds RA, 2013 Evaluation and improvement of an iterative scattering correction scheme for in situ absorption and attenuation measurements. *Journal of Atmospheric and Oceanic Technology*, 30, 1527–1541.
- McKinna LI, Werdell PJ, Proctor CW, 2016 Implementation of an analytical Raman scattering correction for satellite ocean-color processing. *Optics Express*, 24, A1123–A1137. [PubMed: 27410899]
- McKinna LIW, 2015 Three decades of ocean-color remote-sensing *Trichodesmium* spp. in the World's oceans: A review. *Progress in Oceanography*, 131, 177–199.
- McKinna LIW, Fearn PRC, Weeks SJ, Werdell PJ, Reichstetter M, Franz BA, Shea DM, Feldman GC, 2015 A semianalytical ocean color inversion algorithm with explicit water-column depth and substrate reflectance parameterization. *Journal of Geophysical Research: Oceans*, 120, 10.1002/2014JC010224.
- Mélin F, Clerici M, Zibordi G, Holben B, Smirnov A, 2010 Validation of SeaWiFS and MODIS aerosol products with globally distributed AERONET data. *Remote Sensing of Environment*, 114, 230–250.
- Mélin F, Franz BA, 2014 Assessment of satellite ocean colour radiometry and derived geophysical products *Optical Radiometry for Ocean Climate Measurements. Series: Experimental Methods in the Physical Sciences, ISBN: 9780124170117 Elsevier, vol. 47, pp. 609–638, 47, 609–638.*
- Mélin F, Sclep G, Jackson T, Sathyendranath S, 2016 Uncertainty estimates of remote sensing reflectance derived from comparison of ocean color satellite data sets. *Remote Sensing of Environment*, 177, 107–124.
- Mélin F, Vantrepotte V, 2015 How optically diverse is the coastal ocean? *Remote Sensing of Environment*, 160, 235–251.
- Miller RL, Belz M, Castillo CD, Trzaska R, 2002 Determining CDOM absorption spectra in diverse coastal environments using a multiple pathlength, liquid core waveguide system. *Continental Shelf Research*, 22, 1301–1310.
- Mitchell BG, 1990 Algorithms for determining the absorption coefficient for aquatic particulates using the quantitative filter technique Orlando 90, 16-20 4 (pp. 137–148): International Society for Optics and Photonics.

- Mitchell BG, Kahru M, Wieland J, Stramska M, 2003 Determination of spectral absorption coefficients of particles, dissolved material and phytoplankton for discrete water samples In Mueller JL, Fargion GS, McClain CR (Eds.), *Ocean Optics Protocols For Satellite Ocean Color Sensor Validation*, NASA/TM-2003-211621 (pp. 39–64). Greenbelt, MD, USA: NASA Goddard Space Flight Center.
- Mitchell GB, Holm-Hansen O, 1991 Bio-optical properties of Antarctic Peninsula waters: differentiation from temperate ocean models. *Deep Sea Research Part A. Oceanographic Research Papers*, 38, 1009–1028.
- Mobley CD, 1994 *Light and Water: Radiative Transfer in Natural Waters*: Academic Press.
- Mobley CD, 2015 Polarized reflectance and transmittance properties of windblown sea surfaces. *Applied Optics*, 54, 4828–4849. [PubMed: 26192522]
- Mobley CD, Gentili B, Gordon HR, Jin Z, Kattawar GW, Morel A, Reinersman P, Stavn RH, 1993 Comparison of numerical models for computing underwater light fields. *Applied Optics*, 32, 7484–7504. [PubMed: 20861969]
- Mobley CD, Sundman LK, 2008 HYDROLIGHT 5 ECOLIGHT 5. Sequoia Scientific Inc.
- Mobley CD, Sundman LK, Boss E, 2002 Phase function effects on oceanic light fields. *Applied Optics*, 41, 1035–1050. [PubMed: 11900122]
- Mobley CD, Sundman LK, Davis CO, Bowles JH, Downes TV, Leathers RA, Montes MJ, Bissett WP, Kohler DD, Reid RP, 2005 Interpretation of hyperspectral remote-sensing imagery by spectrum matching and look-up tables. *Applied Optics*, 44, 35763592.
- Mobley CD, Werdell J, Franz B, Ahmad Z, Bailey S, 2016 Atmospheric correction for satellite ocean color radiometry. *NASA Technical Memorandum*, 217551, 85 pp.
- Moisan JR, Moisan TAH, Linkswiler MA, 2011 An inverse modeling approach to estimating phytoplankton pigment concentrations from phytoplankton absorption spectra. *Journal of Geophysical Research-Oceans*, 116, 10.1029/2010JC006786.
- Moore L, Goericke R, Chisholm S, 1995 The comparative physiology of *Synechococcus* and *Prochlorococcus* isolated from the subtropical open ocean: growth regulation by light and temperature. *Mar. Ecol. Prog. Ser.*, 116, 259–275.
- Moore TS, Campbell JW, Dowell MD, 2009 A class-based approach to characterizing and mapping the uncertainty of the MODIS ocean chlorophyll product. *Remote Sensing of Environment*, 113, 2424–2430.
- Moore TS, Campbell JW, Feng H, 2001 A fuzzy logic classification scheme for selecting and blending satellite ocean color algorithms. *IEEE Transactions on Geoscience and Remote sensing*, 39, 1764–1776.
- Moore TS, Campbell JW, Feng H, 2015 Characterizing the uncertainties in spectral remote sensing reflectance for SeaWiFS and MODIS-Aqua based on global in situ matchup data sets. *Remote Sensing of Environment*, 159, 14–27.
- Moore TS, Dowell MD, Bradt S, Verdu AR, 2014 An optical water type framework for selecting and blending retrievals from bio-optical algorithms in lakes and coastal waters. *Remote Sensing of Environment*, 143, 97–111. [PubMed: 24839311]
- Morel A, 1968 Note au sujet des constantes de diffusion de la lumière pour l'eau et l'eau de mer optiquement pures. *Cah. Oceanogr*, 20, 157–162.
- Morel A, (Ed.) 1974 *Optical properties of pure water and pure seawater*. London and New York: Academic Press.
- Morel A, 1988 Optical modeling of the upper ocean in relation to its biogenous matter content (Case I waters). *Journal of Geophysical Research*, 93, 10749–10768.
- Morel A, Antoine D, Gentili B, 2002 Bidirectional reflectance of oceanic waters: accounting for Raman emission and varying particle scattering phase function. *Applied Optics*, 41, 62896306.
- Morel A, Gentili B, 1993 Diffuse reflectance of oceanic waters. II. Bidirectional aspects. *Applied Optics*, 32, 6864–6879. [PubMed: 20856540]
- Morel A, Gentili B, Claustre H, Babin M, Bricaud A, Ras J, Tieche F, 2007 Optical properties of the "clearest" natural waters. *Limnology and Oceanography*, 52, 217–229.
- Morel A, Loisel H, 1998 Apparent optical properties of oceanic water: dependence on the molecular scattering contribution. *Applied Optics*, 37, 4765–4776. [PubMed: 18285934]

- Morel A, Maritorena S, 2001 Bio-optical properties of oceanic waters: A reappraisal. *J Geophys Res Oceans*, 106, 7163–7180.
- Morel A, Prieur L, 1977 Analysis of variations in ocean color I. *Limnology and Oceanography*, 22, 709–722.
- Morrow J, Chamberlin W, Kiefer D, 1989 A two-component description of spectral absorption by marine particles. *Limnology and Oceanography*, 34, 1500–1509.
- Moses WJ, Ackleson SG, Hair JW, Hostetler CA, Miller WD, 2016 Spatial scales of optical variability in the coastal ocean: Implications for remote sensing and in situ sampling. *Journal of Geophysical Research: Oceans*, 121, 4194–4208.
- Murakami H, 2016 Ocean color estimation by Himawari-8/AHI. *Proceedings SPIE*, 9878, 10.1117/1.112.2225422.
- Nelson N, Siegel D, Michaels A, 1998 Seasonal dynamics of colored dissolved material in the Sargasso Sea. *Deep Sea Research Part I: Oceanographic Research Papers*, 45, 931–957.
- Nelson NB, Siegel DA, 2002 Chromophoric DOM in the open ocean In Hansell DA, Carlson CA (Eds.), *Biogeochemistry of Marine Dissolved Organic Matter* (pp. 547–578). San Diego, California: Academic Press.
- Neukermans G, Reynolds RA, Stramski D, 2014 Contrasting inherent optical properties and particle characteristics between an under-ice phytoplankton bloom and open water in the Chukchi Sea. *Deep Sea Research Part II: Topical Studies in Oceanography*, 105, 59–73.
- Neukermans G, Reynolds RA, Stramski D, 2016 Optical classification and characterization of marine particle assemblages within the western Arctic Ocean. *Limnology and Oceanography*, 61, 1472–1494.
- Neukermans G, Ruddick K, Bernard E, Ramon D, Nechad B, Deschamps P-Y, 2009 Mapping total suspended matter from geostationary satellites: a feasibility study with SEVIRI in the Southern North Sea. *Optics Express*, 17, 14029–14052. [PubMed: 19654812]
- Neukermans G, Ruddick KG, Greenwood N, 2012 Diurnal variability of turbidity and light attenuation in the southern North Sea from the SEVIRI geostationary sensor. *Remote Sensing of Environment*, 124, 564–580.
- Ogura N, Hanya T, 1966 Nature of ultra-violet absorption of sea water. *Nature*, 212, 758–758.
- Oishi T, 1990 Significant relationship between the backward scattering coefficient of sea water and the scatterance at 120. *Applied Optics*, 29, 4658–4665. [PubMed: 20577448]
- Organelli E, Bricaud A, Antoine D, Uitz J, 2013 Multivariate approach for the retrieval of phytoplankton size structure from measured light absorption spectra in the Mediterranean Sea (BOUSSOLE site). *Applied Optics*, 52, 2257–2273. [PubMed: 23670753]
- Pahlevan N, Lee Z, Wei J, Schaaf CB, Schott JR, Berk A, 2014 On-orbit radiometric characterization of OLI (Landsat-8) for applications in aquatic remote sensing. *Remote Sensing of Environment*, 154, 272–284.
- Pahlevan N, Roger J-C, Ahmad Z, 2017 Revisiting short-wave-infrared (SWIR) bands for atmospheric correction in coastal waters. *Optics Express*, 25, 6015–6035. [PubMed: 28380959]
- Park Y-J, Ruddick K, 2005 Model of remote-sensing reflectance including bidirectional effects for case 1 and case 2 waters. *Applied Optics*, 44, 1236–1249. [PubMed: 15765704]
- Pegau WS, Gray D, Zaneveld JRV, 1997 Absorption and attenuation of visible and nearinfrared light in water: dependence on temperature and salinity. *Applied Optics*, 36, 6035–6046. [PubMed: 18259448]
- Pegau WS, Zaneveld RV, Mueller JL, 2003 Volume absorption coefficients: instruments, characterization, field measurements and data analysis protocols In Mueller JL, Fargion GS, McClain CR (Eds.), *Ocean Optics Protocols For Satellite Ocean Color Sensor Validation, NASA/TM-2003-211621* (pp. 27–38). Greenbelt, MD, USA: NASA Goddard Space Flight Center.
- Peschoud C, Minghelli A, Mathieu S, Lei M, Pairaud I, Pinazo C, 2017 Fusion of SunSynchronous and Geostationary Images for Coastal and Ocean Color Survey Application to OLCI (Sentinel-3) and FCI (MTG). *IEEE Journal of Selected Topics in Applied Earth Observations and Remote Sensing*, 10, 45–56.
- Petrenko A, Zaneveld J, Pegau W, Barnard A, Mobley C, 1998 Effects of a thin layer on reflectance and remote-sensing reflectance. *Oceanography*, 11, 48–50.

- Philpot WD, 1987 Radiative transfer in stratified waters: a single-scattering approximation for irradiance. *Appl. Opt.*, 26, 4123–4132. [PubMed: 20490198]
- Pinkerton MH, Moore GF, Lavender SJ, Gall MP, Oubelkheir K, Richardson KM, Boyd PW, Aiken J, 2006 A method for estimating inherent optical properties of New Zealand continental shelf waters from satellite ocean colour measurements. *New Zealand Journal of Marine and Freshwater Research*, 40, 227–247.
- Pope RM, Fry ES, 1997 Absorption spectrum (380–700 nm) of pure water. II. Integrating cavity measurements. *Applied Optics*, 36, 8710–8723. [PubMed: 18264420]
- Poteau A, Boss E, Claustre H, 2017 Particulate concentration and seasonal dynamics in the mesopelagic ocean based on the backscattering coefficient measured with BiogeochemicalArgo floats. *Geophysical Research Letters*, 44, 6933–6939.
- Preisendorfer RW, Mobley CD, 1988 *Principal component analysis in meteorology and oceanography*: Elsevier Amsterdam.
- Press WH, Flannery BP, Teukolsky SA, Vetterling WT, 1992 *Numerical recipes in C: the art of scientific programming*. Section, 10, 408–412.
- Reynolds RA, Stramski D, Neukermans G, 2016 Optical backscattering by particles in Arctic seawater and relationships to particle mass concentration, size distribution, and bulk composition. *Limnology and Oceanography*, 61, 1869–1890.
- Reynolds RW, Rayner NA, Smith TM, Stokes DC, Wang W, 2002 An Improved In Situ and Satellite SST Analysis for Climate. *Journal of Climate*, 15, 1609–1625.
- Robinson W, Franz B, Patt F, Bailey S, Werdell P, 2003 Masks and flags updates. *Algorithm updates for the fourth Sea-WiFS data reprocessing*, NASA Technical Memorandum, 206892, 34–40.
- Roesler CS, 1998 Theoretical and experimental approaches to improve the accuracy of particulate absorption coefficients derived from the quantitative filter technique. *Limnology and Oceanography*, 43, 1649–1660.
- Roesler CS, Boss E, 2003 Spectral beam attenuation coefficient retrieved from ocean color inversion. *Geophysical Research Letters*, 30, 10.1029/2002GL016185.
- Roesler CS, Etheridge SM, Pitcher GC, 2004 Application of an ocean color algal taxa detection model to red tides in the Southern Benguela Steidinger KA, Lansberg JH, Tomas CR, and Vargo GA [eds.]. *Harmful Algae 2002* (pp. 303–305): Florida Fish and Wildlife Conservation Commission, Florida Institute of Oceanography, and Intergovernmental Oceanographic Commission of UNESCO.
- Roesler CS, Perry MJ, 1995 In situ phytoplankton absorption, fluorescence emission, and particulate backscattering spectra determined from reflectance. *J. Geophys. Res.*, 100, 1327913294.
- Roesler CS, Perry MJ, Carder KL, 1989 Modeling in situ phytoplankton absorption from total absorption spectra in productive inland marine waters. *Limnology and Oceanography*, 34, 1510–1523.
- Röttgers R, Doerffer R, 2007 Measurements of optical absorption by chromophoric dissolved organic matter using a point-source integrating-cavity absorption meter. *Limnology and Oceanography: Methods*, 5, 126–135.
- Rottgers R, Dupouy C, Taylor BB, Bracher A, Wozniak SB, 2014 Mass-specific light absorption coefficients of natural aquatic particles in the near-infrared spectral region. *Limnol. Oceanogr.*, 59, 1449–1460.
- Röttgers R, Gehnke S, 2012 Measurement of light absorption by aquatic particles: improvement of the quantitative filter technique by use of an integrating sphere approach. *Applied Optics*, 51, 1336–1351. [PubMed: 22441480]
- Röttgers R, Häse C, Doerffer R, 2007 Determination of the particulate absorption of microalgae using a point-source integrating-cavity absorption meter: verification with a photometric technique, improvements for pigment bleaching, and correction for chlorophyll fluorescence. *Limnology and Oceanography: Methods*, 5, 1–12.
- Röttgers R, McKee D, Utschig C, 2014 Temperature and salinity correction coefficients for light absorption by water in the visible to infrared spectral region. *Optics Express*, 22, 2509325108.
- Rousseaux CS, Gregg WW, 2015 Recent decadal trends in global phytoplankton composition. *Global Biogeochemical Cycles*, 29, 1674–1688.

- Saba VS, Friedrichs MAM, Antoine D, Armstrong RA, Asanuma I, Behrenfeld MJ, Ciotti AM, Dowell M, Hoepffner N, Hyde KJW, Ishizaka J, Kameda T, Marra J, Melin F, Morel A, O'Reilly J, Scardi M, Smith WO, Smyth TJ, Tang S, Uitz J, Waters K, Westberry TK, 2011 An evaluation of ocean color model estimates of marine primary productivity in coastal and pelagic regions across the globe. *Biogeosciences*, 8, 489–503.
- Salama M, Van der Velde R, Van der Woerd H, Kromkamp J, Philippart C, Joseph A, O'Neill P, Lang R, Gish T, Werdell P, 2012 Calibration and validation of geophysical observation models. *Biogeosciences*, 9, 2195.
- Salama MS, Dekker A, Su Z, Mannaerts CM, Verhoef W, 2009 Deriving inherent optical properties and associated inversion-uncertainties in the Dutch Lakes. *Hydrol. Earth Syst. Sci*, 13, 1113–1121.
- Salama MS, Mélin F, Van der Velde R, 2011 Ensemble uncertainty of inherent optical properties. *Optics Express*, 19, 16772–16783. [PubMed: 21935039]
- Salinas SV, Chang CW, Liew SC, 2007 Multiparameter retrieval of water optical properties from above-water remote-sensing reflectance using the simulated annealing algorithm. *Applied Optics*, 46, 2727–2742. [PubMed: 17446923]
- Sathyendranath S, Cota G, Stuart V, Maass H, Platt T, 2001 Remote sensing of phytoplankton pigments: a comparison of empirical and theoretical approaches. *International Journal of Remote Sensing*, 22, 249–273.
- Sathyendranath S, Platt T, 1988 The spectral irradiance field at the surface and in the interior of the ocean: a model for applications in oceanography and remote sensing. *J. Geophys. Res*, 93, 9270–9280.
- Sathyendranath S, Prieur L, Morel A, 1989 A three-component model of ocean colour and its application to remote sensing of phytoplankton pigments in coastal waters. *International Journal of Remote Sensing*, 10, 1373–1394.
- Sathyendranath S, Stuart V, Platt T, Bouman H, Ulloa O, Maass H, 2005 Remote sensing of ocean colour: Towards algorithms for retrieval of pigment composition. *Indian Journal of Marine Sciences*, 34, 333–340.
- Schaeffer BA, Loftin K, Stumpf RP, Werdell PJ, 2015 Agencies collaborate, develop a cyanobacteria assessment network. *EOS Trans. AGU*, 96, 16–20.
- Schiller H, Doerffer R, 1999 Neural network for emulation of an inverse model operational derivation of Case II water properties from MERIS data. *International Journal of Remote Sensing*, 20, 1735–1746.
- Schofield O, Bergmann T, Oliver M, Irwin A, Bissett P, Moline M, Orrico C, 2004 Inversion of the bulk absorption in the Mid-Atlantic Bight and its utility for water mass analysis in optically complex coastal waters. *J. Geophys. Res*, 109, 10.1029/2003JC002071.
- Sheng MA, Yang X, Tao Z, Li Z, Zhou X, 2014 Assessment of uncertainties of ocean color parameters for the ocean Carbon-based Productivity Model. *IOP Conference Series: Earth and Environmental Science*, 17, 012102.
- Shifrin K, 1988 *Physical optics of ocean water*. New York: American Institute of Physics.
- Siegel DA, Buesseler KO, Doney SC, Sailley SF, Behrenfeld MJ, Boyd PW, 2014 Global assessment of ocean carbon export by combining satellite observations and food-web models. *Global Biogeochemical Cycles*, 28, 181–196.
- Siegel DA, Maritorea S, Nelson NB, Behrenfeld MJ, McClain CR, 2005 Colored dissolved organic matter and its influence on the satellite-based characterization of the ocean biosphere. *Geophysical Research Letters*, 32, 10.1029/2005gl024310.
- Simeon J, Roesler C, Pegau WS, Dupouy C, 2003 Sources of spatial variability in light absorbing components along an equatorial transect from 165 E to 150 W. *Journal of Geophysical Research: Oceans*, 108, 10.1029/2002JC001613.
- Slade WH, Boss ES, 2006 Calibrated near-forward volume scattering function obtained from the LISST particle sizer. *Optics Express*, 14, 3602–3615. [PubMed: 19516507]
- Slade WH, Ransom HW, Musavi MT, Miller RL, 2004 Inversion of ocean color observations using particle swarm optimization. *Geoscience and Remote Sensing, IEEE Transactions on*, 42, 1915–1923.

- Smith RC, 1981 Remote sensing and depth distribution of ocean chlorophyll. *Marine Ecology Progress Series*, 359–361.
- Smith RC, Baker KS, 1981 Optical-Properties of the Clearest Natural-Waters (200–800 Nm). *Applied Optics*, 20, 177–184. [PubMed: 20309088]
- Smyth TJ, Moore GF, Hirata T, Aiken J, 2006 Semianalytical model for the derivation of ocean color inherent optical properties: description, implementation, and performance assessment. *Applied Optics*, 45, 8116–8131. [PubMed: 17068554]
- Sobiechowska-Sasim M, Ston-Egiert J, Kosakowska A, 2014 Quantitative analysis of extracted phycobilin pigments in cyanobacteria - an assessment of spectrophotometric and spectrofluorometric methods. *Journal of Applied Phycology*, 26, 2065–2074. [PubMed: 25346572]
- Soja-Wo niak M, Darecki M, Wojtasiewicz B, Bradtke K, 2017 Laboratory measurements of remote sensing reflectance of selected phytoplankton species from the Baltic Sea. *Oceanologia*, 10.1016/j.oceano.2017.1008.1001.
- Spurr R, Stamnes K, Eide H, Li W, Zhang K, Stamnes J, 2007 Simultaneous retrieval of aerosols and ocean properties: A classic inverse modeling approach. I. Analytic Jacobians from the linearized CAO-DISORT model. *Journal of Quantitative Spectroscopy and Radiative Transfer*, 104, 428–449.
- Stamnes K, Li W, Yan B, Eide H, Barnard A, Pegau WS, Stamnes JJ, 2003 Accurate and self-consistent ocean color algorithm: simultaneous retrieval of aerosol optical properties and chlorophyll concentrations. *Applied Optics*, 42, 939–951. [PubMed: 12617208]
- Stavn RH, Richter SJ, 2008 Biogeo-optics: particle optical properties and the partitioning of the spectral scattering coefficient of ocean waters. *Applied Optics*, 47, 2660–2679. [PubMed: 18470263]
- Steinmetz F, Deschamps P-Y, Ramon D, 2011 Atmospheric correction in presence of sun glint: application to MERIS. *Optics Express*, 19, 9783–9800. [PubMed: 21643235]
- Stramska M, 2009 Particulate organic carbon in the global ocean derived from SeaWiFS ocean color. *Deep-Sea Research Part I-Oceanographic Research Papers*, 56, 1459–1470.
- Stramska M, Stramski D, 2005 Variability of particulate organic carbon concentration in the north polar Atlantic based on ocean color observations with Sea-viewing Wide Field-of-view Sensor (SeaWiFS). *Journal of Geophysical Research*, 110, C10018, 10.1029/2004JC002762.
- Stramska M, Stramski D, Hapter R, Kaczmarek S, Sto J, 2003 Bio-optical relationships and ocean color algorithms for the north polar region of the Atlantic. *Journal of Geophysical Research*, 108(C5), 3143, 10.1029/2001JC001195.
- Stramski D, 1990 Artifacts in measuring absorption spectra of phytoplankton collected on a filter. *Limnol. Oceanogr*, 35, 1804–1809.
- Stramski D, Babin M, Wo niak SB, 2007 Variations in the optical properties of terrigenous mineral-rich particulate matter suspended in seawater. *Limnology and Oceanography*, 52, 2418–2433.
- Stramski D, Boss E, Bogucki D, Voss KJ, 2004a The role of seawater constituents in light backscattering in the ocean. *Progress in Oceanography*, 61, 27–56.
- Stramski D, Bricaud A, Morel A, 2001 Modeling the inherent optical properties of the ocean based on the detailed composition of the planktonic community. *Applied Optics*, 40, 2929–2945. [PubMed: 18357311]
- Stramski D, Reynolds RA, Kaczmarek S, Uitz J, Zheng G, 2015 Correction of pathlength amplification in the filter-pad technique for measurements of particulate absorption coefficient in the visible spectral region. *Applied Optics*, 54, 6763–6782. [PubMed: 26368092]
- Stramski D, Reynolds RA, Kahru M, Mitchell BG, 1999 Estimation of particulate organic carbon in the ocean from satellite remote sensing. *Science*, 285, 239–242. [PubMed: 10398597]
- Stramski D, Wozniak SB, Flatau P, 2004b Optical properties of Asian mineral dust suspended in seawater. *Limnol. Oceanogr*, 49, 749–755.
- Stockley ND, Rottgers R, McKee D, Lefering I, Sullivan JM, Twardowski MS, 2017 Assessing uncertainties in scattering correction algorithms for reflective tube absorption measurements made with a WET Labs ac-9. *Optics Express*, 25, A1139, doi:10.1364/OE.25.0A1139. [PubMed: 29220991]

- Sullivan JM, Twardowski MS, 2009 Angular shape of the oceanic particulate volume scattering function in the backward direction. *Applied Optics*, 48, 6811–6819. [PubMed: 20011022]
- Sullivan JM, Twardowski MS, Ronald J, Zaneveld V, Moore CC, 2013 Measuring optical backscattering in water. *Light Scattering Reviews* 7, 189–224.
- Sullivan JM, Twardowski MS, Zaneveld JRV, Moore CM, Barnard AH, Donaghay PL, Rhoades B, 2006 Hyperspectral temperature and salt dependencies of absorption by water and heavy water in the 400–750 nm spectral range. *Applied Optics*, 45, 5294–5309. [PubMed: 16826267]
- Sydor M, Gould RW, Arnone RA, Haltrin VI, Goode W, 2004 Uniqueness in remote sensing of the inherent optical properties of ocean water. *Applied Optics*, 43, 2156–2162. [PubMed: 15074426]
- Tanaka A, Kishino M, Doerffer R, Schiller H, Oishi T, Kubota T, 2004 Development of a neural network algorithm for retrieving concentrations of chlorophyll, suspended matter and yellow substance from radiance data of the ocean color and temperature scanner. *Journal of Oceanography*, 60, 519–530.
- Tassan S, Ferrari GM, 1995 An alternative approach to absorption measurements of aquatic particles retained on filters. *Limnology and Oceanography*, 40, 1358–1368.
- Tassan S, Ferrari GM, 2003 Variability of light absorption by aquatic particles in the nearinfrared spectral region. *Applied Optics*, 42, 4802–4810. [PubMed: 12952323]
- Taylor KE, 2001 Summarizing multiple aspects of model performance in a single diagram. *Journal of Geophysical Research: Atmospheres*, 106, 7183–7192.
- Tonizzo A, Twardowski M, McLean S, Voss K, Lewis M, Trees C, 2017 Closure and uncertainty assessment for ocean color reflectance using measured volume scattering functions and reflective tube absorption coefficients with novel correction for scattering. *Applied Optics*, 56, 130–146.
- Torrecilla E, Stramski D, Reynolds RA, Millan-Nunez E, Piera J, 2011 Cluster analysis of hyperspectral optical data for discriminating phytoplankton pigment assemblages in the open ocean. *Remote Sensing of Environment*, 115, 2578–2593.
- Twardowski M, Zhang X, Vagle S, Sullivan J, Freeman S, Czerski H, You Y, Bi L, Kattawar G, 2012 The optical volume scattering function in a surf zone inverted to derive sediment and bubble particle subpopulations. *Journal of Geophysical Research: Oceans*, 117, 10.1029/2011JC007347.
- Twardowski MS, Boss E, Macdonald JB, Pegau WS, Barnard AH, Zaneveld JRV, 2001 A model for estimating bulk refractive index from the optical backscattering ratio and the implications for understanding particle composition in case I and case II waters. *Journal of Geophysical Research: Oceans*, 106, 14129–14142.
- Twardowski MS, Boss E, Sullivan JM, Donaghay PL, 2004 Modeling the spectral shape of absorption by chromophoric dissolved organic matter. *Marine Chemistry*, 89, 69–88.
- Twardowski MS, Sullivan JM, Donaghay PL, Zaneveld JRV, 1999 Microscale quantification of the absorption by dissolved and particulate material in coastal waters with an ac-9. *Journal of Atmospheric and Oceanic Technology*, 16, 691–707.
- Twomey S, 1977 Introduction to the mathematics of inversion in remote sensing and the indirect measurements. New York: Elsevier.
- Tzortziou M, Herman JR, Gallegos CL, Neale PJ, Subramaniam A, Harding LW, Jr., Ahmad Z, 2006 Bio-optics of the Chesapeake Bay from measurements and radiative transfer closure. *Estuar. Coast. Shelf Sci*, 68, 348–362.
- Tzortziou M, Neale PJ, Megonigal JP, Pow CL, Butterworth M, 2011 Spatial gradients in dissolved carbon due to tidal marsh outwelling into a Chesapeake Bay estuary. *Marine Ecology Progress Series*, 426, 41–56.
- Tzortziou M, Osburn CL, Neale PJ, 2007 Photobleaching of dissolved organic material from a tidal marsh-estuarine system of the Chesapeake Bay. *Photochemistry and photobiology*, 83, 782–792. [PubMed: 17645648]
- Uitz J, Claustre H, Gentili B, Stramski D, 2010 Phytoplankton class-specific primary production in the world's oceans: Seasonal and interannual variability from satellite observations. *Global Biogeochemical Cycles*, 24, GB3016, doi:10.1029/2009GB003680.
- Uitz J, Stramski D, Reynolds RA, Dubranna J, 2015 Assessing phytoplankton community composition from hyperspectral measurements of phytoplankton absorption coefficient and remote-sensing reflectance in open-ocean environments. *Remote Sensing of Environment*, 171, 58–74.

- Ulloa O, Sathyendranath S, Platt T, 1994 Effect of the particle-size distribution on the backscattering ratio in seawater. *Applied Optics*, 33, 7070–7077. [PubMed: 20941259]
- Vaillancourt RD, Brown CW, Guillard RR, Balch WM, 2004 Light backscattering properties of marine phytoplankton: relationships to cell size, chemical composition and taxonomy. *Journal of plankton research*, 26, 191–212.
- Valente A, Sathyendranath S, Brotas V, Groom S, Grant M, Taberner M, Antoine D, Arnone R, Balch WM, Barker K, Barlow R, Belanger S, Berthon JF, Besiktepe S, Brando V, Canuti E, Chavez F, Claustre H, Crout R, Frouin R, Garcia-Soto C, Gibb S, Gould R, Hooker S, Kahru M, Klein H, Kratzer S, Loisel H, Mckee D, Mitchell BG, Moisan T, Muller-Karger F, O'Dowd L, Ondrusek M, Poulton AJ, Repecaud M, Smyth T, Sosik HM, Twardowski M, Voss K, Werdell J, Wernand M, Zibordi G, 2016 A compilation of global bio-optical in situ data for ocean-colour satellite applications. *Earth System Science Data*, 8, 235–252.
- van de Hulst HC, 1957 Light scattering by small particles: Courier Corporation.
- Van Der Woerd HJ, Pasterkamp R, 2008 HYDROPT: A fast and flexible method to retrieve chlorophyll-a from multispectral satellite observations of optically complex coastal waters. *Remote Sensing of Environment*, 112, 1795–1807.
- Vandermeulen RA, Mannino A, Neeley A, Werdell J, Arnone R, 2017 Determining the optimal spectral sampling frequency and uncertainty thresholds for hyperspectral remote sensing of ocean color. *Optics Express*, 25, A785–A797. [PubMed: 29041046]
- Vanhellemont Q, Neukermans G, Ruddick K, 2014 Synergy between polar-orbiting and geostationary sensors: Remote sensing of the ocean at high spatial and high temporal resolution. *Remote Sensing of Environment*, 146, 49–62.
- Vanhellemont Q, Ruddick K, 2014 Turbid wakes associated with offshore wind turbines observed with Landsat 8. *Remote Sensing of Environment*, 145, 105–115.
- Vanhellemont Q, Ruddick K, 2015 Advantages of high quality SWIR bands for ocean colour processing: Examples from Landsat-8. *Remote Sensing of Environment*, 161, 89–106.
- Vanhellemont Q, Ruddick K, 2016 AOLITE For Sentinel-2: Aquatic Applications of MSI Imagery. ESA Living Planet Symposium (pp. 9–13). Prague, Czech Republic.
- Vantrepotte V, Danhiez FP, Loisel H, Ouillon S, Meriaux X, Cauvin A, Dessailly D, 2015 CDOM-DOC relationship in contrasted coastal waters: implication for DOC retrieval from ocean color remote sensing observation. *Optics Express*, 23, 33–54. [PubMed: 25835652]
- Vantrepotte V, Loisel H, Dessailly D, Meriaux X, 2012 Optical classification of contrasted coastal waters. *Remote Sensing of Environment*, 123, 306–323.
- Verrelst J, Camps-Valls G, Muñoz-Marí J, Rivera JP, Veroustraete F, Clevers JG, Moreno J, 2015 Optical remote sensing and the retrieval of terrestrial vegetation biogeophysical properties—A review. *ISPRS Journal of Photogrammetry and Remote Sensing*, 108, 273–290.
- Vodacek A, Blough NV, DeGrandpre MD, Peltzer ET, Nelson RK, 1997 Seasonal variation of CDOM and DOC in the Middle Atlantic Bight: Terrestrial inputs and photooxidation. *Limnology and Oceanography*, 42, 674–686.
- Walrafen G, 1967 Raman spectral studies of the effects of temperature on water structure. *The Journal of Chemical Physics*, 47, 114–126.
- Walrafen G, Fisher M, Hokmabadi M, Yang WH, 1986 Temperature dependence of the low-and high-frequency Raman scattering from liquid water. *The Journal of Chemical Physics*, 85, 6970–6982.
- Wang G, Cao W, Yang D, Zhao J, 2008 Partitioning particulate absorption coefficient into contributions of phytoplankton and nonalgal particles: A case study in the northern South China Sea. *Estuar. Coast. Shelf Sci*, 78, 513–520.
- Wang P, Boss ES, Roesler C, 2005 Uncertainties of inherent optical properties obtained from semianalytical inversions of ocean color. *Applied Optics*, 44, 4074–4085. [PubMed: 16004055]
- Werdell PJ, Bailey SW, 2005 An improved in-situ bio-optical data set for ocean color algorithm development and satellite data product validation. *Remote Sensing of Environment*, 98, 122–140.
- Werdell PJ, Bailey SW, Franz BA, Harding LW, Jr., Feldman GC, McClain CR, 2009 Regional and seasonal variability of chlorophyll-a in Chesapeake Bay as observed by SeaWiFS and MODIS-Aqua. *Remote Sensing of Environment*, 113, 1319–1330.

- Werdell PJ, Franz BA, Bailey SW, Feldman GC, Boss E, Brando VE, Dowell M, Hirata T, Lavender SJ, Lee Z, Loisel H, Maritorena S, Melin F, Moore TS, Smyth TJ, Antoine D, Devred E, d'Andon OH, Mangin A, 2013a Generalized ocean color inversion model for retrieving marine inherent optical properties. *Applied Optics*, 52, 2019–2037. [PubMed: 23545956]
- Werdell PJ, Franz BA, Lefler JT, Robinson WD, Boss E, 2013b Retrieving marine inherent optical properties from satellites using temperature and salinity-dependent backscattering by seawater. *Opt. Express*, 21, 32611–32622. [PubMed: 24514855]
- Werdell PJ, Proctor CW, Boss E, Leeuw T, Ouhssain M, 2013c Underway sampling of marine inherent optical properties on the Tara Oceans expedition as a novel resource for ocean color satellite data product validation. *Methods in Oceanography*, 7, 40–51, doi:10/1016/j.mio.2013.09.001.
- Werdell PJ, Roesler CS, 2003 Remote assessment of benthic substrate composition in shallow waters using multispectral reflectance. *Limnology and Oceanography*, 48, 557–567.
- Werdell PJ, Roesler CS, Goes JI, 2014 Discrimination of phytoplankton functional groups using an ocean reflectance inversion model. *Appl Opt*, 53, 4833–4849. [PubMed: 25090312]
- Westberry TK, Boss E, Lee Z, 2013 Influence of Raman scattering on ocean color inversion models. *Applied Optics*, 52, 5552–5561. [PubMed: 23913078]
- Westberry TK, Schultz P, Behrenfeld MJ, Dunne JP, Hiscock MR, Maritorena S, Sarmiento JL, Siegel DA, 2016 Annual cycles of phytoplankton biomass in the subarctic Atlantic and Pacific Ocean. *Global Biogeochemical Cycles*, 30, 175–190.
- Westberry TK, Siegel DA, 2006 Spatial and temporal distribution of *Trichodesmium* blooms in the world's oceans. *Global Biogeochemical Cycles*, 20, 10.1029/2005gb002673.
- Whitmire AL, Boss E, Cowles TJ, Pegau WS, 2007 Spectral variability of the particulate backscattering ratio. *Optics Express*, 15, 7019–7031. [PubMed: 19547019]
- Whitmire AL, Pegau WS, Karp-Boss L, Boss E, Cowles TJ, 2010 Spectral backscattering properties of marine phytoplankton cultures. *Optics Express*, 18, 15073–15093. [PubMed: 20639993]
- Willmott CJ, Robeson SM, Matsuura K, 2017 Climate and other models may be more accurate than reported. *EOS Trans. AGU*, 98, 10.1029/2017EO074939.
- Wolanin A, Soppa MA, Bracher A, 2016 Investigation of spectral band requirements for improving retrievals of phytoplankton functional types. *Remote Sensing*, 8, 10.3390/rs8100871.
- Woniak SB, Stramski D, Stramska M, Reynolds RA, Wright VM, Miksic EY, Cichocka M, Cieplak AM, 2010 Optical variability of seawater in relation to particle concentration, composition, and size distribution in the nearshore marine environment at Imperial Beach, California. *Journal of Geophysical Research*, 115, C08027, 10.1029/2009JC005554.
- Wynne TT, Stumpf RP, Briggs TO, 2013 Comparing MODIS and MERIS spectral shapes for cyanobacterial bloom detection. *International Journal of Remote Sensing*, 34, 6668–6678.
- Yang Q, Stramski D, He MX, 2013 Modeling the effects of near-surface plumes of suspended particulate matter on remote-sensing reflectance of coastal waters. *Appl Opt*, 52, 359374.
- Zaneveld JRV, 1982 Remotely sensed reflectance and its dependence on vertical structure: a theoretical derivation. *Applied Optics*, 21, 4146–4150. [PubMed: 20401021]
- Zaneveld JRV, 1989 An asymptotic closure theory for irradiance in the sea and its inversion to obtain the inherent optical properties. *Limnology and Oceanography*, 34, 1442–1452.
- Zaneveld JRV, 1995 A theoretical derivation of the dependence of the remotely sensed reflectance of the ocean on the inherent optical properties. *Journal of Geophysical Research: Oceans*, 100, 13135–13142.
- Zaneveld JRV, Kitchen JC, Bricaud A, Moore CC, 1992 Analysis of in-situ spectral absorption meter data San Diego 92 (pp. 187–200): International Society for Optics and Photonics.
- Zaneveld JRV, Kitchen JC, Moore CC, 1994 Scattering error correction of reflecting-tube absorption meters *Ocean Optics X I I* (pp. 44–55): International Society for Optics and Photonics.
- Zhai P-W, Kattawar GW, Yang P, 2008 Impulse response solution to the three-dimensional vector radiative transfer equation in atmosphere-ocean systems. I. Monte Carlo method. *Applied Optics*, 47, 1037–1047. [PubMed: 18327274]
- Zhang X, Gray DJ, 2015 Backscattering by very small particles in coastal waters. *Journal of Geophysical Research: Oceans*, 120, 6914–6926.

- Zhang X, Gray DJ, Huot Y, You Y, Bi L, 2012 Comparison of optically derived particle size distributions: scattering over the full angular range versus diffraction at near forward angles. *Applied Optics*, 51, 5085–5099. [PubMed: 22858949]
- Zhang X, Hu L, He M-X, 2009 Scattering by pure seawater: Effect of salinity. *Optics Express*, 17, 5698–5710. [PubMed: 19333338]
- Zhang X, Stavn RH, Falster AU, Gray D, Gould RW, 2014 New insight into particulate mineral and organic matter in coastal ocean waters through optical inversion. *Estuarine, coastal and shelf science*, 149, 1–12.
- Zhang X, Twardowski M, Lewis M, 2011 Retrieving composition and sizes of oceanic particle subpopulations from the volume scattering function. *Applied Optics*, 50, 1240–1259. [PubMed: 21460996]
- Zhang XD, Hu LB, 2009 Scattering by pure seawater at high salinity. *Optics Express*, 17, 12685–12691. [PubMed: 19654673]
- Zhang Y, Giardino C, Li L, 2017 Water optics and water colour remote sensing. *Remote Sensing*, 9, 10.3390/rs9080818.
- Zheng G, Stramski D, 2013a A model for partitioning the light absorption coefficient of suspended marine particles into phytoplankton and non-algal components. *Journal of Geophysical Research: Oceans*, 118, 2977–2991, doi:10.1002/jgrc.20206.
- Zheng G, Stramski D, 2013b A model based on stacked-constraints approach for partitioning the light absorption coefficient of seawater into phytoplankton and nonphytoplankton components. *Journal of Geophysical Research: Oceans*, 118, 2155–2174.
- Zheng G, Stramski D, DiGiacomo PM, 2015 A model for partitioning the light absorption coefficient of natural waters into phytoplankton, nonalgal particulate, and colored dissolved organic components: A case study for the Chesapeake Bay. *Journal of Geophysical Research: Oceans*, 120, 2601–2621.

Highlights

- Ocean color algorithms for obtaining marine inherent optical properties are reviewed
- Known uncertainties associated with each approach and knowledge gaps are discussed
- Common performance metrics used to evaluate the satellite retrievals are provided
- Recommendations for future investment for upcoming satellite missions are presented

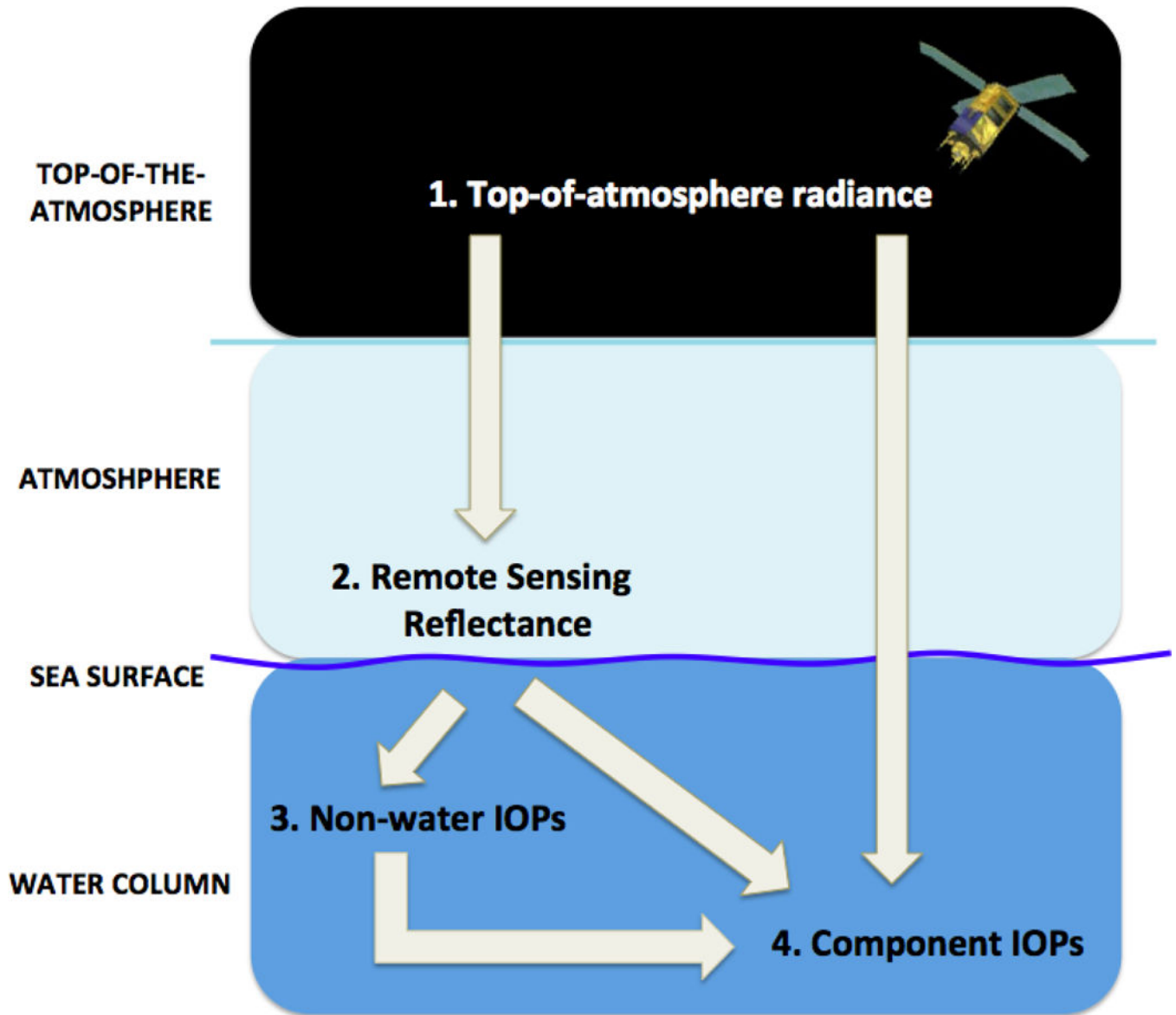
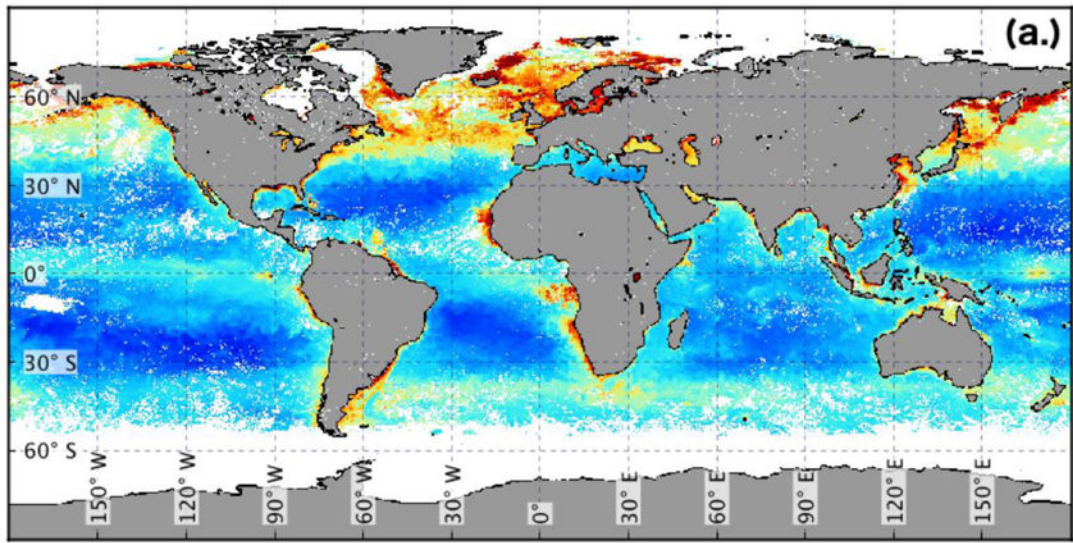


Figure 1: Schematic of inversion methods pathways. Component IOPs can be derived from top-of-atmosphere radiance, remote-sensing reflectance, or non-water IOPs. Each of these approaches requires a different numbers of explicit steps as described in the text.



chlorophyll-a (mg m^{-3})

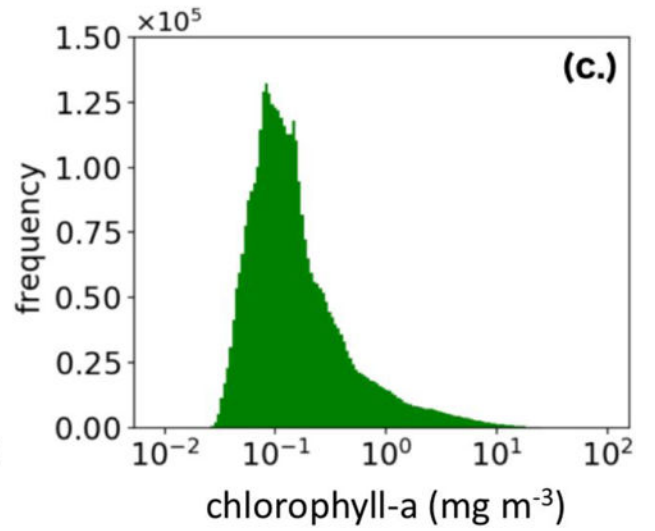
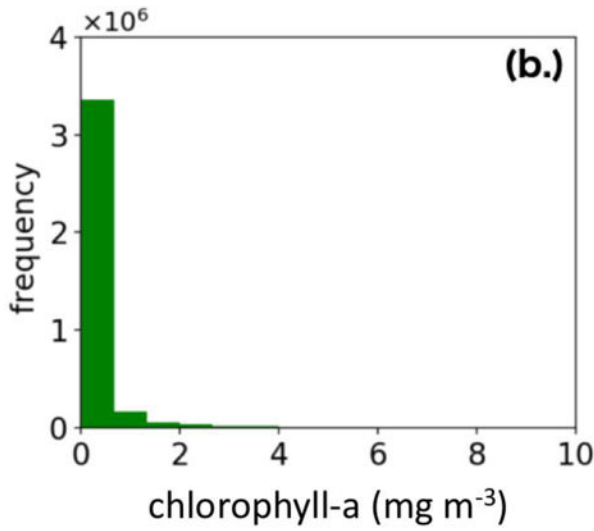
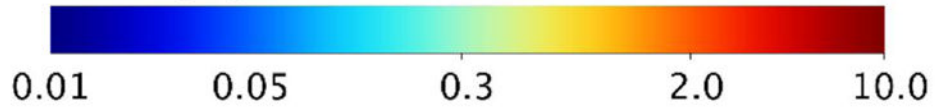


Figure 2:
 (a.) SeaWiFS chlorophyll-a concentration for May 1998. Subplots (b.) and (c.) show how global chlorophyll-a concentration for May 1998 is nearly log-normally distributed.

Table 1:Example methods for deriving normalized $a_{ph}(\lambda)$.

Reference	Uses measured data (Y/N)	Input data required	Description
Prieur and Sathyendranath (1981)	Y	C_a	Single $a_{ph}^*(\lambda)$ vector
Roesler et al. (1989)	Y	C_a	Single $a_{ph}^*(\lambda)$ shape
Lee et al. (1996)	N	C_a	Blends two Gaussian basis vectors
Bricaud et al. (1995)	Y	C_a	Blends two basis vectors
Bricaud et al. (1998)	Y	C_a	Blends two basis vectors
Hoge and Lyon (1996)	N	C_a	Single Gaussian basis vector (Hoepffner and Sathyendranath 1993)
Sathyendranath et al. (2001)	Y	C_a	Blends $a_{ph}^*(\lambda)$ basis vectors for two phytoplankton populations
Ciotti et al. (2002)	Y	Size parameter, S_f	Blends $a_{ph}^*(\lambda)$ basis vectors for micro- and picophytoplankton

Table 2:

Example approaches for partitioning $a(\lambda)$ into $a_{ph}(\lambda)$ and $a_{dg}(\lambda)$.

Reference	Method and assumptions for parameterizing $a_{ph}(\lambda)$ and $a_{dg}(\lambda)$	Additional input data	Applied to ocean color data? (Y/N)
Roesler et al. (1989)	<ul style="list-style-type: none"> $a_{dg}(\lambda)$ has fixed exponential slope, S_{dg} $a_{ph}(\lambda)$ blue-to-red absorption peak defined using pigment data Solves for $a_{dg}(\lambda)$ and $a_{ph}(\lambda)$ 	<ul style="list-style-type: none"> C_a Phaeophytin-a concentration 	N
Lee et al. (2002)	<ul style="list-style-type: none"> $a_{dg}(\lambda)$ has fixed exponential slope, S_{dg} Empirical relationship uses $r_{rs}(\lambda)$ to parameterize band ratio of $a_{ph}(\lambda)$ Solves for $a_{dg}(\lambda)$ and $a_{ph}(\lambda)$ 	<ul style="list-style-type: none"> None 	Y
Ciotti and Bricaud (2006) Method 1	<ul style="list-style-type: none"> $a_{dg}(\lambda)$ assumed to be exponential Empirical relationships uses C_a to parameterize band ratios of $a_{ph}(\lambda)$ Solves for M_{dg}, S_{dg}, $a_{dg}(\lambda)$, and $a_{ph}(\lambda)$ algebraically (Bricaud and Stramski 1990) 	<ul style="list-style-type: none"> C_a 	Y
Ciotti and Bricaud (2006) Method 2	<ul style="list-style-type: none"> $a_{dg}(\lambda)$ assumed to be exponential $a_{ph}(\lambda)$ parameterized through mixing of pico- and microphytoplankton contributions (Ciotti et al. 2002) Solves for M_{dg}, S_{dg}, M_{ph}, and the size parameter of phytoplankton (S_f) via nonlinear optimization 	<ul style="list-style-type: none"> C_a 	Y
Zheng and Stramski (2013b)	<ul style="list-style-type: none"> $a_{dg}(\lambda)$ assumed to be exponential $a_{ph}(\lambda)$ shape expressed through band ratios of 412:443 and 510:490 Searches multiple speculative (feasible) solutions of M_{dg}, S_{dg}, $a_{dg}(\lambda)$, and $a_{ph}(\lambda)$ (Bricaud and Stramski 1990) Computes candidate and selects optimal solution for $a_{dg}(\lambda)$ and $a_{ph}(\lambda)$ using stacked inequality constraints 	<ul style="list-style-type: none"> Pre-determined bounds of inequality constraints 	Y
Zhang et al. (2015)	<ul style="list-style-type: none"> $a_{dg}(\lambda)$ assumed to be exponential $a_{ph}(\lambda)$ parameterized as the sum of mixing of pico-, nano-, and microphytoplankton contributions Solves for M_{dg}, S_{dg}, $a_{dg}(\lambda)$, and $a_{ph}(\lambda)$ including contributions of pico-, nano-, and microphytoplankton using constrained least-squares optimization 	<ul style="list-style-type: none"> C_a-specific $a_{ph}^*(\lambda)$ for pico-, nano-, and microphytoplankton 	N

NASA Author Manuscript

NASA Author Manuscript

NASA Author Manuscript

Table 3:Example methods for deriving normalized S_{bp} .

Method	Uses measured data (Y/N)	Input data required	Description
Morel and Maritorea (2001)	Y	C_a	• S_{bp} defined in terms of \tilde{b}
Gordon et al. (1988)	N	C_a	• Defines $b_p(\lambda)$ from C_a • Assumes $\tilde{b} = F(C_a)$
Ciotti et al. (1999)	Y	C_a	• Logarithmic function from -2 where $C_a = 0.05 \text{ mg m}^{-3}$ to 0 where $C_a = 20 \text{ mg m}^{-3}$
Lee et al. (2002)	Y	$r_{rs}(\lambda)$	• Empirical relationship
Roesler and Boss (2003)	N	$\tilde{b}(\lambda), c_p(\lambda), a_p(\lambda)$	• Solves for for $b_{bp}(\lambda)$ and S_c
Antoine et al. (2011)	Y	C_a or $b_p(555)$	• Empirical relationship
Brewin et al. (2012)	N	C_a	• Empirical relationship for $b_{bp}(\lambda)$

Table 4:

Example of semi-analytical solution classes used in ocean-color algorithms.

Class	Methodology	Example usage
Non-linear spectral optimization	Levenberg Marquardt	Roesler and Perry (1995) Garver and Siegel (1997) Maritorena et al. (2002)
	Nelder-Mead	Evers-King et al. (2014)
	Particle swarm	Slade et al. (2004)
	Genetic algorithm	Haigang et al. (2003)
	Simulated annealing	Salinas et al. (2007)
Direct linear inversion	Linear matrix inversion	Hoge and Lyon (1996) Wang et al. (2005)
Spectral deconvolution	Step-wise algebraic	Lee et al. (2002) Smyth et al. (2006) Pinkerton et al. (2006)
Bulk inversion	Step-wise algebraic solving for each wavelength independently	Loisel and Stramski (2000)
Ensemble inversion	Adaptive linear matrix inversion	Brando et al. (2012)

Table 5:

A sample of recent or soon-to-launch Earth observing satellite missions capable of ocean color observations.

Mission	Agency	Sensor	Launch	Bands [†]	Nadir pixel size (m)	Other Specifications
<i>High spatial resolution missions: O(100 km) swath</i>						
Landsat-8 Landsat-9	USGS/ NASA	OLI OLI-II	2013 2020	• 4 VIS	• 30	• 16 day revisit
Sentinel 2A Sentinel 2B	ESA	MSI	2015 2017	• 4 VIS	• 10	• 10 day revisit • 5 day revisit in constellation
HySpiri	NASA	VSWIR	TBD	• UV-SWIR • Contiguous (10 nm)	• 60	• 19 day revisit
EnMAP	DLR	EnMAP	2017	• UV-SWIR • Contiguous (6.5 nm)	• 30	• 4 day revisit
<i>Geostationary missions</i>						
Geo-Kompsat 2B	KIOST	GOCI-II	2019	• 1 UV • 8 VIS	• 250 local • 1000 global	• Geostationary over NE Asia
<i>Medium spatial resolution missions: O(1000 km) wide swath</i>						
Sentinel 3A Sentinel 3B	ESA	OLCI	2016 2018	• 8 VIS	• 300 coast • 1000 ocean	• 4 day global coverage • 2 day global coverage in constellation
Oceansat-3	ISRO	OCM-3	2018	• 8 VIS	• 360	• 2 day global coverage
Suomi-NPP JPSS-1	NOAA/ NASA	VIIRS	2011 2017	• 5 VIS	• 360	• 1 day global coverage
GCOM-C	JAXA	SGLI	2018	• 1 UV • 6 VIS	• 250 coast • 1000 ocean	• 3 angle polarimetry • 2 day global coverage
PACE	NASA	OCI/ polarimeter	2022	• 350–900 nm • Contiguous (5 nm)	• 1000	• Multi-angle polarimetry • 2 day global coverage

[†]For comparative purposes, SeaWiFS sensor launched in 1997 had six VIS bands

Table 6:

Historical recommendations for the depolarization ratio, δ , of pure water.

δ (unitless)	Reference
0.108	Kratohvil et al. (1965)
0.091	Morel (1974b), Shifrin (1988a)
0.051	Buiteveld et al. (1994a)
0.039	Jonasz and Fournier (2007)